# INFORMATION TO USERS

8015591

ROMANISHIN, WILLIAM

LOW SURFACE BRIGHTNESS SPIRAL GALAXIES

*The University of Arizona*  PH.D.  1980

PLEASE NOTE:

In all cases this material has been filmed in the best possible way from the available copy. Problems encountered with this document have been identified here with a check mark ✓.

1. Glossy photographs ___✓___

2. Colored illustrations _____

3. Photographs with dark background ___✓___

4. Illustrations are poor copy _____

5. Print shows through as there is text on both sides of page _____

6. Indistinct, broken or small print on several pages _____ throughout _____

7. Tightly bound copy with print lost in spine _____

8. Computer printout pages with indistinct print _____

9. Page(s) _____ lacking when material received, and not available from school or author _____

10. Page(s) _____ seem to be missing in numbering only as text follows _____

11. Poor carbon copy _____

12. Not original copy, several pages with blurred type _____

13. Appendix pages are poor copy _____

14. Original copy with light type _____

15. Curling and wrinkled pages _____

16. Other _____

LOW SURFACE BRIGHTNESS

SPIRAL GALAXIES


by

William Romanishin


_____


A Dissertation Submitted to the Faculty of the

DEPARTMENT OF ASTRONOMY

In Partial Fulfillment of the Requirements
For the Degree of

DOCTOR OF PHILOSOPHY

In the Graduate College

THE UNIVERSITY OF ARIZONA


1 9 8 0

## THE UNIVERSITY OF ARIZONA
## GRADUATE COLLEGE

As members of the Final Examination Committee, we certify that we have read

the dissertation prepared by ___William Romanishin___

entitled ___Low Surface Brightness Spiral Galaxies___

and recommend that it be accepted as fulfilling the dissertation requirement

for the Degree of ___Doctor of Philosophy___ .

_Neville J. Woolf_

Date  _5th March 1980_

_William G. Tifft_

Date  _7th March 1980_

_George Rieke_

Date  _March 7, 1980_

_Roger Angel_

Date  _March 7 1980_

Date _____

Final approval and acceptance of this dissertation is contingent upon the
candidate's submission of the final copy of the dissertation to the Graduate
College.

I hereby certify that I have read this dissertation prepared under my
direction and recommend that it be accepted as fulfilling the dissertation
requirement.

_Stephen E. Strom_

Dissertation Director

Date  _6 March, 1980_

STATEMENT BY AUTHOR

This dissertation has been submitted in partial ful-
fillment of requirements for an advanced degree at The
University of Arizona and is deposited in the University
Library to be made available to borrowers under rules of
the Library.

Brief quotations from this dissertation are allow-
able without special permission, provided that accurate
acknowledgment of source is made. Requests for permission
for extended quotation from or reproduction of this manu-
script in whole or in part may be granted by the head of
the major department or the Dean·of the Graduate College
when in his judgment the proposed use of the material is in
the interests of scholarship. In all other instances, how-
ever, permission must be obtained from the author.

SIGNED: _William Romaniski_

ACKNOWLEDGMENTS

During the all-too-numerous years I have been a
graduate student, many people have provided assistance of
various kinds.  Steve and Karen Strom, for the past 3-1/2
years, have provided scientific inspiration, and invaluable
help in obtaining telescope time, fighting with bureaucrats
in my behalf, and arranging for the part-time position at
Kitt Peak which has kept me from starving.  I am particu-
larly grateful for the friendship and companionship of my
colleague Susan Wilkerson, the most interesting, pleasant
and beautiful person I have ever known.  The residents of
the infamous Park Avenue Apartment (Pete Worden, Eric Jensen,
Steve Grandi, Gary Coleman, Todd Boroson and Brad Peterson)
all helped to provide a friendly ambience during the years
I lived there.  I greatly enjoyed the company of numerous
other people at Steward and Kitt Peak, among them Mark
Adams, John Scott, Jim Liebert, John Stocke, Mark Giampapa,
Paul Hintzen and John Kormendy.  The many nights I spent
eating Mexican food and/or drinking beer with some of these
people were among the best times of the last 5-1/2 years.

During the last few months of writing this disser-
tation, when it seemed it would never end, many people went

out of their way to help me. The Stroms and Betty and Herb Schueler provided lodging. Worden, Grandi, Jensen and my parents provided monetary loans.

Many people at Kitt Peak helped in obtaining and reducing the data presented in this dissertation. On the Mountain, all the TA's and LTO's provided their usual high level of competent service, particularly Gus Maxey, who could always repair the telescopes and instruments I managed to put out of commission. Downtown I thank numerous programmers, computer operators, technicians and secretaries, particularly Betty Schueler, the only secretary I know of who works graduate student hours. I thank Dave Monet for helping me with the word processor at Kitt Peak, which I used for rough drafts of this work.

I would like to thank my scientific collaborators who have been patient with me this last year or so while I virtually ignored all the other projects I had started to agonize over this dissertation. These people include Roger Angel, Duane Carbon, Trinh Thuan and the Stroms.

I thank Arecibo Observatory and NRAO for providing telescope time for the 21-cm observations reported here. Nathan Krumm and G. R. Knapp provided invaluable help in obtaining this data, as I didn't know a circular feed from a doober.

Last, but not least, I thank my parents for all they have done for me. The best part of finishing this dissertation is that I can (at last) honestly tell them I won't be a student any longer.

# TABLE OF CONTENTS

LIST OF TABLES

LIST OF TABLES--<u>Continued</u>

# LIST OF ILLUSTRATIONS

ABSTRACT

This dissertation presents an observational overview
of a sample of low surface brightness (LSB) spiral galaxies.
The sample galaxies were chosen to have low surface bright-
ness disks and indications of spiral structure visible on
the Palomar Sky Survey. They are of sufficient angular
size, (diameter > 2.5 arcmin) to allow detailed surface
photometry using Mayall 4-m prime focus plates. In addition
to photographic surface photometry, we obtained optical and
infrared aperture photometry, HII region spectrophotometry,
long-slit spectra and neutral hydrogen 21-cm radio observa-
tions for a selection of the sample galaxies.

The major findings of this dissertation are:

1. The average disk central surface brightness of the
LSB galaxies is 22.88 magnitude/arcsec$^2$ in the B passband.
This is a factor of 3 lower in intensity than the value
found for most spirals studied up to now. The average disk
scale length is about 4 kpc, almost as large as for a
sample of giant late-type systems.

2. From broad-band color measurements of the old stel-
lar population, we infer a low average stellar metallicity,
on the order of 1/5 solar. The old population was

observationally isolated in wavelength, by means of infrared observations, and spatially, by measuring optical colors of points in the disk where there has been no recent star formation.

3. The spectra and optical colors of the HII regions in the LSB galaxies indicate a lack of hot ionizing stars compared to HII regions in other late-type galaxies. We believe this indicates an initial mass function depleted in massive stars.

4. The average surface mass density, measured within the radius containing half the total mass, is less than half that of a sample of normal late-type spirals.

5. The average LSB galaxy neutral hydrogen mass to blue luminosity ratio is about 0.6, significantly higher than in a sample of normal late-type galaxies.

6. We find no conclusive evidence of an abnormal mass-to-light ratio in the LSB galaxies. However, there is a suggestion that the mass-to-light ratio in these galaxies may be slightly larger than normal.

7. Some of the LSB galaxies exhibit well-developed density wave patterns. The amplitude of these wave patterns range up to the amplitude found for normal spirals with well-developed spiral structure. The spiral density wave theory predicts weak shocks in the LSB galaxies.

8. A very crude calculation shows the lower metallicity of the LSB galaxies compared with normal late-type spirals might be explained simply by the deficiency of massive stars in the LSB galaxies.

These galaxies may prove useful in studying the connection between the initial mass function of a galaxy and its metallicity.

# CHAPTER 1

## INTRODUCTION

The detailed study of spiral galaxies has pro-
gressed rapidly in the last decade. Because of the rich
variety of processes we are able to study in spiral gal-
axies, many different observational tools are needed to
obtain even a rudimentary picture of a galaxy. The neces-
sary tools include, but are not limited to: surface pho-
tometry in several colors, photoelectric optical and
infrared aperture photometry, emission-line spectroscopy
of HII regions, and 21-cm radio studies of neutral hydrogen.
Observers have naturally concentrated on the nearby bright
galaxies. Examples of recent detailed studies of the sur-
face brightness distribution in bright spirals is presented
by Schweizer (1976) and Talbot, Jensen and Dufour (1979).
Examples of studies of the emission-line spectra of HII re-
gions in spirals is provided by Searle (1971), Smith (1975)
and Shields and Searle (1978).

Many parameters influence the evolution of spiral
galaxies. We can study samples of galaxies with some ob-
servational parameter which differs from the majority of
galaxies to determine the cause and effect of this

1

parameter on galactic evolution. In this way we hope to
isolate the effects of one parameter. We chose to compare
spirals having particularly low surface brightness disks
with normal spirals. The disk surface brightness provides
a convenient parameter by which to select a sample of
"different" galaxies. It is easy to pick out galaxies with
low surface brightness disks by visual inspection. One
question we wish to answer is: Why do some spiral galaxies
have low optical surface brightness disks, even though they
have total luminosities comparable to some galaxies of
normal surface brightness? Is it due to difference in mass
distribution, or a radically different mass-to-light ratio
or star formation rate? Another question we would like to
ask is: Is the process of star formation different in
these galaxies? By studying these "different" galaxies, we
hope to learn more about the general process of galactic
evolution. This dissertation presents an overview of the
properties of spirals of low surface brightness.

An extensive catalog of low surface brightness gal-
axies was compiled by van den Bergh (1966). This list is
referred to as the David Dunlap Observatory (DDO) dwarf
galaxy list. Van den Bergh defined galaxies with low sur-
face brightness and little central concentration of light
to be "dwarf galaxies", implying low luminosity. Until
1975, little was known about the intrinsic luminosities of

the vast majority of the DDO dwarf galaxies because of the
difficulty of measuring redshifts for these objects. In
1975, Fisher and Tully (1975) published a study of the DDO
dwarf galaxies using observations of their neutral hydrogen
content using the 21-cm radio line. They were able to
measure redshifts for almost 2/3 of the complete DDO dwarf
galaxy catalog. Using eye-estimate magnitudes from the
Palomar Sky Survey, Fisher and Tully found that many of
these galaxies were not intrinsically faint. Over half of
the detected galaxies were brighter than $M_{pg} = -18$ ($H_O = $
50 km/sec/Mpc).

The galaxies studied in this work are intrinsically
luminous low surface brightness galaxies. In order to
study their basic properties, the following types of data
were obtained:

1. Photographic surface photometry in one, two or
three colors to obtain accurate total magnitudes and colors,
and to study the large-scale structure of the galaxies.
The digital surface brightness maps are used to study the
parameters of the spiral pattern, the color of the old disk
stars, and the luminosities of the HII regions.

2. Photoelectric spectrophotometry of HII regions to
study the metal abundance of the ionized gas, and the mass
function of the stars ionizing the gas.

3.  Infrared photometry to study the old stellar population.

4.  Radio observations of the neutral hydrogen 21-cm line to study the gas content.

5.  Long-slit photographic spectra to study the mass-to-light ratio as a function of position, and also to obtain some additional information on line ratios in the emission line spectra of HII regions.

CHAPTER 2

OBSERVATIONS

This chapter first describes the selection of the low surface brightness galaxy sample. Then, the observational techniques used to study these galaxies are described. In addition, the basic observational data on the low surface brightness galaxies is listed in this chapter.

## 2.1 Selection of Galaxies

The low surface brightness (LSB) spiral galaxies observed were chosen by examining most of the Palomar Sky Survey plates with galactic latitude greater than about 30°. The following criteria were used to select LSB spiral galaxies:

1. diameter between about 2.5 and 5 arcmin;

2. low surface brightness disk;

3. clear indications of spiral structure on glass copies of the Palomar Sky Survey.

The lower diameter limit was imposed so the galaxies would be large enough for detailed surface photometry. The upper diameter cutoff was imposed to eliminate galaxies too large to be studied with the 4-m prime focus camera. Many dozens

of LSB spiral galaxies were found below the 2.5 arcmin cut-
off. Only a few were found above the 5 arcmin diameter
cutoff. The sample is not intended to be complete in any
sense. We are interested only in the intrinsic properties
of typical members of the LSB class of galaxies. Discus-
sion of some extrinsic properties of LSB galaxies, such as
their luminosity function and space distribution, can be
found in Thuan and Seitzer (1979).

The final observing list contained about 40 galax-
ies. Because of the varied nature of the observations, it
was possible to obtain complete data for only a few galax-
ies.

## 2.2 UBVR Photometry

Photoelectric UBVR photometry was obtained for 35
galaxies, including all but one of the galaxies for which
we have some plate material. Almost all observations were
obtained with the Kitt Peak National Observatory (KPNO)
1.3-m telescope and the MK II computer-controlled photom-
eter. The filter combinations used to define the band-
passes are listed in Table 1. A few galaxies were observed
with the same equipment using the KPNO 2.1-m telescope.

At the 1.3-m telescope, the galaxies were acquired
by offsetting from nearby stars. The acquisition tele-
vision system, which does not have an integrating capabil-
ity, was not sensitive enough to detect most of the LSB

Table 1. Filter Combinations for Photoelectric
Observations -- All observations are
with an S20 photocathode.

| Photometric Band | Filters |
| --- | --- |
| U | Corning 9863 |
| | $CuSO_4$ |
| B | GG-385 |
| | BG-18 |
| | Corning 5-57 |
| V | BG-18 |
| | GG-495 |
| R | RG-610 |
| | KG-3 |

galaxies.  Positions of the galaxy center, and several
nearby stars, were measured from glass copies of the Palo-
mar Sky Survey, using the KPNO two-dimensional Grant
machine and the ASTRO reduction program.  These positions,
referenced to SAO stars, are accurate to about 1 arcsec.
The 1.3-m computer-controlled drive is able to make offsets
over the distances between the galaxies and the nearby ref-
erence stars (typically 1-3 arcmin) to within 1 or 2 arcsec.
The accuracy of the telescope offsetting was checked many
times each night, particularly after moving the telescope
from one part of the sky to another, by offsetting between
pairs of reference stars.  After setting up on the galaxy
coordinates, an electronic cursor on the television was set
on a star in the field for guiding.  The field was not
visible on the television during an integration.  After a
sequence of galaxy and sky observations in all filters,
lasting a minute or two, the guiding was checked.  We chose
sky measurement positions that were free of stars on the
Palomar Sky Survey prints.  These areas were 200 or more
arcsec from the galaxies.  We estimate that this was suf-
ficient distance from the galaxies so that any correction
for galaxy light in the sky beam would be less than 0.01
magnitude.

At the time of the first photoelectric observing
runs, in late 1977, there was no extensive list of reliable

faint standards available for the standard Johnson R pass-
band. We used standard stars from the list of Sandage
(1973), who lists a red magnitude (which we will denote $R_S$)
which is not exactly the same as the Johnson R. The pri-
mary standard stars used in the photometry were those
listed by Sandage in M 67. Stars from the equatorial UBV
catalog of Landolt (1973) were also observed each run. The
UBV transformations obtained for the Sandage and Landolt
standards were essentially identical.

Recently, R and I magnitudes on the Johnson system
have been measured for a large number of the Landolt equa-
torial standards (Moffett and Barnes 1979). During our
last observing run, we observed a number of these stars
along with the usual Sandage standards. Using these obser-
vations, we derived the following transformations relating
the Johnson R to the Sandage $R_S$:

$$R = R_S - 0.03 \quad , \quad (V-R)_S \leq 0.6 \tag{1}$$

$$R = R_S + 0.19 \ (V-R)_S - 0.15$$
$$0.6 < (V-R)_S < 1.4 \tag{2}$$

The difference between the two R systems is well-defined
and small (< 0.04 mag) over the color range of interest for
the galaxy photometry. All R magnitudes listed in this
work have been corrected to the Johnson R system.

All UBVR photometry is listed in Table 2. The first column gives the galaxy name, the second the aperture diameter for the photoelectric photometry, in arcsec; the remaining columns list the V magnitude and the (B-V), (U-B) and (V-R) colors. Integration times were adjusted so that photometric uncertainties, derived from photon statistics, were typically 0.03 magnitude in V and 0.04 magnitude in all colors. All measurements with errors between 0.08 and 0.11 magnitudes are followed by a colon in Table 2.

## 2.3 Surface Photometry

We obtained photographic plates of 17 LSB galaxies. The prime focus camera of the Mayall 4-m telescope was used to obtain U, $B_3$ or R plates. The following plate, filter and exposure time combinations were used, resulting in an average photographic sky density of 0.7:

1. U -- IIIa-J plates baked in nitrogen or hydrogen were used with a UG2 filter for a typical exposure time of 2 hours and 15 minutes.

2. $B_3$ -- Baked IIIa-J plates were used with a GG385 filter. The typical exposure time was 45 minutes.

3. R -- Baked IIIa-F plates were used, with a RG610 filter, with sky reached in about 50 minutes.

The scale of these plates (18.55 arcsec/mm) is adequate for detailed surface photometry. One problem with

Table 2.  UBVR Photometry[a]

|  | Aperture | V | B–V | U–B | V–R |
|---|---|---|---|---|---|
| UGC 00334 | 35ʺ3 | 16.03 | 0.55 | −0.23 | 0.67 |
|  | 58.6 | 15.31 | 0.47 | −0.08 | 0.71 |
|  | 82.2 | 14.95 | 0.49 | −0.24 | 0.72 |
| UGC A0033 | 35.3 | 15.37 | 0.79: | −0.12: | 0.51 |
|  | 82.2 | 14.30 | 0.51 | 0.09 | 0.50 |
| DDO 48 | 82.2 | 15.27 | 0.49 | −0.25: | 0.64 |
| UGC 04841 | 17.7 | 16.18 | 0.67 | −0.01 | 0.74 |
| UGC 04922 | 35.3 | 15.14 | 0.69 | 0.04 | 0.66 |
|  | 58.6 | 14.52 | 0.57 | 0.04 | 0.66 |
| DDO 79 | 82.2 | 14.32 | 0.55 | −0.11 | 0.58 |
| UGC 06446 | 82.2 | 14.39 | 0.48 | −0.29 | 0.36 |
| UGC 06682 | 82.2 | 14.77 | 0.65: | −0.11: | 0.61: |
| NGC 3913 | 58.6 | 13.57 | 0.61 | −0.09 | 0.64 |
|  | 82.2 | 13.26 | 0.60 | −0.04 | 0.64 |
| UGC 06922 | 82.2 | 14.09 | 0.61 | −0.12 | 0.64 |
| UGC 06955 | 82.2 | 13.75 | 0.56 | −0.07 | 0.58 |
| UGC 06983 | 82.2 | 13.53 | 0.54 | −0.14 | 0.58 |
| NGC 4411B | 35.3 | 14.33 | 0.68 | −0.04 | 0.68 |
|  | 82.2 | 13.25 | 0.56 | −0.12 | 0.61 |
| UGC 07557 | 35.3 | 15.19 | 0.41 | −0.04 | 0.61 |
|  | 82.2 | 13.89 | 0.61 | −0.26 | 0.49 |
| DDO 128 | 82.2 | 14.65 | 0.42 | −0.13 | 0.51 |
| UGC 07685 | 35.3 | 14.76 | 0.65 | −0.08 | 0.62 |
| DDO 144 | 13.3 | 16.39 | 0.48 | −0.10 | 0.63 |
| DDO 142 | 35.3 | 14.57 | 0.69 | 0.16 | 0.74 |
|  | 82.2 | 13.30 | 0.68 | −0.07 | 0.58 |

Table 2.--<u>Continued</u>

| | Aperture | V | B-V | U-B | V-R |
|---|---|---|---|---|---|
| MCG-2-33-15 | 82.2 | 13.21 | 0.45 | -0.13 | 0.59 |
| UGC 08253 | 35.3 | 16.43: | 0.23: | -0.02: | 0.56: |
| UGC A0333 | 35.3 | 15.37 | 0.54 | -0.15 | 0.63 |
| | 82.2 | 14.16 | 0.51 | -0.17 | 0.54 |
| UGC 08409 | 35.3 | 15.35 | 0.49: | 0.06: | 0.58: |
| | 82.2 | 14.62 | 0.44 | -0.07 | 0.52: |
| UGC 09061 | 35.3 | 13.78 | 0.94 | 0.52 | 0.92 |
| | 58.6 | 13.33 | 1.01 | 0.45 | 0.86 |
| NGC 5774 | 35.3 | 13.93 | 0.60 | -0.05 | 0.61 |
| | 58.6 | 13.41 | 0.54 | -0.07 | 0.64 |
| UGC 09614 | 35.3 | 16.10 | 0.48 | 0.03 | 0.62 |
| | 58.6 | 15.24 | 0.47 | -0.31 | 0.41: |
| | 82.2 | 15.19 | 0.38 | -0.14 | 0.53 |
| UGC 09875 | 35.3 | 15.96 | 0.64 | -0.17 | 0.64 |
| | 58.6 | 14.90 | 0.39 | -0.01 | 0.57 |
| UGC 09910 | 35.3 | 16.06 | 0.12: | -0.14: | 0.52 |
| | 58.6 | 15.71 | 0.14: | -0.16: | 0.73: |
| | 82.2 | 15.30: | 0.37: | -0.29: | 0.43: |
| NGC 5964 | 82.2 | 13.01 | 0.70 | 0.11 | 0.71 |
| UGC 09938 | 58.6 | 15.88: | 0.33: | -0.31: | 0.47: |
| DDO 203 | 82.2 | 13.84 | 0.52 | -0.12 | 0.57 |
| UGC 11868 | 35.3 | 15.21 | 0.74 | -0.01 | 0.78 |
| DDO 214 | 35.3 | 14.95 | 0.46: | 0.07: | 0.74: |
| | 82.2 | 13.57 | 0.81 | -0.25 | 0.51 |
| UGC 12522 | 35.3 | 15.88 | 0.52: | 0.12: | 0.85: |
| | 58.6 | 15.18 | 0.77: | -0.05: | 0.71: |

Table 2.--<u>Continued</u>

|  | Aperture | V | B-V | U-B | V-R |
|---|---|---|---|---|---|
| DDO 219 | 35.3 | 15.60 | 0.66 | 0.10: | 0.61 |
|  | 82.2 | 14.56 | 0.50 | -0.11 | 0.62 |
| UGC 12845 | 35.3 | 15.06 | 0.89 | 0.17 | 0.81 |

a.  The nominal uncertainties are $\pm$ 0.04 magnitude in V
    and $\pm$ 0.05 in all colors.  Values followed by a colon
    have uncertainties approximately twice the nominal
    value.

the prime focus camera is the complex large-scale background variation resulting from scattered light and the radial scale change. The galaxies studied here, with maximum size of 5 arcmin, are large enough that the background variations cannot be ignored, particularly in the outer, faint parts of the galaxies. A fairly simple method, described in detail below, was devised to correct for the background variation.

The first step in the reduction process was to scan the plates on the KPNO PDS microdensitometer. All scanning was done in the 12 bit density mode, which records plate density from 0.00 to 5.115 in 4096 steps. The aperture was a square 100 microns (1.86 arcsec) on a side, with a step size of 50 microns. Generally, a 1024 x 1024 raster or matrix of points was scanned around each galaxy, yielding an image 15.8 arcmin on a side. Each prime focus plate has a 16 step intensity calibration, exposed simultaneously with the galaxy exposure. A small raster on each of the density levels was scanned, along with a portion of the plate chemical fog.

All subsequent picture processing operations made use of the Interactive Picture Processing System (IPPS) at KPNO (Wells 1975). The densities of the step calibration exposure were fit to the following characteristic curve function (Goad 1975):

$$\log I = P_0 + P_1 Y + P_2 Y^2 + P_3 Y^3 \qquad (3)$$

where

$$Y = D + P_4 \log_{10} (1 - 10^{-D}); \qquad (4)$$

I is the intensity; D the photographic density; and the P's are constants determined by the fit. All galaxy density rasters were converted to intensity rasters using the parameters determined for each individual plate.

Next, the intensity rasters were corrected for the 4-m background variation. Experimentation showed that the variation could be modeled, at least locally (i.e., over the area covered by a $1024^2$ raster) as a linear decrease in the sky intensity I as a function of radius, with the radius measured from some point near the plate center:

$$I = I_0 - sR \qquad (5)$$

where R is the distance of a pixel from the imaginary center point, $I_0$ the extrapolated intensity at the center point and s is a constant derived as explained below. In reality, the background variation is not radially symmetric over the entire plate, so the center of intensity is not necessarily the center of the plate. This variation is, of course, not the same as a simple tilted plane, as the sky isophotes were portions of approximately circular arcs. The procedures used to correct the background are outlined here:

1.  We estimated the apparent center of the sky iso-
phote arcs in the coordinate system of the raster, using
the shape of the arcs as seen on the COMTAL display and a
print of the plate.

2.  We took an intensity scan along the longest possi-
ble radius vector appearing on the raster, yielding a plot
and listing of the values of I(R).

3.  We made a linear fit to the radial intensity scan,
ignoring the portions of the scan containing the galaxy or
bright stars.  This fit gives the constant s.

4.  We created a raster containing a model of the back-
ground.  This was done by first creating a raster, using
the R subroutine in the EDIT menu, where each pixel was as-
signed the value $-(s/I_0)R$.  The arithmetic subroutines were
used to add 1.000 to this raster, yielding a raster with
the intensity fulfilling equation 5, normalized so that $I_0$
was 1.000.

5.  We divided the galaxy image by this raster.

After applying this correction algorithm, the next
steps in the reduction were to find the basic properties
describing the galaxy image:  coordinates of center, posi-
tion angle ($\theta$) of the major axis, and ellipticity or ratio
of semiminor axis b to semimajor axis a, (b/a).  The center
was usually found by setting the COMTAL image display

cursor on the center of the galaxy and reading the coordi-
nates (in pixels) of the cursor. There is an automatic,
digital image center finding procedure, but in general
these galaxies did not have the small sharp, well-defined
nuclei needed to use this feature. The values of b/a and θ
were found using the B/A subroutine. In this routine, the
galaxy image was displayed so that the galaxy isophotes
were clearly visible. The COMTAL cursor was positioned at
either ends of the major and minor axes of a particular
isophote and an ellipse was fit to these four points,
yielding b/a and θ of the major axis. This was usually
done for several isophotes and the results averaged. We
used fairly faint isophotes, beyond the extent of the spi-
ral arms, to try to derive parameters for the underlying
disk.

The transformation constant s relating the photo-
graphic instrumental magnitudes to the absolute magnitude
scale were found by comparing photoelectric aperture pho-
tometry with simulated aperture photometry done with the
IPPS routine PHOT. PHOT sums the intensity of all pixels
within a specified radius of a given point, and subtracts
a sky value found by averaging the intensity values in a
number of small apertures spaced along a circle at a large
distance from the center of the aperture. This sky value
is corrected for the presence of stars or plate defects

which might affect individual sky aperture measurements
using a point rejection algorithm. Each plate was cali-
brated separately, using our photoelectric aperture photom-
etry for all galaxies except NGC 45, where the R magnitude
was extrapolated from the UBV magnitudes given by de
Vaucouleurs and de Vaucouleurs (1972). The most signifi-
cant source of uncertainty in this calibration procedure is
the uncertainty in the photoelectric magnitudes, typically
0.04 magnitude. A potential major source of error is the
centering of the aperture: if the aperture used in PHOT is
not placed relative to the galaxy as was the photoelec-
tric aperture, the calibration constant will be in error.
When observing the galaxies photoelectrically, the error in
centering was estimated to be no larger than 2"-3". The
location of this same center on the digital image is prob-
ably better than 2". Changing the center of the PHOT aper-
ture by 3" from the measured central position seldom
changed the transformation coefficient by more than 0.01
magnitude, except for the smaller apertures, diameters
13.3" or 17.7". Some galaxies were observed photoelectric-
ally with more than one aperture size. In these cases, the
transformation coefficient was the average of the values
for the individual values, with half weight given to the
small aperture measurements.

To study the large-scale structure of a galaxy, we derived I(r), the azimuthally averaged surface brightness as a function of the geometric mean radius, $r = \sqrt{ab}$. The intensity values, with the sky subtracted, in small (usually 2" diameter) apertures placed along elliptical paths are averaged for various values of b. A point rejection algorithm rejects particularly high or low points along each scan, to remove stars or plate defects. The values of b/a and position angle found using B/A are used for all b. This procedure can smear out some of the features in the profile, such as bars near the nucleus, which can have both different ellipticities and position angles from those adopted for the galaxy as a whole.

The first step in the profile measurement is the determination of the local sky value at each point in the image. Although the flattening procedure discussed above removed most of the systematic sky variations, we used as a final algorithm the Fourier sky fit discussed by Strom and Strom (1978). The sky intensity is measured in a large number of small apertures along a circle, centered on the galaxy, of radius $R_o$. The resulting distribution of intensity as a function of angle, $I(\phi)$, was fit with a low-order Fourier series of the form $a_o + f(\phi)$, after removing those points affected by stars or plate defects. At any point at radius r from the galaxy center, the background intensity

is computed as $a_o + (r/R_o)f(\phi)$. This implicitly assumes that the sky varies linearly along a ray drawn from the galaxy center to $R_o$, $\phi$. Many of the galaxies did not require this type of fit, as the intensity was constant along the circle. Some required a first order Fourier fit, i.e., a tilted plane, while only a very few required a second order Fourier fit.

At the IPPS the surface brightness profile is displayed on an interactive terminal. The $I(r)$ distribution is computed for increasing values of b until the sky level is reached, at which point $I(r)$ remains constant or changes very slowly compared to its change within the galaxy image. The final sky value is set equal to the average of the values of $I(r)$ from the edge of the galaxy to the sky point at the greatest galactocentric distance measured. Alternatively, an estimated value can be specified if this average value is not judged appropriate, following visual inspection. For example, an estimated sky value is entered if there is still a slight gradient in $I(r)$ past the maximum extent of the galaxy image. All the values of $I(r)$ are corrected for this final sky value, and a table listing values of a, b, r, $M(r)$ and $M_{tot}(r)$ is produced. $M(r)$ is simply 2.5 log $I(r)$, and $M_{tot}(r)$ is the integrated magnitude within the ellipse with geometric mean radius r. This surface brightness profile routine is known as ISOPH.

One problem we discovered late in the reduction process is that the point rejection algorithm, designed to delete star images, was also deleting a few pixels in particularly high surface brightness knots within the galaxy image. We estimated the size of this effect by comparing values of the total intensity derived from PHOT, which sums all pixels within a given radius, to the integrated intensity measured with ISOPH, for several galaxies with only faint superposed stars. The effect was detectable on the U images, but not on the R. This is as expected, as the contrast between the bright knots of newly formed stars and the surrounding galaxy is much greater in U than in R. The comparison of PHOT and ISOPH magnitudes shows the effect to be less than 0.05 magnitude in total U magnitude for NGC 3913, one of the galaxies which from visual inspection would appear to be affected the most.

Unfortunately, as is well known, (Burnstein 1978), surface photometry is often susceptible to large systematic errors, which are often difficult to evaluate internally. The best way to discover such errors is to compare results obtained by independent observers. As one form of external check, we derived profiles for three LSB galaxies using plates taken with the Palomar 1.2-m Schmidt telescope. These profiles agree well with the profiles obtained from the 4-m plates. These data are discussed below. The basic

integrity of the observing and reduction system, such as the calibration of the 4-m spot sensitometer, the accuracy of the density to intensity routine, and the correct performance of the IPPS algorithms, has been documented (Strom and Strom 1978).

The profiles of three galaxies, NGC 4411A and B, and UGC 07557, were measured on U and R plates obtained with the Palomar 1.2-m Schmidt telescope. These plates were scanned with a 20 micron square (1.34 arcsec square) aperture, at 20 micron separations. The calibration was provided by a set of Palomar spots on the plate. The spot densities were fit to a characterisitc curve of the form (Strom et al. 1977):

$$\log I = a_0 + a_1 D + a_2 \log (1-10^{-D}) + 10^{a_3 (D-a_4)} \qquad (6)$$

where the a's are constants determined by the fit. The a's for these particular plates have been determined by Strom (1978, personal communication). This calibration has yielded accurate profiles for elliptical galaxies on the same Schmidt plates. The subsequent analysis of these galaxy profiles proceeded as for the 4-m plates, except that no flattening or Fourier fit sky was necessary because of the uniform sky background on the Schmidt plates.

For NGC 4411A and B, and UGC 07557, the profiles derived from the 4-m plates and the Schmidt plates agreed very well. We compared each pair of 4-m and Schmidt profiles at each value of r. For surface brightness levels brighter than $\mu$ = 24 mag/arcsec$^2$ in both U and R, the average difference for all points was 0.01 magnitude, with a scatter of 0.04 magnitude. For 24 < $\mu$ < 26.5 mag/arcsec$^2$, the average difference was 0.01, with a scatter of 0.21 magnitude. In this lower surface brightness range, small errors in setting the sky value can result in sizable systematic errors in the profiles. The scatter in the values of I(r) averaged in ISOPH to obtain the sky provides an estimate of the uncertainty in the sky level. Appropriate small adjustments in the sky levels of the Schmidt profiles, within the errors in setting the sky, were made to improve the agreement between the 4-m and Schmidt profiles. With these adjustments, the scatter in the difference for the lower surface brightness region is decreased by a factor of two. We feel the error in setting the sky is primarily in the Schmidt profiles, because the estimated error in the sky was much less for the 4-m plates, simply because of the greater amount of information contained in the higher-scale 4-m images.

The small average difference between the 4-m and Schmidt profiles at $\mu$ < 26.5 mag/arcsec$^2$ shows that the

intensity scales are consistent. The small scatter in the differences for individual values of $r$, especially after small adjustments in the Schmidt sky levels, indicates that the level of random errors in the profiles is probably less than 0.05 mag for $\mu < 24$ mag/arcsec$^2$ and less than 0.10 mag for $24 < \mu < 26.5$ mag/arcsec$^2$.

The luminosity profiles are listed in Table 3. The first two columns list $r$, in arcsec, and the R surface brightness, in mag/arcsec$^2$, at that $r$. The (U-R) and ($B_3$-R) colors are listed when available. The last column lists the B surface brightness. For galaxies with only an R plate, the B surface brightness was obtained from the R using a constant (B-R), equal to that observed in the largest photoelectric aperture for the galaxy (see Table 2). The B profile for galaxies with both a U and R plates was obtained from the R profile and the value of (B-R) calculated at each $r$ from (U-R), using the color interpolation equations (equations 9 and 10). For galaxies with plates in U, $B_3$, and R the B profile was obtained from the $B_3$ profile by the equation

$$B = B_3 + 0.3 \ (B-V) \tag{7}$$

(Schweizer 1976), where the (B-V) value at each $r$ was found from the (U-R) color and the color interpolation formula.

Table 3. Luminosity and Color Profiles

| | $\sqrt{ab}$ | $\mu_R$ | U-R | $B_3$-R | $\mu_B$ |
|---|---|---|---|---|---|
| NGC 45 | 2.3 | 20.91 | | | 22.12 |
| (b/a=0.76) | 7.0 | 21.08 | | | 22.29 |
| | 11.7 | 21.17 | | | 22.38 |
| | 16.4 | 21.28 | | | 22.49 |
| | 21.1 | 21.40 | | | 22.61 |
| | 25.8 | 21.51 | | | 22.72 |
| | 30.4 | 21.64 | | | 22.85 |
| | 35.1 | 21.82 | | | 23.03 |
| | 44.5 | 21.96 | | | 23.17 |
| | 58.5 | 22.26 | | | 23.47 |
| | 72.6 | 22.53 | | | 23.74 |
| | 86.6 | 22.86 | | | 24.07 |
| | 100.7 | 23.03 | | | 24.24 |
| | 114.7 | 23.23 | | | 24.44 |
| | 128.8 | 23.47 | | | 24.68 |
| | 142.8 | 23.69 | | | 24.90 |
| | 156.8 | 23.80 | | | 25.01 |
| | 170.9 | 23.90 | | | 25.11 |
| | 184.9 | 24.10 | | | 25.31 |
| | 199.0 | 24.38 | | | 25.59 |
| | 213.0 | 24.63 | | | 25.84 |
| | 227.1 | 24.73 | | | 25.94 |
| | 241.1 | 25.12 | | | 26.33 |
| | 255.2 | 25.70 | | | 26.91 |
| | 269.2 | 25.86 | | | 27.07 |
| | 283.2 | 26.44 | | | 27.65 |
| | 297.3 | 26.73 | | | 27.94 |

Table 3. Luminosity and Color Profiles--<u>Continued</u>

| | $\sqrt{ab}$ | $\mu_R$ | U-R | $B_3$-R | $\mu_B$ |
|---|---|---|---|---|---|
| UGC 04841 | 1.2 | 20.97 | 1.68 | | 22.52 |
| (b/a=0.76) | 3.4 | 21.27 | 1.47 | | 22.68 |
| | 5.7 | 21.44 | 1.39 | | 22.80 |
| | 8.0 | 21.61 | 1.35 | | 22.94 |
| | 10.3 | 21.73 | 1.41 | | 23.10 |
| | 12.6 | 21.85 | 1.29 | | 23.14 |
| | 14.9 | 21.94 | 1.14 | | 23.14 |
| | 17.2 | 22.09 | 1.06 | | 23.24 |
| | 19.5 | 22.28 | 1.06 | | 23.43 |
| | 21.8 | 22.40 | 1.11 | | 23.58 |
| | 24.1 | 22.49 | 1.10 | | 23.66 |
| | 26.4 | 22.59 | 1.06 | | 23.74 |
| | 28.7 | 22.62 | 1.07 | | 23.78 |
| | 31.0 | 22.67 | 1.15 | | 23.88 |
| | 33.3 | 22.75 | 0.99 | | 23.85 |
| | 35.6 | 22.82 | 1.04 | | 23.95 |
| | 37.9 | 22.86 | 1.04 | | 23.99 |
| | 40.2 | 22.93 | 1.04 | | 24.07 |
| | 42.4 | 23.01 | 1.03 | | 24.14 |
| | 44.7 | 23.11 | 1.07 | | 24.26 |
| | 47.0 | 23.17 | 1.07 | | 24.33 |
| | 49.3 | 23.24 | 1.06 | | 24.39 |
| | 51.6 | 23.33 | 1.05 | | 24.47 |
| | 53.9 | 23.37 | 1.02 | | 24.49 |
| | 56.2 | 23.43 | 1.03 | | 24.56 |
| | 58.5 | 23.48 | 0.97 | | 24.57 |
| | 60.8 | 23.55 | 0.99 | | 24.65 |
| | 63.1 | 23.59 | 0.98 | | 24.69 |
| | 65.4 | 23.65 | 1.01 | | 24.77 |

Table 3. Luminosity and Color Profiles--<u>Continued</u>

| | $\sqrt{ab}$ | $\mu_R$ | U-R | $B_3$-R | $\mu_B$ |
|---|---|---|---|---|---|
| | 70.0 | 23.81 | 0.91 | | 24.86 |
| | 76.9 | 24.05 | 0.88 | | 25.08 |
| | 83.7 | 24.39 | 0.89 | | 25.43 |
| | 90.6 | 24.74 | 0.84 | | 25.75 |
| | 97.5 | 25.01 | 0.79 | | 25.99 |
| | 104.4 | 25.29 | 0.72 | | 26.22 |
| | 111.3 | 25.62 | 0.67 | | 26.52 |
| | 118.2 | 25.91 | 0.73 | | 26.85 |
| <u>UGC 04922</u> | 1.5 | 20.92 | | | 22.15 |
| <u>(b/a=0.47)</u> | 2.9 | 21.09 | | | 22.32 |
| | 4.4 | 21.30 | | | 22.53 |
| | 5.8 | 21.49 | | | 22.72 |
| | 7.3 | 21.68 | | | 22.91 |
| | 8.8 | 21.78 | | | 23.01 |
| | 10.2 | 21.91 | | | 23.14 |
| | 13.1 | 22.07 | | | 23.30 |
| | 17.5 | 22.31 | | | 23.54 |
| | 21.9 | 22.57 | | | 23.80 |
| | 26.3 | 22.78 | | | 24.01 |
| | 30.6 | 22.94 | | | 24.17 |
| | 35.0 | 23.10 | | | 24.33 |
| | 39.4 | 23.27 | | | 24.50 |
| | 43.8 | 23.44 | | | 24.67 |
| | 48.1 | 23.67 | | | 24.90 |
| | 52.5 | 23.95 | | | 25.18 |
| | 56.9 | 24.04 | | | 25.27 |
| | 61.3 | 24.22 | | | 25.45 |
| | 65.6 | 24.60 | | | 25.83 |

Table 3. Luminosity and Color Profiles--<u>Continued</u>

|  | $\sqrt{ab}$ | $\mu_R$ | U-R | $B_3$-R | $\mu_B$ |
|---|---|---|---|---|---|
|  | 70.0 | 24.99 |  |  | 26.22 |
|  | 74.4 | 25.20 |  |  | 26.43 |
|  | 78.8 | 25.84 |  |  | 27.07 |
|  | 83.1 | 25.83 |  |  | 27.06 |
| <u>NGC 3913</u> <u>(b/a=1</u>.00) | 1.0 | 19.09 | 1.54 |  | 20.55 |
|  | 3.0 | 19.56 | 1.42 |  | 20.94 |
|  | 5.0 | 20.12 | 1.36 |  | 21.46 |
|  | 7.0 | 20.53 | 1.38 |  | 21.88 |
|  | 9.0 | 20.82 | 1.34 |  | 22.15 |
|  | 11.0 | 21.03 | 1.26 |  | 22.31 |
|  | 13.0 | 21.20 | 1.20 |  | 22.44 |
|  | 15.0 | 21.37 | 1.14 |  | 22.57 |
|  | 17.0 | 21.58 | 1.11 |  | 22.76 |
|  | 19.0 | 21.77 | 1.14 |  | 22.97 |
|  | 21.0 | 22.03 | 1.10 |  | 23.20 |
|  | 23.0 | 22.18 | 1.08 |  | 23.34 |
|  | 25.0 | 22.32 | 1.01 |  | 23.44 |
|  | 27.0 | 22.40 | 1.02 |  | 23.52 |
|  | 29.0 | 22.50 | 1.01 |  | 23.62 |
|  | 31.0 | 22.62 | 1.00 |  | 23.73 |
|  | 33.0 | 22.78 | 1.03 |  | 23.91 |
|  | 35.0 | 22.91 | 1.11 |  | 24.09 |
|  | 37.0 | 23.03 | 1.15 |  | 24.24 |
|  | 39.0 | 23.12 | 1.10 |  | 24.29 |
|  | 41.0 | 23.20 | 1.09 |  | 24.37 |
|  | 43.0 | 23.28 | 1.13 |  | 24.47 |
|  | 45.0 | 23.33 | 1.16 |  | 24.54 |
|  | 49.0 | 23.50 | 1.04 |  | 24.64 |

Table 3. Luminosity and Color Profiles--<u>Continued</u>

| | $\sqrt{ab}$ | $\mu_R$ | U-R | $B_3$-R | $\mu_B$ |
|---|---|---|---|---|---|
| | 55.0 | 23.76 | 0.93 | | 24.83 |
| | 61.0 | 23.85 | 0.94 | | 24.92 |
| | 67.0 | 24.01 | 0.93 | | 25.08 |
| | 73.0 | 24.35 | 0.94 | | 25.42 |
| | 79.0 | 24.67 | 0.95 | | 25.75 |
| | 85.0 | 25.03 | 0.92 | | 26.09 |
| | 91.0 | 25.40 | 0.91 | | 26.45 |
| | 97.0 | 25.97 | 0.75 | | 26.92 |
| | 103.0 | 26.58 | 0.66 | | 27.47 |
| <u>UGC 06922</u> | 1.2 | 20.03 | 1.52 | | 21.47 |
| <u>(b/a=0.70)</u> | 3.6 | 20.40 | 1.44 | | 21.79 |
| | 6.0 | 20.85 | 1.40 | | 22.22 |
| | 8.4 | 21.30 | 1.36 | | 22.64 |
| | 10.8 | 21.65 | 1.32 | | 22.96 |
| | 13.2 | 21.94 | 1.20 | | 23.18 |
| | 15.5 | 22.24 | 1.15 | | 23.45 |
| | 17.9 | 22.45 | 1.05 | | 23.59 |
| | 20.3 | 22.72 | 1.07 | | 23.87 |
| | 22.7 | 23.00 | 1.12 | | 24.19 |
| | 25.1 | 23.20 | 1.09 | | 24.37 |
| | 27.5 | 23.34 | 1.06 | | 24.49 |
| | 29.9 | 23.48 | 1.01 | | 24.60 |
| | 32.3 | 23.67 | 1.04 | | 24.81 |
| | 34.7 | 23.87 | 0.93 | | 24.94 |
| | 37.1 | 24.04 | 0.96 | | 25.12 |
| | 39.4 | 24.18 | 0.96 | | 25.26 |
| | 41.8 | 24.36 | 0.91 | | 25.41 |
| | 44.2 | 24.46 | 0.88 | | 25.49 |

Table  3.  Luminosity and Color Profiles--<u>Continued</u>

| | $\sqrt{ab}$ | $\mu_R$ | U-R | $B_3$-R | $\mu_B$ |
|---|---|---|---|---|---|
| | 49.0 | 24.67 | 0.95 | | 25.75 |
| | 56.2 | 25.00 | 0.87 | | 26.03 |
| | 63.4 | 25.53 | 0.68 | | 26.44 |
| | 70.5 | 26.09 | 0.67 | | 26.99 |
| | 77.7 | 26.67 | 0.58 | | 27.51 |
| | 84.9 | 27.05 | 0.60 | | 27.90 |
| <u>DDO 102</u> | 1.0 | 22.06 | 1.07 | | 23.21 |
| (b/a=1.00) | 3.0 | 22.21 | 1.11 | | 23.39 |
| | 5.0 | 22.42 | 1.20 | | 23.66 |
| | 7.0 | 22.60 | 1.12 | | 23.79 |
| | 9.0 | 22.85 | 1.09 | | 24.02 |
| | 13.0 | 23.14 | 1.27 | | 24.42 |
| | 19.0 | 23.71 | 1.20 | | 24.95 |
| | 25.0 | 24.09 | 1.17 | | 25.31 |
| | 31.0 | 24.37 | 1.02 | | 25.49 |
| | 37.0 | 24.59 | 0.84 | | 25.60 |
| | 43.0 | 24.88 | 0.92 | | 25.94 |
| | 49.0 | 25.12 | 0.77 | | 26.08 |
| | 55.0 | 25.48 | 0.58 | | 26.32 |
| | 61.0 | 25.69 | 0.58 | | 26.53 |
| | 67.0 | 25.92 | 0.78 | | 26.89 |
| | 73.0 | 26.26 | 0.71 | | 27.18 |
| | 79.0 | 26.49 | 0.61 | | 27.35 |
| <u>UGC 06983</u> | 1.2 | 20.24 | 1.02 | 1.02 | 21.42 |
| (b/a=0.67) | 3.7 | 20.68 | 1.13 | 1.03 | 21.88 |
| | 6.1 | 21.17 | 1.34 | 1.22 | 22.59 |
| | 8.6 | 21.42 | 1.29 | 1.30 | 22.90 |

Table  3.  Luminosity and Color Profiles--<u>Continued</u>

| | $\sqrt{ab}$ | $\mu_R$ | U-R | $B_3$-R | $\mu_B$ |
|---|---|---|---|---|---|
| | 11.0 | 21.71 | 1.20 | 1.12 | 23.00 |
| | 13.4 | 21.92 | 1.22 | 1.02 | 23.12 |
| | 15.9 | 22.05 | 1.20 | 1.05 | 23.28 |
| | 18.3 | 22.16 | 1.15 | 1.05 | 23.38 |
| | 20.8 | 22.26 | 1.12 | 1.03 | 23.46 |
| | 23.2 | 22.33 | 1.12 | 1.00 | 23.50 |
| | 25.7 | 22.41 | 1.09 | 0.99 | 23.57 |
| | 28.1 | 22.56 | 1.03 | 0.96 | 23.68 |
| | 30.5 | 22.57 | 1.05 | 0.97 | 23.70 |
| | 35.4 | 22.77 | 0.94 | 0.91 | 23.83 |
| | 42.8 | 23.07 | 0.90 | 0.90 | 24.11 |
| | 50.1 | 23.37 | 0.88 | 0.88 | 24.39 |
| | 57.4 | 23.57 | 0.95 | 0.91 | 24.63 |
| | 64.8 | 23.64 | 0.87 | 0.84 | 24.62 |
| | 72.1 | 23.98 | 0.83 | 0.85 | 24.96 |
| | 79.4 | 24.38 | 1.14 | 0.96 | 25.51 |
| | 86.7 | 24.69 | 1.14 | 0.94 | 25.81 |
| | 94.1 | 25.08 | 1.09 | 0.82 | 26.07 |
| | 101.4 | 25.44 | 1.10 | 0.83 | 26.44 |
| | 108.7 | 25.89 | 1.17 | 0.76 | 26.82 |
| <u>NGC 4411A</u> | 1.0 | 20.39 | 1.17 | | 21.61 |
| <u>(b/a=1.00)</u> | 3.0 | 20.72 | 1.21 | | 21.96 |
| | 5.0 | 21.03 | 1.28 | | 22.32 |
| | 7.0 | 21.13 | 1.26 | | 22.41 |
| | 9.0 | 21.35 | 1.31 | | 22.66 |
| | 11.0 | 21.50 | 1.19 | | 22.73 |
| | 13.0 | 21.57 | 1.15 | | 22.78 |
| | 15.0 | 21.68 | 1.15 | | 22.89 |
| | 17.0 | 21.85 | 1.11 | | 23.03 |

Table 3. Luminosity and Color Profiles--<u>Continued</u>

| | $\sqrt{ab}$ | $\mu_R$ | U−R | $B_3$−R | $\mu_B$ |
|---|---|---|---|---|---|
| | 19.0 | 21.99 | 1.16 | | 23.20 |
| | 21.0 | 22.05 | 1.10 | | 23.22 |
| | 23.0 | 22.14 | 1.04 | | 23.28 |
| | 25.0 | 22.22 | 1.05 | | 23.36 |
| | 27.0 | 22.33 | 1.02 | | 23.45 |
| | 29.0 | 22.44 | 0.93 | | 23.51 |
| | 31.0 | 22.59 | 1.02 | | 23.71 |
| | 35.0 | 22.78 | 1.00 | | 23.89 |
| | 41.0 | 23.09 | 1.13 | | 24.28 |
| | 47.0 | 23.32 | 1.16 | | 24.53 |
| | 53.0 | 23.54 | 1.25 | | 24.81 |
| | 59.0 | 23.84 | 1.29 | | 25.14 |
| | 65.0 | 24.14 | 1.34 | | 25.47 |
| | 71.0 | 24.45 | 1.38 | | 25.80 |
| | 77.0 | 24.82 | 1.51 | | 26.26 |
| | 83.0 | 25.14 | 1.59 | | 26.63 |
| | 89.0 | 25.58 | 1.41 | | 26.95 |
| | 95.0 | 25.94 | 1.82 | | 27.57 |
| <u>NGC 4411B</u> <br> (b/a=1.00) | 1.0 | 19.73 | 1.49 | | 21.15 |
| | 3.0 | 20.40 | 1.49 | | 21.82 |
| | 5.0 | 20.73 | 1.43 | | 22.12 |
| | 7.0 | 20.93 | 1.33 | | 22.25 |
| | 9.0 | 21.12 | 1.26 | | 22.40 |
| | 11.0 | 21.30 | 1.25 | | 22.57 |
| | 13.0 | 21.41 | 1.31 | | 22.72 |
| | 15.0 | 21.46 | 1.17 | | 22.68 |
| | 17.0 | 21.62 | 1.09 | | 22.79 |
| | 19.0 | 21.73 | 1.18 | | 22.96 |

Table 3. Luminosity and Color Profiles--<u>Continued</u>

| | $\sqrt{ab}$ | $\mu_R$ | U-R | $B_3$-R | $\mu_B$ |
|---|---|---|---|---|---|
| | 21.0 | 21.80 | 1.14 | | 23.00 |
| | 23.0 | 21.87 | 1.10 | | 23.04 |
| | 25.0 | 21.93 | 1.06 | | 23.08 |
| | 27.0 | 22.07 | 1.05 | | 23.21 |
| | 29.0 | 22.19 | 1.11 | | 23.37 |
| | 31.0 | 22.33 | 1.07 | | 23.48 |
| | 35.0 | 22.48 | 1.06 | | 23.63 |
| | 41.0 | 22.71 | 1.07 | | 23.86 |
| | 47.0 | 22.94 | 1.11 | | 24.12 |
| | 53.0 | 23.05 | 1.06 | | 24.20 |
| | 59.0 | 23.18 | 1.12 | | 24.37 |
| | 65.0 | 23.43 | 1.14 | | 24.63 |
| | 71.0 | 23.61 | 1.12 | | 24.80 |
| | 77.0 | 23.87 | 1.11 | | 25.05 |
| | 83.0 | 24.17 | 1.27 | | 25.45 |
| | 89.0 | 24.61 | 1.49 | | 26.03 |
| | 95.0 | 25.06 | 1.69 | | 26.61 |
| | 101.0 | 25.44 | 1.68 | | 26.99 |
| | 107.0 | 25.88 | 1.70 | | 27.44 |
| <u>UGC 07557</u> <u>(b/a=0.80)</u> | 1.1 | 21.12 | 1.10 | | 22.29 |
| | 3.4 | 21.36 | 1.13 | | 22.55 |
| | 5.6 | 21.63 | 1.14 | | 22.83 |
| | 7.8 | 21.90 | 1.10 | | 23.07 |
| | 10.1 | 22.04 | 1.00 | | 23.15 |
| | 12.3 | 22.23 | 0.96 | | 23.31 |
| | 14.5 | 22.41 | 1.00 | | 23.52 |
| | 16.8 | 22.51 | 0.85 | | 23.52 |
| | 19.0 | 22.59 | 0.86 | | 23.61 |

Table 3. Luminosity and Color Profiles--<u>Continued</u>

| | $\sqrt{ab}$ | $\mu_R$ | U-R | $B_3$-R | $\mu_B$ |
|---|---|---|---|---|---|
| | 21.2 | 22.64 | 0.77 | | 23.60 |
| | 23.5 | 22.78 | 0.85 | | 23.79 |
| | 25.7 | 22.87 | 0.91 | | 23.92 |
| | 28.0 | 22.99 | 0.87 | | 24.02 |
| | 30.2 | 22.98 | 0.95 | | 24.06 |
| | 34.7 | 23.18 | 0.81 | | 24.17 |
| | 41.4 | 23.40 | 0.83 | | 24.40 |
| | 48.1 | 23.54 | 0.76 | | 24.50 |
| | 54.8 | 23.68 | 0.77 | | 24.64 |
| | 61.5 | 23.98 | 0.72 | | 24.91 |
| | 68.2 | 24.19 | 0.72 | | 25.12 |
| | 74.9 | 24.50 | 0.65 | | 25.39 |
| | 81.6 | 24.95 | 0.50 | | 25.74 |
| | 88.3 | 25.25 | 0.54 | | 26.07 |
| | 95.0 | 25.51 | 0.57 | | 26.34 |
| | 101.7 | 25.79 | 0.68 | | 26.70 |
| | 108.5 | 26.33 | 0.83 | | 27.33 |
| NGC 4517A <br> (b/a=0.62) | 1.3 | 20.80 | 1.27 | 1.12 | 22.11 |
| | 3.8 | 20.97 | 1.24 | 1.09 | 22.24 |
| | 6.4 | 21.31 | 1.21 | 1.01 | 22.50 |
| | 8.9 | 21.51 | 1.26 | 1.07 | 22.77 |
| | 11.4 | 21.68 | 1.17 | 1.05 | 22.91 |
| | 14.0 | 21.88 | 1.23 | 1.04 | 23.10 |
| | 16.5 | 22.04 | 1.20 | 1.02 | 23.24 |
| | 19.1 | 22.13 | 1.14 | 1.03 | 23.33 |
| | 21.6 | 22.23 | 1.20 | 0.99 | 23.40 |
| | 24.1 | 22.33 | 1.09 | 0.96 | 23.46 |
| | 26.7 | 22.46 | 1.11 | 0.95 | 23.58 |
| | 29.2 | 22.57 | 1.06 | 0.93 | 23.66 |

Table  3.   Luminosity and Color Profiles--<u>Continued</u>

| | $\sqrt{ab}$ | $\mu_R$ | U-R | $B_3$-R | $\mu_B$ |
|---|---|---|---|---|---|
| | 34.3 | 22.69 | 1.02 | 0.92 | 23.77 |
| | 41.9 | 22.86 | 0.96 | 0.86 | 23.87 |
| | 49.5 | 23.04 | 0.95 | 0.88 | 24.07 |
| | 57.2 | 23.29 | 0.86 | 0.80 | 24.23 |
| | 64.8 | 23.57 | 0.90 | 0.83 | 24.54 |
| | 72.4 | 23.90 | 0.91 | 0.80 | 24.85 |
| | 80.0 | 24.17 | 0.89 | 0.81 | 25.12 |
| | 87.6 | 24.39 | 0.90 | 0.81 | 25.35 |
| | 95.3 | 24.66 | 0.99 | 0.84 | 25.65 |
| | 102.9 | 25.12 | 1.11 | 0.85 | 26.14 |
| | 110.5 | 25.57 | 1.34 | 0.91 | 26.67 |
| | 118.1 | 26.05 | 1.42 | 0.99 | 27.24 |
| DDO 144 | 1.1 | 20.65 | 1.01 | | 21.77 |
| (b/a=0.80) | 3.4 | 21.02 | 1.02 | | 22.14 |
| | 5.6 | 21.28 | 1.15 | | 22.49 |
| | 7.8 | 21.45 | 0.88 | | 22.48 |
| | 10.1 | 21.69 | 0.90 | | 22.74 |
| | 12.3 | 21.98 | 0.94 | | 23.05 |
| | 14.5 | 22.15 | 1.00 | | 23.26 |
| | 16.8 | 22.23 | 0.93 | | 23.30 |
| | 19.0 | 22.41 | 0.94 | | 23.48 |
| | 21.2 | 22.53 | 1.02 | | 23.65 |
| | 23.5 | 22.58 | 1.04 | | 23.72 |
| | 25.7 | 22.62 | 0.96 | | 23.70 |
| | 28.0 | 22.66 | 1.13 | | 23.85 |
| | 30.2 | 22.77 | 1.11 | | 23.95 |
| | 34.7 | 22.98 | 0.99 | | 24.08 |
| | 41.4 | 23.19 | 0.91 | | 24.24 |

Table 3. Luminosity and Color Profiles--<u>Continued</u>

| | $\sqrt{ab}$ | $\mu_R$ | U-R | $B_3$-R | $\mu_B$ |
|---|---|---|---|---|---|
| | 48.1 | 23.38 | 0.90 | | 24.43 |
| | 54.8 | 23.50 | 0.90 | | 24.55 |
| | 61.5 | 23.69 | 0.82 | | 24.68 |
| | 68.2 | 23.96 | 0.85 | | 24.97 |
| | 74.9 | 24.50 | 1.02 | | 25.62 |
| | 81.6 | 25.01 | 1.02 | | 26.13 |
| | 88.3 | 25.53 | 0.97 | | 26.62 |
| | 95.0 | 26.55 | 0.65 | | 27.44 |
| <u>DDO 142</u> (b/a=0.86) | 1.1 | 20.29 | 1.51 | 1.12 | 21.62 |
| | 3.2 | 20.90 | 1.60 | 1.22 | 22.34 |
| | 5.4 | 21.11 | 1.66 | 1.24 | 22.58 |
| | 7.6 | 21.21 | 1.60 | 1.23 | 22.66 |
| | 9.7 | 21.30 | 1.54 | 1.19 | 22.71 |
| | 11.9 | 21.38 | 1.52 | 1.18 | 22.78 |
| | 14.0 | 21.49 | 1.48 | 1.15 | 22.85 |
| | 16.2 | 21.61 | 1.48 | 1.14 | 22.96 |
| | 18.3 | 21.75 | 1.38 | 1.12 | 23.07 |
| | 20.5 | 21.84 | 1.35 | 1.14 | 23.18 |
| | 22.6 | 21.93 | 1.32 | 1.12 | 23.24 |
| | 24.8 | 22.00 | 1.35 | 1.08 | 23.28 |
| | 27.0 | 22.09 | 1.25 | 1.04 | 23.31 |
| | 29.1 | 22.18 | 1.24 | 1.05 | 23.41 |
| | 31.3 | 22.27 | 1.21 | 1.05 | 23.50 |
| | 35.6 | 22.52 | 1.16 | 1.02 | 23.71 |
| | 42.1 | 22.80 | 1.12 | 1.00 | 23.97 |
| | 48.5 | 23.05 | 1.10 | 0.99 | 24.21 |
| | 55.0 | 23.24 | 1.11 | 0.98 | 24.39 |
| | 61.5 | 23.42 | 0.99 | 0.91 | 24.48 |

Table 3. Luminosity and Color Profiles--<u>Continued</u>

| | $\sqrt{ab}$ | $\mu_R$ | U-R | $B_3$-R | $\mu_B$ |
|---|---|---|---|---|---|
| | 67.9 | 23.65 | 0.97 | 0.92 | 24.72 |
| | 74.4 | 23.85 | 0.96 | 0.92 | 24.92 |
| | 80.9 | 24.00 | 0.83 | 0.89 | 25.03 |
| | 87.3 | 24.13 | 0.80 | 0.86 | 25.12 |
| | 93.8 | 24.39 | 0.86 | 0.85 | 25.38 |
| | 100.3 | 24.64 | 0.80 | 0.84 | 25.61 |
| | 106.8 | 24.88 | 0.79 | 0.80 | 25.81 |
| | 113.2 | 25.08 | 0.82 | 0.80 | 26.02 |
| | 119.7 | 25.20 | 0.86 | 0.87 | 26.21 |
| | 126.2 | 25.69 | 0.82 | 0.81 | 26.64 |
| | 132.6 | 26.38 | 0.79 | 0.70 | 27.21 |
| <u>DDO 146</u> | 1.2 | 21.27 | 1.70 | 1.38 | 22.89 |
| (b/a=0.71) | 3.6 | 21.38 | 1.42 | 1.16 | 22.74 |
| | 5.9 | 21.37 | 1.42 | 1.20 | 22.77 |
| | 8.3 | 21.47 | 1.45 | 1.22 | 22.90 |
| | 10.7 | 21.60 | 1.43 | 1.18 | 22.99 |
| | 13.1 | 21.71 | 1.46 | 1.21 | 23.13 |
| | 15.4 | 21.80 | 1.48 | 1.23 | 23.24 |
| | 17.8 | 21.93 | 1.43 | 1.20 | 23.34 |
| | 20.2 | 22.03 | 1.43 | 1.18 | 23.42 |
| | 22.6 | 22.10 | 1.42 | 1.20 | 23.50 |
| | 24.9 | 22.18 | 1.42 | 1.19 | 23.57 |
| | 27.3 | 22.27 | 1.36 | 1.21 | 23.68 |
| | 29.7 | 22.36 | 1.35 | 1.11 | 23.67 |
| | 32.0 | 22.41 | 1.30 | 1.13 | 23.73 |
| | 36.8 | 22.53 | 1.21 | 1.10 | 23.81 |
| | 43.9 | 22.69 | 1.15 | 1.08 | 23.94 |
| | 51.0 | 22.94 | 1.21 | 1.11 | 24.23 |
| | 58.2 | 23.18 | 1.28 | 1.13 | 24.50 |

Table  3.  Luminosity and Color Profiles--<u>Continued</u>

| | $\sqrt{ab}$ | $\mu_R$ | U-R | $B_3$-R | $\mu_B$ |
|---|---|---|---|---|---|
| | 65.3 | 23.30 | 1.30 | 1.17 | 24.66 |
| | 72.4 | 23.48 | 1.30 | 1.14 | 24.81 |
| | 79.5 | 23.67 | 1.31 | 1.16 | 25.02 |
| | 86.6 | 23.96 | 1.28 | 1.21 | 25.36 |
| | 93.8 | 24.33 | 1.40 | 1.25 | 25.78 |
| | 100.9 | 24.72 | 1.41 | 1.28 | 26.20 |
| | 108.0 | 25.07 | 1.32 | 1.29 | 26.55 |
| | 115.1 | 25.50 | 1.21 | 1.26 | 26.94 |
| | 122.2 | 25.92 | 1.02 | 1.14 | 27.22 |
| | 129.4 | 26.31 | 1.16 | 1.10 | 27.58 |
| | 136.5 | 26.75 | 1.01 | 1.04 | 27.95 |
| | 143.6 | 27.13 | 1.00 | 0.90 | 28.19 |
| <u>UGC A0333</u><br>(b/a=1.00) | 1.0 | 21.13 | | | 22.17 |
| | 3.0 | 21.30 | | | 22.34 |
| | 5.0 | 21.61 | | | 22.65 |
| | 7.0 | 21.89 | | | 22.93 |
| | 9.0 | 22.15 | | | 23.19 |
| | 11.0 | 22.35 | | | 23.39 |
| | 13.0 | 22.54 | | | 23.58 |
| | 15.0 | 22.69 | | | 23.73 |
| | 17.0 | 22.80 | | | 23.84 |
| | 19.0 | 22.92 | | | 23.96 |
| | 21.0 | 23.07 | | | 24.11 |
| | 25.0 | 23.30 | | | 24.34 |
| | 31.0 | 23.58 | | | 24.62 |
| | 37.0 | 23.67 | | | 24.71 |
| | 43.0 | 23.87 | | | 24.91 |
| | 49.0 | 24.12 | | | 25.16 |
| | 55.0 | 24.52 | | | 25.56 |

Table 3. Luminosity and Color Profiles--<u>Continued</u>

| | $\sqrt{ab}$ | $\mu_R$ | U-R | $B_3$-R | $\mu_B$ |
|---|---|---|---|---|---|
| | 61.0 | 24.94 | | | 25.98 |
| | 67.0 | 25.34 | | | 26.38 |
| | 73.0 | 25.26 | | | 26.30 |
| | 79.0 | 26.08 | | | 27.12 |
| <u>NGC 5774</u> | 1.2 | 19.79 | 1.13 | 1.16 | 21.12 |
| (b/a=0.75) | 3.5 | 19.94 | 1.29 | 1.23 | 21.36 |
| | 5.8 | 20.44 | 1.14 | 1.02 | 21.63 |
| | 8.1 | 20.62 | 1.07 | 1.03 | 21.81 |
| | 10.4 | 20.76 | 1.23 | 1.15 | 22.09 |
| | 12.7 | 21.03 | 1.18 | 1.04 | 22.25 |
| | 15.0 | 21.32 | 1.10 | 0.92 | 22.41 |
| | 17.3 | 21.46 | 1.26 | 0.99 | 22.64 |
| | 19.6 | 21.60 | 1.15 | 1.00 | 22.77 |
| | 21.9 | 21.75 | 1.12 | 0.97 | 22.89 |
| | 24.3 | 21.87 | 1.08 | 0.98 | 23.02 |
| | 26.6 | 22.01 | 1.10 | 0.95 | 23.13 |
| | 28.9 | 22.12 | 1.00 | 0.94 | 23.22 |
| | 31.2 | 22.23 | 1.13 | 0.92 | 23.32 |
| | 33.5 | 22.37 | 1.23 | 0.92 | 23.47 |
| | 35.8 | 22.55 | 1.09 | 0.93 | 23.65 |
| | 38.1 | 22.68 | 1.15 | 0.94 | 23.79 |
| | 42.7 | 22.88 | 1.15 | 0.87 | 23.92 |
| | 49.7 | 23.03 | 1.15 | 0.90 | 24.10 |
| | 56.6 | 23.15 | 1.18 | 0.90 | 24.23 |
| | 63.5 | 23.37 | 1.08 | 0.87 | 24.41 |
| | 70.4 | 23.55 | 1.18 | 0.96 | 24.69 |
| | 77.4 | 23.83 | 1.31 | 1.01 | 25.03 |
| | 84.3 | 24.18 | 1.36 | 0.99 | 25.37 |

Table 3. Luminosity and Color Profiles--<u>Continued</u>

| | $\sqrt{ab}$ | $\mu_R$ | U-R | $B_3$-R | $\mu_B$ |
|---|---|---|---|---|---|
| | 91.2 | 24.49 | 1.47 | 1.07 | 25.77 |
| | 98.2 | 24.90 | 1.76 | 1.11 | 26.25 |
| | 105.1 | 25.17 | 2.00 | 1.31 | 26.75 |
| | 112.0 | 25.52 | 1.92 | 1.25 | 27.03 |
| <u>UGC 11868</u> | 1.1 | 21.11 | | | 22.63 |
| (b/a=0.78) | 3.4 | 21.41 | | | 22.93 |
| | 5.7 | 21.58 | | | 23.10 |
| | 7.9 | 21.74 | | | 23.26 |
| | 10.2 | 21.92 | | | 23.44 |
| | 12.5 | 22.01 | | | 23.53 |
| | 14.7 | 22.17 | | | 23.69 |
| | 17.0 | 22.23 | | | 23.75 |
| | 19.3 | 22.37 | | | 23.89 |
| | 21.5 | 22.46 | | | 23.98 |
| | 23.8 | 22.54 | | | 24.06 |
| | 26.0 | 22.65 | | | 24.17 |
| | 28.3 | 22.78 | | | 24.30 |
| | 30.6 | 22.83 | | | 24.35 |
| | 32.8 | 22.89 | | | 24.41 |
| | 35.1 | 22.99 | | | 24.51 |
| | 37.4 | 23.10 | | | 24.62 |
| | 39.6 | 23.19 | | | 24.71 |
| | 41.9 | 23.25 | | | 24.77 |
| | 44.2 | 23.35 | | | 24.87 |
| | 46.4 | 23.51 | | | 25.03 |
| | 48.7 | 23.58 | | | 25.10 |
| | 51.0 | 23.78 | | | 25.30 |
| | 53.2 | 23.92 | | | 25.44 |

Table 3. Luminosity and Color Profiles--<u>Continued</u>

| $\sqrt{ab}$ | $\mu_R$ | U-R | $B_3$-R | $\mu_B$ |
|---|---|---|---|---|
| 55.5 | 24.04 | | | 25.56 |
| 57.8 | 24.17 | | | 25.69 |
| 60.0 | 24.17 | | | 25.69 |
| 62.3 | 24.36 | | | 25.88 |
| 64.5 | 24.54 | | | 26.06 |
| 66.8 | 24.77 | | | 26.29 |
| 69.1 | 24.81 | | | 26.33 |
| 71.3 | 24.93 | | | 26.45 |
| 75.9 | 25.20 | | | 26.72 |
| 82.7 | 25.61 | | | 27.13 |
| 89.5 | 26.00 | | | 27.52 |
| 96.2 | 26.30 | | | 27.82 |
| 103.0 | 26.49 | | | 28.01 |

Most of the surface photometry data reduction was carried out using the interactive IPPS routines mentioned. In addition, a number of non-interactive programs were written to analyze the digital data. The most useful of these found the intensity values in small square rasters around a specified pixel. The COMTAL cursor was first used to read the coordinates of the desired spot on the picture. The program is similar in purpose to PHOT, but is more flexible. The intensity values are written to a disk file for further use.

For most galaxies, we obtained U and R plates. These colors provide a relatively long baseline in wavelength. The U plate emphasizes the young stellar population and the R the old. In order to estimate other colors from (U-R), we plotted all the UBVR colors against (U-R) and derived least-squares fits to all colors versus (U-R). This is necessary as most published models and analyses concern only UBV colors. This procedure yielded the following relations, which we will refer to as the color interpolation equations:

$$(U-B) = 0.38 \ (U-R) - 0.49 \qquad (8)$$

$$(B-V) = 0.38 \ (U-R) + 0.14 \qquad (9)$$

$$(V-R) = 0.24 \ (U-R) + 0.35. \qquad (10)$$

Figures 1-3 show plots of the color-color data. The rms
deviation of individual points from the mean line is about
0.08 magnitude for (U-B) and (B-V), 0.06 for (V-R). These
errors are larger than the observational errors, but not by
a large factor. Apparently (U-R) contains much the same
information as the other broad-band colors, at least for
this set of photometry restricted to LSB galaxies.

## 2.4 Infrared Photometry

We obtained infrared photometry of 14 LSB galaxies,
using the KPNO 1.3-m telescope and InSb detector system.
There were two motivations for these observations: (1) the
infrared magnitudes provide long-baseline colors useful in
studying the stellar populations in galaxies and (2) we
wished to see where the LSB galaxies fell in the H
magnitude-HI velocity width plane (Aaronson, Huchra and
Mould 1979), since one might expect the H mag-HI width re-
lation to be different for galaxies of low surface bright-
ness. Discussion of the second topic will be deferred
until a more complete calibration of the H magnitude-HI
velocity width correlation is available.

The galaxies were acquired as for the UBVR photom-
etry, by offsetting from nearby stars using a television
acquisition system. We observed 8 to 10 standard stars
each night from the list of Frogel et al. (1978). These
stars are on a magnitude system in which α Lyr has a
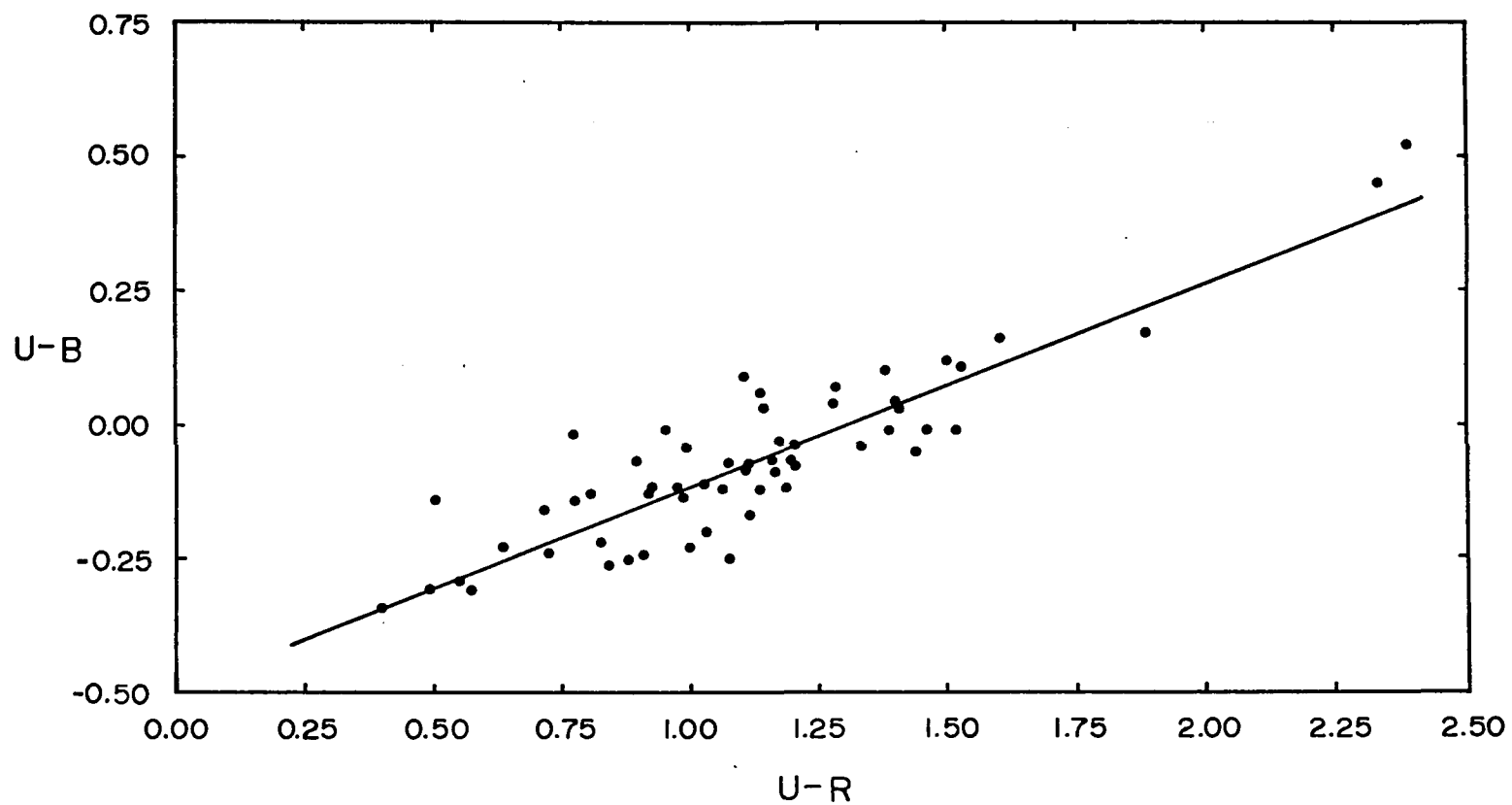
Figure 1.   (U-B) vs. (U-R) Color-color Plot.
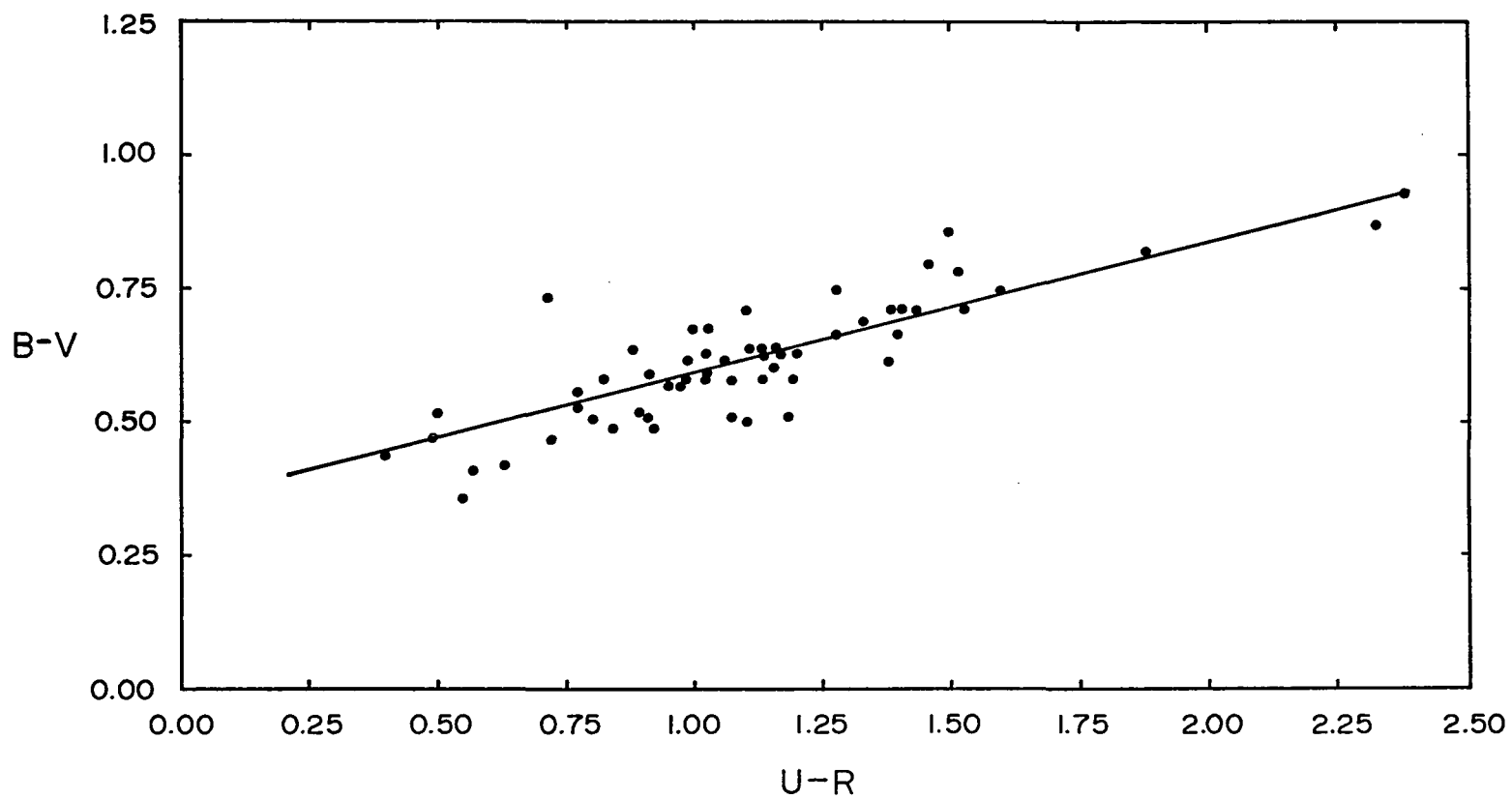
Figure 2. (B-V) vs. (U-R) Color-color Plot.
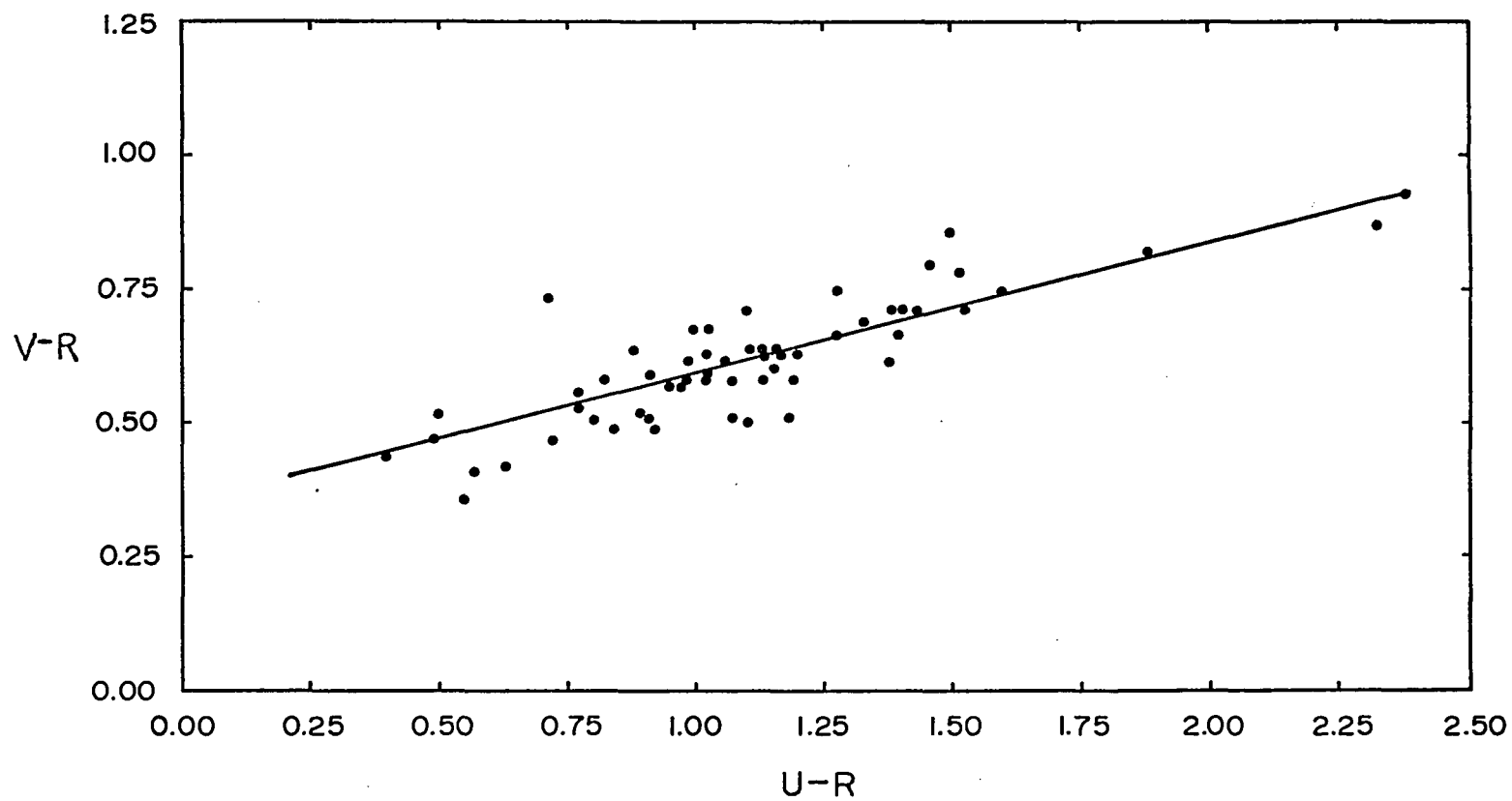
Figure 3. (V-R) vs. (U-R) Color-color Plot.

magnitude of 0.00 at all wavelengths. Most observations were made through an aperture of diameter 47 arcsec, with a very few made with a 33 arcsec diameter aperture. The 47 arcsec aperture provides a value of log A/D(0), the aperture size divided by the de Vaucouleurs diameter, near -0.6 for most of the galaxies in our sample. This aperture was chosen as this value of log A/D(0) is one of the standard aperture sizes used by Aaronson (1977). Internal errors were assigned to the measurements from the statistical fluctuations of repeated 10 or 20 second integrations. We checked these error estimates by observing a few galaxies on two or more nights to provide independent measurements. The assigned errors were found to be good estimates of the actual repeatibility measured by the independent measurements. Because of the low surface brightness nature of these galaxies, they required long total integration times. First priority was given to obtaining H magnitudes for a number of galaxies, therefore J and K magnitudes were measured for only a fraction of the sample.

Sky positions were chosen to be free of all stars on the Palomar Sky Survey. These regions were typically 250 to 300 arcsec from the galaxy. At this beam size/throw ratio, and aperture/galaxy size ratio, the correction for flux in the reference beam is $\leq$ 0.01 magnitude (Aaronson 1977), so no correction was applied. A few galaxies were

observed with sky positions at 150 to 250 arcsec. We used
the procedure of Aaronson (1977) to correct for the flux in
the reference beam for these galaxies. This correction was
always < 0.05 magnitude.

One problem affecting these observations is the
variation of the response across the aperture caused by the
optics necessary to image the signal on the small detector.
We mapped the relative response across the aperture by driv-
ing a bright star across the aperture and recording the out-
put of the PAR amplifier on a strip chart recorder. Using
these cuts across the aperture, we made a model of the
relative response across the beam. We then convolved this
model beam with the digital image of the R photograph of
each galaxy, using the IPPS system, and integrated the
total flux in the convolved image. This flux was compared
to the flux measured through a uniform aperture of the nom-
inal diameter. The differences of these two measurements,
in magnitudes, were used to correct the observed infrared
magnitudes to magnitudes that would have been observed
through a perfect aperture of the nominal size. This
scheme was tested by observing the EO galaxy NGC 3379 which
was observed by Frogel et al. (1978). We first corrected
the Frogel et al. K magnitude to our aperture size (a very
small extrapolation) by using their standard growth curve.
The difference between this magnitude and our raw,

uncorrected K magnitude was 0.10 magnitude. A simple model of the light distribution of NGC 3379 was created, using the de Vaucouleurs $r^{\frac{1}{4}}$ law and the photometric parameters for NGC 3379 given by de Vaucouleurs (1953). Our procedure to measure the aperture correction yielded a correction of 0.10 magnitude using this artificial galaxy image, confirming the basic soundness of the procedure. The typical correction for the spiral galaxy magnitudes was 0.15 magnitudes. This value is larger than that computed for NGC 3379. This is expected, since the spirals do not have their light so strongly concentrated towards the center of the aperture where the relative response is greatest. We found no variation of the beam profile in the different infrared colors.

By far the largest error in the infrared magnitudes was simply the statistical uncertainty in the signal measurement. This produced a typical error of 0.05 magnitude. Observations of four bright galaxies observed by Frogel et al. (1978) showed very good agreement between our measured infrared colors and theirs, with a mean difference of 0.01 magnitude. This indicates that our measurements are on the same color system as theirs. We could not measure the accuracy of the beam correction procedure on any other galaxy than NGC 3379, as there was not sufficient information to create artificial galaxy images.

The results of the infrared photometry are listed in Table 4. The first column gives the measuring aperture diameter in arcsec, the second the H magnitude, and the remaining columns the (J-K), (H-K), (V-K) and (U-V) colors. The U and V magnitudes were derived from the plate material, using PHOT magnitudes for the appropriate aperture size, and the color interpolation formula. For a few galaxies, with only an R plate available, the U and V magnitudes were derived from the R PHOT magnitude and colors from the photoelectric photometry. All colors have been corrected for Galactic reddening and redshift following the precepts of Aaronson (1977). These corrections are very small, the largest being 0.03 magnitude.

For some of the galaxies in Table 4, an (H-K) color of 0.23 was assumed, in order to derive a K magnitude when only an H magnitude was measured.

## 2.5 HII Region Spectroscopy and Photometry

Measurements of the emission line ratios in the LSB spiral HII regions comes from two sources: (1) IIDS scans of individual HII regions obtained with the KPNO 2.1-m telescope and (2) the photographic spectra obtained for rotation curve study, described in detail in Section 2.6. The IIDS scans covered the spectral region from about 4500 Å to 7500 Å. The lines observed were [OIII] $\lambda\lambda$ 4959, 5007,

Table 4. UVJHK Photometry

| | Aperture | H | J-H | H-K[a] | J-K | V-K | U-V |
|---|---|---|---|---|---|---|---|
| UGC 04841 | 33".0 | 12.70 | 0.44 | 0.36 | 0.80 | 2.68 | 0.69 |
| UGC 04922 | 47.0 | 12.43 | 0.56 | 0.22 | 0.78 | 2.47 | 0.69 |
| UGC 06922 | 47.0 | 12.02 | 0.47 | 0.21 | 0.68 | 2.68 | 0.57 |
| NGC 4411B | 47.0 | 11.56 | 0.47 | 0.21 | 0.68 | 2.56 | 0.57 |
| NGC 4517A | 47.0 | 12.13 | 0.48 | 0.24 | 0.72 | 2.46 | 0.52 |
| NGC 5774 | 47.0 | 12.43 | 0.56 | 0.22 | 0.78 | 2.53 | 0.51 |
| UGC 06983 | 47.0 | 11.96 | | (0.23) | | 2.54 | 0.50 |
| UGC 07557 | 47.0 | 12.44 | | (0.23) | | 2.55 | 0.38 |
| DDO 144 | 47.0 | 12.41 | | (0.23) | | 2.48 | 0.38 |
| DDO 142 | 47.0 | 11.63 | | (0.23) | | 2.70 | 0.78 |
| DDO 146 | 47.0 | 12.00 | | (0.23) | | 2.59 | 0.71 |
| DDO 48 | 47.0 | 13.27 | | | | | |
| UGC 05633 | 47.0 | 12.59 | | | | | |
| UGC 06446 | 47.0 | 12.23 | | | | | |
| UGC 06554 | 47.0 | 11.53 | | | | | |
| DDO 128 | 47.0 | 13.00 | | | | | |
| MCG-2-33-15 | 47.0 | 11.90 | | | | | |
| DDO 203 | 47.0 | 12.16 | | | | | |

a. H-K values in parentheses are assumed, not measured.

Hβ, Hα, [SII] λλ 6717, 6731 in first order and [OII] λ 3727
in second order.  Because of the poor resolution of these
scans (~15 A full width at half maximum) the [NII] λλ 6548,
6584 lines are not cleanly split from the much stronger Hα
line, and little useful data can be obtained for the [NII]
lines.  The photographic spectra provide relative intensi-
ties for the [NII], Hα, and [SII] lines.

At the time of our IIDS observations, problems with
the IIDS reduction software prevented us from readily de-
riving an absolute calibration of our scans from observation
of a standard star.  We overcame this problem by observing
a number of HII regions in M 101 that had been observed
previously, and using the published line ratios as "stan-
dards".  The published observations were taken from Searle
(1971), Smith (1975) and Shields and Searle (1978).  The
following summarizes our procedure:

1.  We first measured the height above the local con-
tinuum of the maximum of all the lines in all the HII re-
gions.  These measurements were in counts per channel.  The
lines were unresolved, so measurement of the height is
equivalent to and much simpler than measuring the line in-
tegral.

2.  We corrected intensities for each line for atmos-
pheric extinction.

3. The published line ratios are presented corrected for reddening within the HII regions. We "uncorrected" these ratios for reddening by using the same reddening curve as was used by the original authors and by using the listed values of the reddening parameter for each individual region. This provided us with a list of line ratios as actually observed.

4. We took the logarithm of the ratios of the heights for various line pairs and compared these "instrumental" ratios to the actual observed logarithmic ratios. For each line ratio, the difference between the two logarithmic quantities should be constant. This difference provides a "calibration constant" to convert the instrumental ratios to real intensity ratios. This comparison was done between our measurements in M 101 and those of Smith (1975) and Shields and Searle (1978), separately.

One major potential problem in this calibration technique arises from the large spatial extent of the M 101 HII regions; a typical region has an angular size of order 20 arcsec. If our measurements were taken at a different position than the calibration observations, our ratios could be in error, as spatial inhomogeneities in the line ratios are not insignificant within a given HII region. The observations of Smith (1975) were taken with a 2 arcsec wide slit, centered on the highest surface brightness section of

the region.  The Shields and Searle (1978) observations were made with a 7 arcsec diameter circular aperture, centered so as to maximize the Hα count rate.  Our data, obtained through an 8 arcsec aperture centered visually on the HII region, is thus very similar to the Shields and Searle data.  Comparison of the calibration constants obtained from the two sets of published data enable a check on possible errors, such as any introduced by spatial inhomogeneities in the calibrating HII regions.  The comparison is very encouraging -- the calibration constants differ by 0.04, 0.03 and 0.13 dex,  for the [OII]/Hβ, Hα/Hβ, and [SII]/Hα ratios, respectively.  The difference in the [SII]/Hα calibration is in the sense expected for spatial inhomogeneities, as the [SII] lines form preferentially in the outer parts of the nebulae, and the Shields and Searle (1978) observations yield a higher [SII]/Hα ratio than those of Smith (1975).  Even though we had only three M 101 regions in common with Shields and Searle, as opposed to five in common with Smith, we adopt the calibration constants derived from the Shields and Searle (1978) observations for two reasons:

1.  Their observations were obtained through an aperture almost identical to ours, and

2.  The internal consistency of the calibration constants obtained for the separate regions is better, with a

standard deviation of 0.01, 0.02, and 0.06 for the 3 line ratios mentioned above, significantly better than those obtained from the Smith (1975) observations.

Considering the indirect nature of our calibration, it appears to have worked very well.  The final errors in the intensity ratios measured for the HII regions in the LSB galaxies are certainly dominated by random errors, not systematic calibration errors.

The [OIII]/Hβ ratio does not need to be calibrated in this way, as the lines are so close in wavelength that there should be no wavelength-dependent sensitivity change. Hence, our tabulated ratios are simply the ratio of the measured heights of the lines.  Our [OIII]/Hβ ratios for the M 101 regions were found to be in excellent agreement with those of Smith (1975) and Shields and Searle (1978), with a scatter in the difference between our measurements and the published ones of about 0.03 dex, with a negligible zero-point shift.  Our measurements also yield the equivalent width of lines, in particular the equivalent width of Hβ, W(Hβ).  This measurement does not, of course, depend on the intensity calibration, but only on the linearity of the detector.  Smith (1975) and Shields and Searle (1978) do not list equivalent widths, but Searle (1971) gives W(Hβ) for three M 101 HII regions we observed.  Our values of W(Hβ) are larger, by a factor of 1.6 in the mean.  As Searle

(1971) used a large aperture (14 or 20 arcsec diameter) for his measurements, we might expect our W(Hβ) to be slightly larger, as his measurements must include more background continuum than our measurements, which would dilute the Hβ line. One potential problem in the measurement of W(Hβ) in the LSB regions is their relatively small angular size. If the continuum flux in the 8 arcsec aperture is dominated by background light because the HII region does not fill the aperture, we would measure an artificially small W(Hβ). We tested for this effect by measuring the magnitude, on both the U and R plates, of an 8 arcsec diameter region centered on each HII region and in a nearby comparison region. The magnitudes of the region centered on the HII regions were in general a magnitude or more brighter than the comparison area, in both U and R. This implies that the majority of the continuum flux in the HII region comes from stars ioniz-ing the region. We could derive an estimate of the correc-tion to the W(Hβ) for each individual region, but this was not done as equivalent data were not available for the pub-lished HII region data. .

In Section 2.6, we describe the reduction of the photographic spectra and indicate how we can average rows of pixels to obtain the spectrum of a given region along the slit. To use the intensity ratio of [SII]/Hα measured from these spectra, we first must see if there is a significant

change of sensitivity with wavelength in the system between

6560 and 6730 Å. There are two wavelength dependent fac-

tors in the variation of the response of this system with

wavelength -- the blaze of the grating and the sensitivity

of the image tube. The efficiency of the grating, blazed

at 8000 Å, is rising with increasing wavelength in this

spectral region, while the image tube response is falling

(Kitt Peak National Observatory 1977). The changes are

only a few percent in this spectral region, and to a good

approximation they cancel, resulting in a uniform response

with wavelength. Thus, the photographic line ratios were

not corrected for variation of response with wavelength.

The visual absorption, $A_V$, was derived from the ob-

served Balmer decrement, using the Purcell (1969) fit to

the Whitford (1958) reddening curve. An intrinsic $I(H\alpha)/$

$I(H\beta)$ ratio of 2.85 (log = 0.45) was assumed. This is

identical to the procedure used by Smith (1975). Because

of the relatively small difference in extinction between $H\alpha$

and $H\beta$, small errors in the observed $H\alpha/H\beta$ ratio or in the

assumed intrinsic intensity ratio can lead to large errors

in $A_V$. For example, a change of only 10% (0.04 dex) in the

observed $H\alpha/H\beta$ ratio leads to a change in $A_V$ of about 0.25

magnitude. The only intensity ratio we measured signifi-

cantly affected by reddening is the [OII]/$H\beta$ ratio. We

corrected this ratio, using the computed $A_V$ for each region

and the Purcell fit to the reddening curve. This correction was small, averaging 0.07 dex, and was made only to make our [OII]/Hβ ratio consistent with other published data.

The broad-band magnitudes of HII regions are useful in studying the properties of the associated star clusters. Table 5 lists the U magnitude and (U-R) color in an 8 arcsec diameter circular aperture, for all HII regions observed with the IIDS. These magnitudes were obtained using the IPPS routine PHOT. We derived the equivalent (U-V) color, using the color interpolation formula, and $M_U$, the absolute U magnitude. Values of (U-V) and $M_U$ are also listed in Table 5. These values have been corrected for internal reddening, assuming $A_V = 0.5$ magnitude for all regions. This $A_V$ value is the average obtained from the Hα/Hβ ratio for all LSB regions.

Table 6 lists the observed logarithmic line ratios for all HII regions observed with the IIDS. Also listed is the equivalent width of Hβ, W(Hβ), in Ångstroms, and the visual extinction, $A_V$, derived from the Hα/Hβ ratio for each region. The last column lists the distance of the HII region from the center of the galaxy, in units of the Holmberg radius, $R_H$. Table 7 lists the logarithmic line ratios observed photographically. The third column of Table 7 lists the equivalent [OIII]/Hβ, estimated from Hα/[NII] and

Table 5. Magnitudes of HII Regions

|  | U | U-R | U-V[a] | $M_u$[a] |
|---|---|---|---|---|
| NGC 3913-2 | 17.64 | -0.37 | -0.9 | -14.4 |
| UGC 06922-4 | 18.57 | 0.77 | 0.0 | -13.4 |
| -5 | 19.04 | 0.50 | -0.2 | -13.0 |
| UGC 06983-5 | 17.70 | 0.02 | -0.6 | -14.3 |
| -7 | 17.28 | 0.92 | 0.1 | -13.9 |
| -8 | 18.09 | 0.30 | -0.4 | -14.7 |
| NGC 4411A-17 | 18.40 | 0.46 | -0.3 | -13.9 |
| -18 | 18.68 | 0.58 | -0.2 | -13.6 |
| NGC 4411B-3 | 17.78 | 0.88 | 0.0 | -14.5 |
| -11 | 18.18 | 0.35 | -0.3 | -14.1 |
| UGC 07557-3 | 18.42 | 0.45 | -0.3 | -13.8 |
| -13 | 18.07 | -0.09 | -0.7 | -14.2 |

a. Corrected for average internal reddening.

Table  6.  IIDS HII Region Data

|  | [OII]/Hβ | [OIII]/Hβ | [SII]/Hα | W(Hβ) | $A_V$ | $r/R_H$ |
|---|---|---|---|---|---|---|
| NGC 3913-2 | 0.73 | -0.10 | -0.40 | 117 | 1.3 | 0.3 |
| UGC 06922-4 | 0.69 | -0.08 | -0.30 | 15 | 0.3 | 0.2 |
| -5 | 0.65 | 0.85 | ---- | 19 | 1.3 | 0.5 |
| UGC 06983-5 | 1.00 | 0.68 | -0.36 | 25 | 1.1 | 0.8 |
| -7 | 0.66 | 0.43 | -0.49 | 49 | 0.6 | 0.6 |
| -8 | 0.46 | 0.23 | -0.42 | 12 | 0.6 | 0.1 |
| NGC 4411A-17 | 0.46 | 0.35 | -0.23 | 16 | 0.1 | 0.5 |
| -18 | 0.55 | 0.13 | -0.58 | 34 | 0.4 | 0.4 |
| NGC 4411B-3 | 0.52 | -0.23 | -0.41 | 14 | 1.2 | 0.1 |
| -11 | 0.43 | 0.42 | -0.50 | 58 | 0.1 | 0.6 |
| UGC 07557-3 | 0.39 | 0.43 | -0.46 | 45 | 0.0 | 0.3 |
| -13 | 0.49 | 0.52 | -0.32 | 25 | 0.0 | 0.6 |

Table 7.  HII Region Photographic Emission Line Ratios

| | [SII]/Hα | Hα/[NII] | [OIII]/Hβ | $r/R_H$ |
|---|---|---|---|---|
| UGC 06983-4 | -0.96 | 0.99 | 0.71 | 0.7 |
| -5 | -0.71 | 0.88 | 0.67 | 0.8 |
| -8 | -0.47 | 0.47 | 0.24 | 0.1 |
| -Bar | -0.54 | 0.50 | 0.36 | 0.0 |
| -A | -0.80 | 0.93 | 0.69 | 0.8 |
| UGC 07557-3 | -0.59 | 0.59 | 0.56 | 0.5 |
| -5 | -0.44 | 0.81 | 0.65 | 0.8 |
| -8 | -0.46 | 0.75 | 0.62 | 0.4 |
| -29 | -0.29 | 0.57 | 0.56 | 0.3 |
| -A | -0.03 | 0.42 | 0.05 | 0.0 |
| NGC 4517A-1 | -0.66 | 0.65 | 0.59 | 0.0 |
| -16 | -0.58 | 0.77 | 0.63 | 0.6 |
| -20 | -0.51 | 0.63 | 0.58 | 0.1 |
| -30 | -0.50 | 0.76 | 0.63 | 0.6 |

the relation between [OIII]/Hβ and Hα/[NII] given by Searle (1971).

Table 8 lists the coordinates of all HII regions on the galaxy prints, (Section 3.4). These coordinates are measured from the upper left hand corner of each set of four galaxy images, with x parallel to the short dimension of the page. The coordinates are in millimeters.

## 2.6 Long Slit Spectra Reduction

We obtained long slit spectra of three of the LSB galaxies, using the RC spectrograph on the Mayall 4-m telescope. These spectra provide the data which permit derivation of detailed rotation curves and also some emission line ratios. All spectra were taken approximately along the major axes of the galaxy. The exact position angle and slit center were chosen so the slit passed through as many condensations (HII regions) as possible. Because the exposures were long, 2 to 3 hours, we were only able to obtain one spectrum per galaxy. Along with each galaxy spectrum, we obtained a curvature plate with the telescope set at the hour angle corresponding to the midpoint of the galaxy spectrum and an intensity calibration wedge on a separate plate.

The 1200 line/mm grating was used, yielding a dispersion of about 28 Å/mm; the scale perpendicular to the dispersion was 25 arcsec/mm. The spectra were centered at 6600 Å and include the Hα, [NII], and [SII] emission lines.

Table 8.  X, Y Positions of HII Regions on
Prints -- Coordinates are measured
from the upper left hand corner of
each set of four galaxy images.
The X axis is parallel to the
short dimension of the page.

|  | X(mm) | Y(mm) |
|---|---|---|
| NGC 3913-2 | 34 | 47 |
| UGC 06922-4 | 41 | 111 |
| -5 | 48 | 109 |
| UGC 06983-Bar | 37 | 37 |
| -4 | 10 | 40 |
| -5 | 7 | 41 |
| -7 | 42 | 50 |
| -8 | 33 | 37 |
| -11 | 63 | 35 |
| NGC 4411A-17 | 23 | 33 |
| -18 | 28 | 31 |
| NGC 4411B-3 | 33 | 118 |
| -11 | 29 | 131 |
| UGC 07557-A | 38 | 37 |
| -3 | 47 | 43 |
| -5 | 55 | 50 |
| -8 | 24 | 25 |
| -13 | 54 | 28 |
| -29 | 42 | 39 |
| NGC 4517A-1 | 37 | 40 |
| -16 | 62 | 40 |
| -20 | 31 | 37 |
| -30 | 8 | 33 |

The galaxy spectra, along with the corresponding curvature plate, were digitized on the PDS microdensitometer. The resulting digital images were analyzed using the IPPS system, using the program RV written by A. Phillips and D. Tody. The entire operation is fairly complex. A brief outline of the process follows:

1. The spectra are converted from density to intensity using the same programs described earlier for the direct plates.

2. The curvature is mapped by tracing the lines on the curvature plate. The curvature parameters obtained from this mapping are used to create a new raster in which the effects of the curvature are removed from the galaxy spectra.

3. The vignetting perpendicular to the dispersion is mapped by measuring the intensity of a night-sky emission line across the spectra. The galaxy spectrum is divided by the inverse of the night-sky line intensity, yielding a spectrum with uniform response perpendicular to the dispersion.

4. The night-sky spectrum is obtained by averaging several regions which do not contain emission lines from the galaxy. This night-sky spectrum is subtracted from the entire raster, yielding a spectrum with only the galaxy emission lines left.

At this point we have a relative intensity raster containing the galaxy spectrum corrected for curvature, with the vignetting perpendicular to the dispersion removed, and with the night-sky emission spectra removed. We can now measure a rotation curve or emission line ratios. To measure the rotation curve, the program scans perpendicular to the dispersion in a small region flanking the specified emission line and measures the wavelength of the centroid of any emission regions. This produces a plot showing the velocity of each point on the spectra where the emission line signal was larger than some specified noise limit, specified in terms of the pixel-to-pixel variation in a blank region of the spectra near the emission line. To measure emission line ratios, we can obtain a plot of intensity versus wavelength for a given row of the matrix, or we can use the COMTAL cursor to specify a range of rows to be averaged together to obtain a spectrum of an entire emission region.

### 2.7 Neutral Hydrogen Radio Observations

Neutral hydrogen observations of LSB spiral galaxies were obtained with both the 91-m transit telescope of the National Radio Astronomy Observatory (NRAO) and the 305-m telescope of the National Astronomy and Ionosphere Center (NAIC) in Arecibo.

The NRAO 21-cm observations were obtained in December of 1977. We used the autocorrelator spectrometer with 192 channels, usually with a channel separation of 11 km/sec, although a few observations were made with 22 km/sec channel spacing. The signals from the two polarizations were averaged. Transformation of the data from antenna temperature to Jansky units was carried out through a standard curve of gain as a function of declination. This gain was checked several times during the run by observing continuum sources of known flux density. Comparison of our flux values with those of Fisher and Tully (1975) for 8 galaxies in common show the ratio of our measured flux to theirs to be 1.13 ± 0.11 (m.e.). One galaxy (DDO 146) had much larger than average discrepancies in both flux and line width. Without this galaxy, the flux ratio is 1.05 ± 0.11 (m.e.). Thus our flux scale is very close to that of Fisher and Tully, who went to great lengths to calibrate their scale.

The Arecibo 21-cm observations were obtained in August 1977. A 504 channel spectrometer was used, yielding spectra with a channel spacing of 4.1 km/sec. The system was calibrated by observing continuum sources to fix the temperature of the noise tubes. As the feed efficiency is dependent on frequency, separate calibrations were obtained for different velocity ranges.

Some of the galaxies observed at Arecibo were
larger than the 3.2 arcmin FWHM size of the beam. Several
galaxies were observed at a number of positions in an at-
tempt to observe all the HI associated with a galaxy or to
determine the separate HI content of galaxies in close
pairs. These observations were made with beam centers of
about 2 arcmin, using a 3 x 3 or 3 x 5 grid of points.

It is, of course, impossible to obtain a detailed
HI map of an object comparable in size to the telescope
beam. However, it is possible to use a grid of observations
to derive a reasonable estimate of the total mass of HI. A
simple model of the HI distribution in each galaxy was con-
structed, using the optical diameter of the galaxy and an
HI versus radius curve similar to those obtained by Rogstad
and Shostak (1972) for Scd galaxies. The model was con-
volved with the average profile of the Arecibo beam, includ-
ing sidelobes. The model was iteratively altered to obtain
better agreement between the actual observations and those
predicted by the model. Once the differences between the
model predictions and the actual observations were similar
in size to the random errors in the observations, we inte-
grated the best fit flux-position model to derive the total
flux. This flux value is listed as $F_{corr}$ in Column 6 of
Table 9. Different initial models yielded final flux
values within a few percent of one another, but with

Table 9. Neutral Hydrogen Data

| Name (1) | V (2) | $V_o$ (3) | $\Delta V$ (4) | $F_H$ (5) | $F_{corr}$ (6) | Telescope (7) |
|---|---|---|---|---|---|---|
| UGC 04841 | 1127 | 1288 | 167 | 5.79 | 6.48 | NRAO |
| UGC 04922 | 1992 | 2024 | 247 | 3.44 | 3.75 | NRAO |
| UGC 05633 | 1383 | 1257 | 177 | 3.68 | 3.86 | NRAO |
| UGC 06446 | 646 | 729 | 139 | 8.04 | 8.85 | NRAO |
| UGC 06682 | 1325 | 1436 | 83 | 2.96 | 3.08 | NRAO |
| NGC 3913 | 953 | 1050 | 43 | 2.51 | 2.71 | NRAO |
| UGC 06922 | 892 | 971 | 136 | 2.02 | 2.12 | NRAO |
| DDO 105 | 901 | 922 | 155 | 6.66 | 7.79 | NRAO |
| UGC 06983 | 1080 | 1168 | 189 | 7.83 | 8.85 | NRAO |
| NGC 4411A | 1280 | 1184 | 80 | 1.89 | 2.39 | AO |
| NGC 4411B | 1269 | 1174 | 77 | 2.33 | 3.61 | AO |
| UGC 07557 | 937 | 835 | 144 | 3.50 | 6.16 | AO |
| NGC 4517A | 1530 | 1404 | 160 | 8.34 | 9.43 | NRAO |
| NGC 4571 | 343 | 277 | 152 | 9.12 | 10.40 | NRAO |
| DDO 144 | 1182 | 1064 | 112 | 3.10 | 3.32 | NRAO |
| DDO 142 | 1433 | 1292 | 131 | 8.20 | 8.86 | NRAO |
| DDO 146 | 1476 | 1334 | 168 | 4.86 | 5.30 | NRAO |
| MCG-2-33-15 | 2390 | 2236 | 254 | 7.11 | 8.32 | NRAO |
| UGC 08253 | 3317 | 3264 | 147 | 1.73 | 2.27 | AO |
| UGC 08409 | 2804 | 2809 | 162 | 1.74 | 2.37 | AO |
| UGC 09061 | 5442 | 5460 | 182 | 5.30 | 6.62 | NRAO |

Table 9.--<u>Continued</u>

| Name (1) | V (2) | $V_O$ (3) | $\Delta V$ (4) | $F_H$ (5) | $F_{corr}$ (6) | Telescope (7) |
|---|---|---|---|---|---|---|
| NGC 5774 | 1563 | 1561 | 142 | 6.66 | 13.58 | AO |
| UGC 09614 | 3062 | 3086 | 130 | 1.25 | 1.61 | AO |
| UGC 09875 | 1991 | 2094 | 86 | 1.15 | 1.55 | AO |
| NGC 5964 | 1456 | 1502 | 180 | 5.08 | 10.77 | AO |
| UGC 09938 | 1858 | 1989 | 101 | 0.92 | 1.20 | AO |
| UGC 11868 | 1094 | 1349 | 118 | 2.11 | 2.25 | NRAO |
| DDO 214 | 1693 | 1867 | 98 | 3.65 | 3.80 | NRAO |
| DDO 219 | 2682 | 2844 | 130 | 1.90 | 2.02 | NRAO |

somewhat different distributions of HI. Another way to obtain the total HI content from a grid of observations is to treat the superposition of the beams as one large beam, and the sum of the antenna temperatures at each point in the grid as the flux of a point source in the large beam. The summed antenna temperature can then be converted to Jansky units, using the central gain of the artificial large beam. As expected, this method gave slightly smaller total flux values as the method described above, as each galaxy, although smaller than the large artificial beam, is large enough so it cannot be considered a point source relative to this beam.

The galaxy pair NGC 4411 A and B was observed with a 3 x 5 grid of points. The model fit was performed on the entire grid at once, and HI fluxes were ascribed to the individual galaxies by dividing the final model on a line halfway between the galaxies. The galaxy pair NGC 5774-5775 was also observed with a 3 x 5 grid of points. It was possible to crudely divide the flux from the points between the galaxies into contributions from the separate galaxies because of the different velocity profiles of the two galaxies. Then the model fit was performed on the separate 3 x 3 grids.

A direct comparison between our Arecibo and NRAO observations is possible for the galaxy UGC 07557. A single

NRAO observation gives a flux value, corrected for source to beam size, only 5% different from the flux obtained by the model fit to the Arecibo 3 x 3 point grid of observations. As the procedure applied to the Arecibo data is straightforward, with little chance of sizable error in deriving the total flux, this close agreement in final flux values suggests the flux density scales are similar.

By comparing the flux from the central beam to the total derived flux for the five galaxies for which total fluxes were obtained by the model fit, we derived the following equation to correct single-point Arecibo observations for source to beam size:

$$F_{corr} = F \left[ 1 + (0.65 \, a/\theta)^2 \right]^{\frac{1}{2}} \left[ 1 + (0.65 \, b/\theta)^2 \right]^{\frac{1}{2}} \qquad (11)$$

In this equation, F is the single-beam flux, $F_{corr}$ is the total flux, $\theta$ is 3.2 arcmin, the FWHM size of the Arecibo beam, and a and b are the Holmberg major and minor axes diameters, estimated from the Nilson diameter as in Fisher and Tully (1975). Use of the more accurate diameters available from the surface photometry change $F_{corr}$ by only a few percent.

The observational data for the LSB spirals is listed in Table 9. The columns are as follows:

Column (1) -- The name of the galaxy.

Column (2) -- V, the heliocentric velocity (in km/sec).
For most profiles, the velocity was determined in two inde-
pendent ways.  For straight sided profiles, we averaged the
velocity of four points, the two where the profile reached
zero intensity and the two at the high-intensity ends of
the straight side portion of the scan.  We also visually
estimated the center of the profile and found the channel
velocity corresponding to this point.  The final velocity
is the average of the two velocities obtained, which usu-
ally agreed to 5-10 km/sec.  For gaussian or asymmetric
profiles, we averaged the two points where the profile
reached zero intensity and also estimated the centroid of
the profile visually.  These two velocities agreed to
within 15 km/sec for most of these galaxies, and were aver-
aged to obtain the final velocity.

Column (3) -- $V_o$, the velocity of the galaxy corrected
for galactic rotation.  The form of the correction is from
de Vaucouleurs, de Vaucouleurs and Corwin (1976) and as-
sumes a galactic rotation velocity of 300 km/sec.

Column (4) -- $\Delta V$, the full profile width at one-quarter
of the peak intensity.  We made a crude correction for the
effects of instrumental resolution by subtracting 6 km/sec
from the raw line widths obtained with the NRAO telescope
and 3 km/sec from those obtained with the Arecibo telescope.
Comparison of the line widths for seven objects observed by
us and by Fisher and Tully (1975) (excluding DDO 146) shows

a mean difference of less than 1 km/sec and an rms differ-
ence of 12 km/sec. Comparison of three objects (not LSBs)
observed by us at 11 km/sec channel spacing and by Dickel
and Rood (1978) (NGC 2805, NGC 3319, NGC 4145) shows our
line widths to be smaller by about 25 km/sec. As the
Fisher and Tully line widths are measured at one-half peak
intensity, we would expect our line widths to be slightly
larger than theirs, but do not observe this. This, com-
bined with the difference from the Dickel and Rood widths,
suggests our line widths may be slightly underestimated.
A comparison of 38 line widths for galaxies in common be-
tween Dickel and Rood (1978) and Shostak (1978) shows a
rms difference of 22 km/sec. If we assume this as the size
of the typical uncertainty in their line widths, the dif-
ference between our line widths and those of Dickel and
Rood may simply be due to uncertainty in the measurements.

Column (5) -- The observed integrated hydrogen flux
density $F_H$ in units of $10^6$ $M_\odot/Mpc^2$. For the galaxies ob-
served at more than one position with the Arecibo telescope,
the flux in the beam centered on the object is listed in
this column.

Column (6) -- The integrated hydrogen flux density cor-
rected for source to beam size, $F_{corr}$, in units of $10^6$
$M_\odot/Mpc^2$. All NRAO observations were corrected as in
Fisher and Tully (1975). The Arecibo observations were

corrected with equation 11, except for the galaxies ob-
served at more than one position, for which the total flux
determination was described previously.

The total hydrogen mass, $M_H$, can be derived from
$F_{corr}$ and the distance of the galaxy, D, in Mpc:

$$M_H = F_{corr}D^2 \tag{12}$$

Column (7) -- The telescope used to make the observa-
tions, where AO denotes the Arecibo telescope and NRAO the
91-m telescope.

CHAPTER 3

ANALYSIS

In this chapter, we use the observational material
presented in Chapter 2 to study the physical properties of
the LSB spiral galaxies.  We also make extensive compari-
sons between the properties of the LSB and normal late-type
spirals.

In the first section, the large-scale photometric
properties of the LSB and normal galaxies are compared.  We
find that the LSB disk scale lengths are almost as large as
those of Sb I and Sc I galaxies, while the average central
surface brightness of the LSB disks is a factor of 3 lower
than that characterizing the majority of spiral galaxies.
In the second section, broad-band infrared and optical
colors are used to show that the stellar metallicity in the
LSB galaxies is significantly less than the solar value.
Using the spectra and colors of the LSB HII regions, we
show in the third section that the initial mass function
for massive stars is significantly steeper in these galax-
ies than in other late-type spirals.  The fourth section
compares the properties of the spiral structure of normal
and LSB spirals.  This section includes a discussion of the

properties of the LSB spirals in terms of the spiral
density-wave theory. In the fifth section, we compare the
surface mass density of the LSB and normal galaxies. In
the sixth section, we compare the neutral hydrogen content
of normal and LSB spirals. We find that the LSBs have a
high HI mass to luminosity ratio, and perhaps a high HI
mass to total mass ratio. In the last section, we examine
the mass-to-light ratio of the LSB galaxies. We find no
conclusive evidence for an unusual mass-to-light ratio in
these galaxies, although a slightly high value may be
masked by the large uncertainties in our derived values.

### 3.1 Large-scale Photometric Properties

In this section, we use the luminosity profiles
discussed in Section 2.3 to analyze two aspects of the
large-scale structure of the LSB galaxies: (1) the posi-
tion of the galaxies in the size versus absolute magnitude
plane and (2) the decomposition of the luminosity profiles
into disk and bulge components.

The positions of the LSB galaxies in the size-
absolute B magnitude plane are shown in Figure 4. Total B
magnitudes were determined from the photographic R magni-
tudes, using (B-R) from the color interpolation equations
(Section 2.3) for galaxies with U and R plates or from the
photoelectric photometry for galaxies with no U plate. The
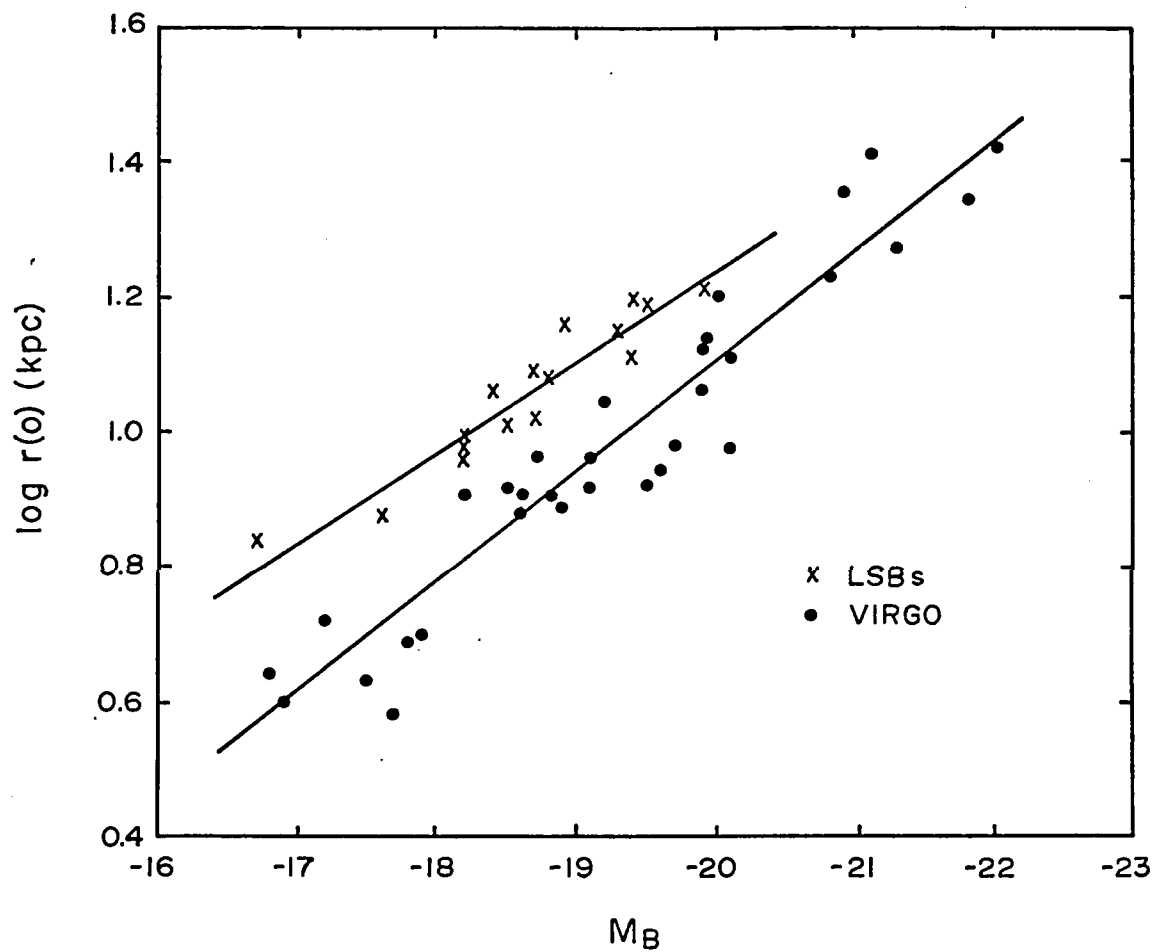
Figure 4. Size vs. Absolute Magnitude Plot.

vertical axis is the logarithm of the Holmberg radius, r(0), corrected to face-on value. Also shown in Figure 4 are a number of normal spiral galaxies in the Virgo cluster studied by Peterson, Strom and Strom (1979). The LSB data was analyzed in a manner identical to the Virgo data. Galaxy distances were derived from the 21-cm velocities using $H_o$ = 50 km/sec/Mpc, or were taken as group distances consistent with this distance scale. The diameters were corrected to face-on values using the correction factor $(b/a)^{0.4}$. Peterson, Strom and Strom (1979) did not correct their magnitudes for internal reddening. Because the LSB galaxy sample is strongly biased towards face-on galaxies, while the normal Virgo sample is not, there will be a systematic error in the comparison if an internal absorption correction is not made. To crudely correct for this, we have corrected all galaxy magnitudes to face-on values, using the simple correction used by Tully and Fisher (1977):

$$A_B = 0.28 \ (a/b-1) \qquad (13)$$

Figure 4 reveals the expected result: the LSB galaxies are too faint at a given size or too large at a given absolute B magnitude. Least squares fits to the two sets of data yield the following relations between log r(0) and $M_B$:

$$\text{LSB:} \quad \log r(0) = 1.449 - 0.1344 \ M_B$$
$$0.225 \qquad 0.0121 \qquad\qquad (14)$$

$$\text{Virgo:} \quad \log r(0) = 2.167 - 0.1634 \, M_B \qquad (15)$$
$$0.185 \qquad 0.0096$$

Standard one-sigma errors are listed under each coefficient. These errors were calculated with the program LINFIT (Bevington 1969). At $M_B$ = -18.5, the LSB galaxies have Holmberg radii a factor of over 1.5 times larger than the normal Virgo galaxies. At a fixed Holmberg radius of 10 kpc, the LSB galaxies are on average fainter than the normal Virgo galaxies by about 1.3 magnitudes.

A typical LSB galaxy luminosity profile, the R profile for NGC 4517A, is shown in Figure 5. The profile can be divided into three fairly distinct sections: (1) The dominant section of the profile is the exponential disk, extending from about r = 30 arcsec to r = 100 arcsec. (2) Near the center of the galaxy, the profile rises above the exponential disk extrapolated from further out. This section will be referred to as the central bulge. (3) Beyond 100 arcsec, the profile falls below the extrapolated disk.

Our analysis of the profiles was carried out using only the R profiles, as they are much less affected by the presence of spiral arms than the U or $B_3$ profiles. Disk parameters found using the R profiles were transformed to the B passband for galaxies with both U and R plates, using the color interpolation equations and the total (U-R) color of the galaxy.
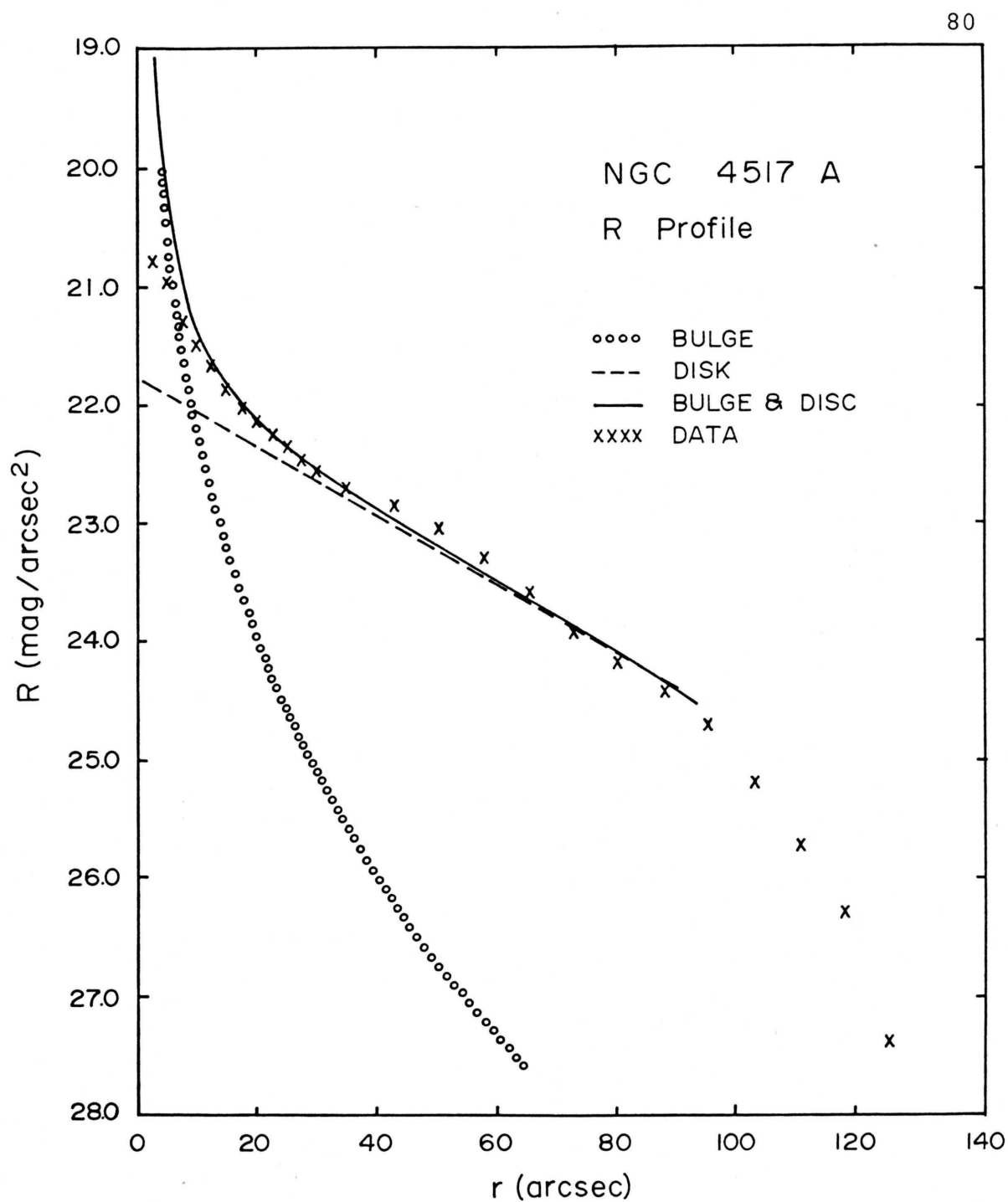
Figure 5. R Profile for NGC 4517A.

We decomposed the profiles into a contribution from the exponential disk, with intensity as a function of radius:

$$I(r) = I_0 \exp(-\alpha r) \qquad (16)$$

where $\alpha^{-1}$ is the scale length of the disk, and $I_0$ the central intensity, and a contribution from a spheroidal bulge component which follows the de Vaucouleurs law:

$$\log I(r) = I_{ov} \; 10^{-3.33 \; [(r/r_0)^{\frac{1}{4}} -1]} \qquad (17)$$

where $r_0$ is the radius containing half the total light, and $I_{ov}$ is the intensity at $r_0$. The de Vaucouleurs function is referred to as the "$r^{\frac{1}{4}}$" law. The fits were made with an iterative least-squares fitting routine, similar to that used by Kormendy (1977a). We fit an exponential to the region where the disk was clearly dominant, subtracted this from the profile, and fit a $r^{\frac{1}{4}}$ profile to the difference. We then subtracted the $r^{\frac{1}{4}}$ fit from the profile, fit the difference with an exponential from r = 0 to the maximum extent of the disk as determined visually from the profile, and iterated the procedure several times. This procedure yielded well-determined parameters for the exponential disk. The parameters for the bulge were not as well determined, primarily because the bulge component in most of the LSB spirals does not seem to follow the $r^{\frac{1}{4}}$ law exactly. The

intensitites at small radii were always too faint for the best fit de Vaucouleurs law component. Also, small changes in the limits of the disk fit changed the bulge parameters much more than the disk parameters.

The extrapolated disk central surface brightness values have been corrected for the geometric tilt effects and Galactic absorption as in Freeman (1970), to derive $B(0)_c$, the corrected central disk surface brightness. Values of $B(0)_c$ and $\alpha^{-1}$, in kpc, are listed in Table 10. For 12 LSB galaxies with both U and R profiles, the average disk parameters are listed below, along with their standard deviations:

$$B(0)_c = 22.88 \, \text{mag/arcsec}^2 \quad (\sigma = 0.39)$$
$$\alpha^{-1} = 4.04 \, \text{kpc} \quad (\sigma = 1.24)$$

Schweizer (1976) found the following average disk parameters for six high-luminosity Sb I and Sc I spirals:

$$B(0)_c = 21.67 \, \text{mag/arcsec}^2 \quad (\sigma = 0.35)$$
$$\alpha^{-1} = 4.95 \, \text{kpc} \quad (\sigma = 1.24)$$

Disk scale lengths for the LSB galaxies were calculated with galaxy distances derived using $H_o = 55$ km/sec/Mpc for consistency with the distances used by Schweizer. The value of $B(0)_c$ found by Schweizer is virtually identical to the value of 21.65 that Freeman (1970) found to characterize

Table 10.  Disk Parameters

| | $\alpha^{-1}$ (kpc) | $B(0)_c$ (mag/arcsec$^2$) |
|---|---|---|
| UGC 04841 | 4.97 | 22.76 |
| NGC 3913 | 2.91 | 22.74 |
| UGC 06922 | 2.22 | 23.82 |
| UGC 06983 | 3.12 | 22.94 |
| NGC 4411A | 2.47 | 22.27 |
| NGC 4411B | 3.65 | 22.49 |
| UGC 07557 | 3.62 | 23.04 |
| NGC 4517A | 5.49 | 23.24 |
| DDO 144 | 3.95 | 22.95 |
| DDO 142 | 4.80 | 22.60 |
| DDO 146 | 5.30 | 22.90 |
| NGC 5774 | 5.94 | 22.77 |

the majority of spiral galaxies for which he could find
surface photometry. Freeman (1976) put forward the hypoth-
esis that all non-dwarf disk galaxies have this same cen-
tral surface brightness. Clearly, this is not the case.
We use the normal z statistical test (Crow, Davis and Max-
field 1960) to determine whether or not there is a statis-
tically significant difference between the means of samples
of data from the LSB and normal galaxies. We use the ex-
perimental standard deviation, calculated from each sample,
as an estimate of the true standard deviation. The normal
test shows that the probability of there being no signifi-
cant difference between $B(0)_c$ for the LSB and normal
galaxies is less than 0.002%. The probability of there
being no significant difference for $\alpha^{-1}$ is about 10%. The
average LSB central surface intensity is a factor of 3
lower than Freeman's value. The LSB disk scale lengths are
slightly smaller, on average, than the Sc I disk scale
lengths, although the average values for the two samples
are statistically only marginally different. Thus, the
difference in $B(0)_c$ cannot be understood as an effect of
the disk size.

The ratio of the bulge luminosity to total lumi-
nosity in a spiral galaxy is correlated with Hubble type
(Yoshizawa and Wakamatsu 1975; de Vaucouleurs 1977). This
ratio will be denoted $K_1$, following de Vaucouleurs. We

determined the bulge luminosity following the procedure of Yoshizawa and Wakamatsu, by numerically integrating the luminosity above the exponential disk. Because the $K_1$-type relation is defined for B magnitudes, we cannot directly use our $K_1$, determined from the R profile. Since the bulge is redder than the disk, $K_1$ determined from the R profile will be too large. Therefore, we decreased $K_1$ by 0.7 magnitudes, the difference in B-R between the disk (B-R $\approx$ 1.1) and the estimated bulge color (B-R $\approx$ 1.8). The bulge color was estimated from the $M_V$-(U-V) plot of Aaronson (1977) and the color interpolation equations, using a typical bulge absolute magnitude ($M_V \sim -16$). Table 11 lists the values of $K_1$, corrected to the B magnitude, and the type from the $K_1$-type relation of de Vaucouleurs. Ten of the twelve galaxies listed in Table 11 have types in the Second Reference Catalog of Bright Galaxies (RC2) (de Vaucouleurs et al. 1976). In the RC2, all ten galaxies are classified as type Scd or later. The types listed in Table 11 derived from $K_1$ are, in general, slightly earlier than the RC2 types. Some of the disagreement is probably due to the intrinsic scatter in the $K_1$-type relation. However, at least three galaxies (NGC 3913, UGC 06922 and NGC 5774) are definitely of early Hubble type as judged from their $K_1$ values.

Table 11.  Morphological Types from $K_1$

| | Log $K_1$ | $K_1$ Type | RC2 Type |
|---|---|---|---|
| UGC 04841 | −1.55 | Sd | Sd |
| NGC 3913 | −0.78 | Sa | Sd |
| UGC 06922 | −0.61 | SO/a | --- |
| UGC 06983 | −1.62 | Sdm | Scd |
| NGC 4411A | −1.44 | Scd | Sdm |
| NGC 4411B | −1.26 | Sc | Sdm |
| UGC 07557 | −1.70 | Sdm | --- |
| NGC 4517A | −1.40 | Scd | Sdm |
| DDO 144 | −1.44 | Scd | Sm |
| DDO 142 | −1.33 | Scd | Sm |
| DDO 146 | −2.12 | Im | Im |
| NGC 5774 | −1.00 | Sb | Sd |

## 3.2 Stellar Metal Abundance from
## Broad-band Colors

In this section we discuss the interpretation of the optical and infrared colors of the LSB spiral galaxies. The primary factors affecting the intrinsic broad-band colors of a galaxy are: (1) the amount of light contributed by young stars, (2) the average stellar metallicity and (3) the initial mass function (IMF). It is often quite difficult to disentangle the effects of low metallicity from the effects of young stars on the basis of integrated colors, since both produce blue integrated colors. However, we are able to show that the blue colors observed for the LSB galaxies almost certainly result from the dominance of a metal-poor stellar population, with a characteristic metal abundance on the order of 1/10 to 1/2 solar.

We would like to compare the colors of the LSB galaxies with those of normal spirals of similar type. Of the six LSB spirals with measured (J-K) colors, four have types listed in the RC2. All four are listed as Sd or Sdm. The average colors for the four galaxies (Section 2.4), and standard deviation from the mean, are:

$$(U-V) = 0.57 \ (\sigma = 0.08)$$

$$(V-K) = 2.56 \ (\sigma = 0.09)$$

$$(J-K) = 0.75 \ (\sigma = 0.06)$$

These colors are not corrected for internal reddening. As discussed earlier, these measurements are measured at an aperture corresponding to approximately log A/D(0) = -0.6, one of the standard apertures used by Aaronson. We compare these colors with those of galaxies of type Scd and Sd observed by Aaronson (1977). The Scd and Sd spirals are the latest spirals observed by Aaronson. As there is a significant radial variation in the (U-V) and (V-K) colors, we use the (U-V) and (V-K) colors from his "restricted" class, which does not include galaxies measured only at very small values of A/D(0). The (J-K) color is the average of all the Scd and Sd galaxies measured, as Aaronson finds no significant color gradient in (J-H) or (H-K), thus the measurement aperture size is not important. The average colors, uncorrected for internal reddening, are:

$$(U-V) = 0.62 \ (\sigma = 0.17)$$

$$(V-K) = 2.91 \ (\sigma = 0.10)$$

$$(J-K) = 0.90 \ (\sigma = 0.08).$$

The colors of the LSB galaxies are remarkably uniform. The average colors of the six galaxies with measured (J-K) colors, including the two without types listed in the RC2, are:

$$(U-V) = 0.59 \ (\sigma = 0.08)$$

$$(V-K) = 2.56 \ (\sigma = 0.10)$$

$$(J-K) = 0.74 \ (\sigma = 0.05)$$

The average colors of the 11 LSB galaxies with (V-K) colors, including those for which a (H-K) color was assumed (see Section 2.4), are:

$$(U-V) = 0.57 \ (\sigma = 0.13)$$

$$(V-K) = 2.57 \ (\sigma = 0.09).$$

The observed colors of spiral galaxies are affected not only by metallicity and the amount of light contributed by young stars, but also by reddening. We expect that a purely infrared color, like (J-K), will not be affected much either by reddening or by the light contributed by young stars. Thus (J-K) should be sensitive primarily to the metallicity and perhaps initial mass function of the old population. We computed several models of galaxies with constant star formation rates, using a galactic evolution program written by J. Huchra (see Huchra 1977 for details of this program). Huchra's models contain only stars of solar composition. These models reveal that (J-K) changes by only a small amount (0.02 magnitude at most) as (U-V) changes by up to one magnitude as the proportion of light from young stars changes in the course of the evolution of a model galaxy. Thus the effect on (J-K) of differences in the proportion of light from young stars should be negligible. We can estimate the maximum effect of reddening on (J-K), by making use of the ratio of the excess in (J-K), $(E_{J-K})$, to the visual absorption $(A_V)$ and

an estimate of $A_V$. The ratio $E_{J-K}/A_V$ has a value of 0.16 from the standard reddening curve (Aaronson 1977). Using the individual values of $a/b-1$ for the Scd and Sd galaxies observed by Aaronson (1977), and the simple Tully and Fisher (1977) internal reddening law used in Section 3.1, we estimate that the average value of $A_V$ for these galaxies is 0.2 magnitude or less. Thus, the correction to face-on colors makes the Scd and Sd galaxies 0.03 magnitude bluer in (J-K). The corresponding correction for the LSB galaxies makes them 0.01 magnitude bluer in (J-K). Thus the difference in (J-K) color between the LSB and Aaronson Scd and Sd galaxies should not be much affected by reddening differences. We would really like to compare intrinsic, rather than face-on, colors of the LSB and normal galaxies. As discussed below, we assume that any difference caused by a different face-on to intrinsic color transformation for the two samples of galaxies is negligible. Using the normal z test (Section 3.1) we find that the probability the face-on (J-K) values for the LSB and Scd, Sd spirals do not differ significantly is less than 0.2%.

The results from the galactic evolution models show that the light from young stars has negligible effect on (J-K). This implies that the blue and red supergiants do not affect (J-K) much. However, even if the supergiants do contribute a significant amount of light, the difference

between the (J-K) colors of the LSB and normal galaxies can-
not be due to the difference in supergiant colors caused by
differing metallicity between the two groups of galaxies.
The ratio of blue to red supergiants (B/R) decreases with
increasing radius in M 33 (Walker 1964). As the metal
abundance also decreases with increasing radius, B/R de-
creases with decreasing metal abundance. Thus, the inte-
grated supergiant colors become redder with decreasing metal
abundance. We have two independent pieces of evidence that
the average metal abundance in the LSB galaxies is less
than that of normal galaxies of similar type: (1) the
upper limit implied by the HII region line ratios (see Sec-
tion 3.3), and (2) the optical colors of the old disk popu-
lation (discussed later in this section). Because the LSB
galaxies have lower metal abundance than the normal galax-
ies, proper inclusion of the supergiants in a model would
tend to make the LSBs redder, not bluer, relative to normal
spirals than if the difference in supergiant colors were
not taken into account.

We investigated the effect of a change in the ini-
tial mass function (IMF) on (J-K) for a spiral galaxy,
using the galactic evolution program mentioned above.
Models were computed for a 15 billion year old galaxy with
a constant star formation rate, and with a power-law IMF
characterized by $x = 0.5$, 1.35 and 2.5. The (J-K) color

for x = 2.5 was 0.04 magnitude redder than that for x = 1.35 and 0.07 magnitude redder than that for x = 0.5. Thus, changes in the IMF do not make a large change in the (J-K) color. In Section 3.3 we argue that the IMF in the LSB galaxies, at least for the massive stars, is steeper than that in a normal galaxy. If this holds true for less massive stars, we would expect this effect to tend to make the LSB galaxies redder in (J-K) than normal galaxies. However, we have no information on the low mass IMF in the LSB galaxies.

The LSB galaxies are significantly bluer in (J-K) than normal galaxies. We have argued that this difference cannot be due to the presence of young stars or reddening differences. Also, we have argued that a plausible difference in IMF between the LSBs and normal galaxies would make the LSB galaxies redder than normal in (J-K).

Aaronson et al. (1978) present evidence that, at least for globular clusters and elliptical galaxies, (J-K) is related directly to metallicity. This relation is defined primarily by globular cluster data, where the metal abundance of individual stars can be measured spectroscopically. The elliptical galaxies overlap with and extend the globular cluster color-metallicity relation to higher metallicity. All relations between color and line strength and metallicity found for globular clusters extrapolate

smoothly to elliptical galaxies (Faber 1977). Because of
this smooth continuation, it seems reasonable to assume that
the relations between color and metallicity found from
globular clusters can be extrapolated to elliptical galax-
ies. We shall therefore assume (J-K) provides a good mea-
sure of metallicity in old stellar populations. As (J-K)
is not much affected by the presence of young stars, red-
dening, or variations in the IMF, its use as a metallicity
indicator appears justified for spiral as well as ellipti-
cal galaxies. This is a reasonable assumption, as (J-K)
essentially measures the effective temperature of the giant
branch, which depends primarily on the chemical composition
of the giants. From the globular cluster (J-K) versus
metallicity plots of Aaronson et al. (1978), we estimate
that the face-on LSB (J-K) of 0.74 corresponds to a metal
abundance about 1/5 solar. This estimate has a large un-
certainty, which is difficult to precisely estimate, as
there are few clusters near this (J-K) to define the scat-
ter in the (J-K), metallicity diagram. Using an estimate of
the scatter at lower metallicity as an estimate of scatter
in (J-K) versus metallicity at (J-K) of 0.74, and an esti-
mate of the error of the mean of the LSB (J-K) value, we
estimate this value of (J-K) could correspond to metal-
licity between about 1/10 and 1/2 solar.

Another method of investigating the metal abundance of the older population is provided by the optical colors of the underlying disk stars. The color of the underlying old disk for seven LSB spirals was determined by measuring the colors in many small regions visually determined to be free of star formation, using the COMTAL display and the programs described in Section 2.3. These disk colors can be compared to the disk colors obtained by Schweizer (1976) for several giant spiral galaxies. The galaxies studied by Schweizer were brighter and more luminous than the LSB galaxies. Thus, Schweizer was able to make an estimate of the disk intensity level and color by finding the two minima corresponding to troughs between spiral arms, using azimuthal profiles in several bandpasses. We could not use this technique, as the signal-to-noise in azimuthal profiles of the LSB galaxies was not great enough. We measured (U-R) disk colors only for those galaxies for which there appeared to be patches of old disk stars not contaminated by obvious regions of active star formation. Schweizer measured (U-R) disk colors for four galaxies. One of these galaxies (M 81) is of early type (Sb) and will not be included in our average of the Schweizer disk colors. The other three galaxies are of type Sc or Scd and have similar disk colors. The average (U-R) disk color for these three galaxies is 1.71, with a standard deviation of

0.10, and the average (U-B) is 0.23 ($\sigma$ = 0.03). These colors were measured at galactocentric distances from about 5 to 10 kpc. In M 101, one of these three galaxies, we know that the metal abundance in this region, at least in the gas, is approximately solar (Smith 1975). The (U-R) colors for the disks in the LSB galaxies are listed in Table 12.

Table 12. Old Disk Colors

|            | U-R  | U-B  |
|------------|------|------|
| NGC 3913   | 1.21 |      |
| NGC 4411A  | 1.46 |      |
| NGC 4411B  | 1.41 |      |
| UGC 06983  | 1.14 | 0.04 |
| UGC 07557  | 0.99 |      |
| NGC 4517A  | 1.19 | 0.04 |
| DDO 144    | 1.05 |      |

These colors are the average of 30 to 50 separate disk points. Only disk points within the de Vaucouleurs radius ($\mu_B$ = 25) were used, as the dispersion for points at fainter levels increased significantly. The typical standard deviation in (U-R) of the points within one galaxy was

0.15 magnitude. The colors were computed for both 3 x 3
and 5 x 5 pixel boxes around each disk point. Strong con-
tamination by young stars should show up as a difference
between the two measurements, as the bigger box would pick
up more of the region of star formation surrounding the
disk points. The average colors of the small and large
boxes agreed to within a few hundredths of a magnitude in
all cases, with no systematic behavior as a function of box
size. The average (U-R) disk color for the LSB spirals is
1.21 ($\sigma$ = 0.17). The (U-B) color for the two galaxies for
which $B_3$ plates are available is 0.04. The B magnitudes
were calculated from the $B_3$ magnitudes using equation 7,
with (B-V) estimated from the observed (U-R) and the color
interpolation equations (Section 2.3). Thus the underlying
disk colors in the LSB galaxies are bluer than the Schwei-
zer spiral disks by about 0.5 magnitude in (U-R) and 0.19
magnitude in (U-B). Using the normal z test (Section 3.1),
we find the probability that the (U-R) colors of the LSB
and Schweizer spirals do not differ significantly is less
than 0.02%. The (U-R) difference corresponds to a differ-
ence in both (U-B) and (B-V) of about 0.19 magnitude, using
the color interpolation equations. Therefore, the old disk
populations of the LSB spirals are about 0.2 magnitude
bluer in both (U-B) and (B-V) than the disks of the galax-
ies studied by Schweizer.

The Schweizer spirals are all observed close to face-on (b/a > 0.9) as are the LSB galaxies, so there should be negligible difference in the optical colors caused by any correction to face-on colors. We would really like to compare the intrinsic disk colors, rather than the face-on colors. The correction from face-on to intrinsic color in a spiral galaxy is very complicated, as it depends on the distribution of the stars and dust, and the scattering and absorption properties of the dust. The small ($E_{B-V} \leq 0.02$ magnitude) Galactic polar reddening found by Sandage (1973) and Burnstein and Heiles (1978) is consistent with there being little or no correction from face-on to intrinsic color for the disks of spiral galaxies. Even if this correction is not negligible, we need only worry about the differential effect between normal and LSB galaxies. We, therefore, ignore any possible effect on our color comparisons caused by any correction from face-on to intrinsic colors.

The color difference between the LSB and normal disks can be attributed to a difference in metallicity between the old disk populations of the two classes of galaxies. Part of the color difference could be due to a difference in the residual star formation rate in the old disk regions measured. We assume this effect is negligible, although we cannot test the validity of this

assumption. Larson and Tinsley (1978) present a rough·calibration of the change in UBV colors of a galaxy for a change in metal abundance. They give two vectors in the (U-B), (B-V) color plane for a change of metallicity of a factor of 4, one for red galaxies ([U-B] = 0.5, [B-V] = 0.8) the other for blue galaxies ([U-B] = -0.2, [B-V] = 0.6). If we start with the Schweizer disk colors and change the colors as appropriate to changing Z by a factor of 4, interpolation between the two vectors shows (U-B) would be 0.16 magnitude bluer at the lower metallicity and (B-V) 0.1 magnitude bluer. Larson and Tinsley state that the color vectors are uncertain by perhaps a factor of two. The difference in the optical colors of the old disk populations in the LSB and Schweizer galaxies can be plausibly understood as a metallicity difference, with the LSB disk stars a factor of four, or perhaps more, lower in metallicity than those in the Schweizer galaxies.

We have presented two methods of estimating the old stellar population metal abundance: (1) using (J-K) to measure the effective temperature of the giant branch and (2) using the difference in optical colors of the spatially isolated old disk population between the LSB and a sample of normal galaxies. Although both methods clearly have large uncertainties in calibration and observational data, they give similar results: the old stellar population in

the LSB spirals is metal-poor, with a metal abundance per-
haps 1/4 solar.

## 3.3 HII Regions

In this section we use the LSB HII region observa-
tions presented in Section 2.5 to study the metal abundance
in the ionized gas and the mass function of the stars ioniz-
ing the HII regions. The LSB HII regions appear to have a
softer ionizing radiation field than HII regions of similar
metal abundance in normal spirals. We interpret this as a
relative lack of massive stars in the clusters ionizing
these HII regions. The optical colors of the HII regions
also yield evidence for a lack of massive stars. The soft
radiation field makes it difficult to use our measurements
to directly measure the metal abundance in the ionized gas.

We averaged all the spectroscopic and photometric
data presented in Section 2.5 to obtain values for a typ-
ical HII region in a LSB galaxy. Although there are of
course differences among the HII regions in the LSB galax-
ies, as a group these regions are systematically different
than HII regions in normal galaxies. The average values,
along with their standard deviations from the scatter of
the individual measurements are listed in Table 13.

Ideally, to study the ionizing radiation field, we
would like to compare these measurements to measurements of
HII regions of comparable metal abundance in normal

Table 13.   Average LSB HII Region Parameters

Log [OIII]/Hβ = 0.30 (σ = 0.33)   (IIDS only)

Log [OII]/Hβ  = 0.59 (σ = 0.17)   (IIDS only)

Log [SII]/Hα  =-0.48 (σ = 0.19)   (IIDS and
                                   Photographic)

Log Hα/[NII]  = 0.69 (σ = 0.18)  (Photographic
                                   only)

W(Hβ)      = 36 Å (σ = 30)      (IIDS only)

$M_U$       =-13.9 (σ = 0.48)

$A_V$       = 0.6 Mag   (σ = 0.5)

(U-V)      =-0.32 (σ = 0.30)

galaxies. Unfortunately, we cannot directly determine abundances from our data as we did not observe any lines sensitive to the electron temperature.

The [OIII]/Hβ ratio is used as a crude metallicity indicator (see Jensen, Strom and Strom 1976 for a discussion). Therefore, we will compare the line ratios of the LSB HII regions with those of a similar range of [OIII]/Hβ in galaxies of similar type. We took ratios for M 33 and M 101, both Scd galaxies, from Sarazin (1976). We isolated a range in [OIII]/Hβ by taking only those HII regions observed with the IIDS with log [OIII]/Hβ between -0.03 and 0.63, a range within one standard deviation of the LSB average. The average values for the line ratios and W(Hβ) for HII regions with [OIII]/Hβ in the restricted range in both the LSB galaxies and in M 33 and M 101 are listed in Table 14.

The line ratios for the LSB galaxy HII regions with log [OIII]/Hβ between -0.03 and 0.63 were compared with those of the normal galaxies in the same [OIII]/Hβ range. We used the normal z test (Section 3.1) to compare the line ratio samples. The probability that there is no significant difference between both W(Hβ) and [SII]/Hβ in the LSB and normal spirals is less than 0.1%. The probability that [OII]/Hβ does not differ significantly is less than 2%. The differences suggest that the radiation field in the LSB

Table 14. Comparison of HII Regions in
LSBs and M 33, M 101

### LSB with IIDS Observations

| | | |
|---|---|---|
| [OIII]/Hβ | −0.03 $\longrightarrow$ 0.63 | |
| [OII]/Hβ | 0.49 | ($\sigma$ = 0.17) |
| [SII]/Hβ | 0.02 | ($\sigma$ = 0.10) |
| W(Hβ) | 34 Å | ($\sigma$ = 17) |

### M 33, M 101

| | | |
|---|---|---|
| [OIII]/Hβ | −0.03 $\longrightarrow$ 0.63 | |
| [OII]/Hβ | 0.33 | ($\sigma$ = 0.08) |
| [SII]/Hβ | −0.58 | ($\sigma$ = 0.28) |
| W(Hβ) | 105 Å | ($\sigma$ = 38) |

HII regions is softer than the in normal galaxies. The low-ionization lines [OII] and [SII] are stronger relative to Hβ in the LSB galaxies. W(Hβ), which decreases with decreasing hardness of the radiation field (Shields and Tinsley 1976), is smaller. The soft radiation field and consequent strong low-ionization lines could be caused by a large dust-to-gas ratio, or a relative dearth of the hottest, most massive stars, caused either by a steep mass function or a relatively low upper mass limit for stellar masses. These possibilities will be discussed in detail below.

Recall that the [OIII]/Hβ ratio increases with decreasing O/H abundance ratio, as the lower O abundance results in decreased cooling, a higher gas temperature and consequently a higher [OIII]/[OII] ratio. Taking the LSB average [OIII]/Hβ at face value, and a linear fit to the log [OIII]/Hβ -log O abundance values derived by Shields and Searle (1978), we derive a metal abundance slightly less than solar. However, the apparently unusual nature of the ionizing radiation field in the LSB HII regions forces us to reconsider the relation between [OIII]/Hβ and metallicity. Ideally, we would like a grid of detailed HII region models such as those of Sarazin (1976) for various metal abundances and ionizing radiation fields. However, since these models do not exist, we do not know in detail

the behavior of [OIII]/Hβ with differing metal abundance and $T_{upp}$, the effective temperature of the hottest star ionizing the HII region. Below, using W(Hβ), we show that $T_{upp}$ for the LSB regions is in the range 40,000 K to 43,000 K. A grid of simple dust-free HII regions models, for various values of abundances and $T_{upp}$ have been published by Balick and Sneden (1976). From these models, we find that [OIII]/Hβ drops as $T_{upp}$ is lowered from 50,000 K, a typical value for an HII region in M 101 (Shields and Tinsley 1976), to 40,000 K. This implies that the metal abundance inferred from the [OIII]/Hβ ratio for the LSB HII regions must be an upper limit. If there were more hot stars, producing a more normal radiation field, [OIII]/Hβ would increase, resulting in our estimating a lower O abundance. Thus, because of the soft ionizing radiation field in the LSB HII regions, we cannot directly estimate the metal abundance from [OIII]/Hβ, but can only infer an upper limit. We need observations of some lines sensitive to the electron temperature in these HII regions to allow a more detailed chemical abundance analysis.

As Sarazin (1976, 1977) suggests, absorption of ionizing photons by dust can soften the radiation field in an HII region, if the dust absorption cross section varies with frequency in the Lyman continuum. He attributes the W(Hβ) gradient seen in normal galaxies to a decrease in the

dust-to-gas ratio with increasing radius, and implicitly with decreasing metal abundance. High metal abundance (very low [OIII]/Hβ) HII regions can have W(Hβ) values as low as those for the average LSB HII region. The prime argument against dust softening the radiation field in the LSB HII regions is the moderate to low metal abundance inferred above, and the assumption of a correlation of dust-to-gas ratio with metal abundance. We might hope to directly estimate the amount of dust in the HII regions by examining the reddening derived from the Hα/Hβ ratio. The average value of $A_V$ for the LSB HII regions is 0.5 magnitude ($\sigma$ = 0.5). For comparison, we used the values of $A_V$ listed by Smith (1975) for the HII regions in M 101. Dividing the M 101 regions into two groups of equal number on the basis of metallicity, we find an average $A_V$ of 0.5 magnitude ($\sigma$ = 0.5) for the high metal abundance group and 0.7 magnitude ($\sigma$ = 0.5) for the low metal abundance group. Thus, there is apparently no correlation of reddening and metallicity, and implicity dust-to-gas ratio, detectable from the optical data alone. We can only note that the reddening of the LSB HII regions is similar to that derived in the same way for metal-poor HII regions in M 101. We believe it unlikely that dust-driven radiation softening is a significant effect in the LSB HII regions as compared with normal galaxies primarily because of the overall low

metallicity of the LSB galaxies, which we take to imply a
low dust-to-gas ratio.

Unfortunately, we do not have enough data on any
one galaxy to say very much about the presence or absence
of abundance gradients in the ionized gas across the galac-
tic disk.  The fragmentary data which we do have suggests
the presence of a small gradient in [OIII]/Hβ, of the order
of 0.4 dex, from center to outer regions in a typical LSB
spiral.  In M 33 and M 101, [OIII]/Hβ changes by at least
2.0 dex from the center to the outer regions of the galaxy.

If we assume the low value of W(Hβ) in the LSB HII
regions is caused by a lack of massive, hot ionizing stars,
what can we learn about the IMF or upper stellar mass limit
($M_{upp}$) in the ionizing star clusters?  Shields and Tinsley
(1976) present a quantitative discussion of W(Hβ) of an HII
region as a function of the parameters of its ionizing star
cluster.  They consider an HII region ionized by a star
cluster with a power-law IMF:

$$\frac{dN}{d(\log M)} = CM^{-x} \tag{18}$$

where M is the stellar mass and N is the number of stars
per unit mass interval.  They find that the outer regions
in M 101, such as NGC 5471 (W(Hβ) = 165 A) require ionizing
clusters with $T_{upp}$, the temperature of their hottest star,
of about 55,000 K.  They present a graph of W(Hβ),

normalized to the value for NGC 5471, for various values of $T_{upp}$ and two values of x, representing a flat (x $\cong$ 0.5) and a steep (x $\cong$ 3.0) IMF. The average LSB HII region has a value of log W(H$\beta$) about 0.7 dex smaller than that for NGC 5471. Using the Shields and Tinsley graph, we find the LSB HII region $T_{upp}$ is about 40,000 K for a steep IMF and 43,000 K for a flat IMF. These $T_{upp}$ can be converted to approximate $M_{upp}$, by using the main-sequence models of Chiosi, Nasi and Sreenivasan (1978). The corresponding $M_{upp}$ are about 30 $M_{\odot}$ for the steep IMF and 40 $M_{\odot}$ for the flat IMF. These values are far below the $M_{upp}$ of ~ 100 $M_{\odot}$ required for NGC 5471 ($T_{upp}$ = 55,000 K). Are there other differences between the LSB and M 101 HII regions which can account for this difference, or is $M_{upp}$ actually different in the LSB and M 101 HII regions? One difference between the LSB and M 101 HII regions which could be important is the absolute luminosities of the HII regions. An apparently small value of $M_{upp}$ might be due to the relative rarity of very massive stars, even for a normal IMF, for intrinsically faint clusters of low population. The absolute magnitudes of the 3 brightest HII regions in M 101 are given by Sandage and Tammann (1974b). After applying a correction for extinction, using the values of $A_V$ given by Smith (1975) for these HII regions, we find their average absolute U magnitude, $M_U$, to be -16.6 ($\sigma$ = 0.27). From

Section 2.5, we find the average $M_U$ for the brightest HII

regions in the LSB galaxies, (the ones chosen to be ob-

served with the IIDS), to be -13.9 ($\sigma$ = 0.48). Below, we

present a quantitative discussion of the possible impor-

tance of the low absolute magnitude of the ionizing clus-

ters of the LSB HII regions, by means of simple models of

these star clusters. The aim is to answer the following

question: Is $M_{upp}$ or the IMF significantly different in

the LSB HII regions as compared to those in M 101?

The model calculations were carried out as follows:

1. We assumed an IMF with separate power-law sections

from 0.1-2 $M_\odot$, 2-10 $M_\odot$ and 10-60 $M_\odot$. This approximates the

behavior of the IMF found by Miller and Scalo (1979) who

find that the slope of the IMF changes with mass. We found

the number of stars in small mass ranges for various combi-

nations of x for the three power law sections. We calcu-

lated the number versus mass interval for a cluster

containing $10^3$ $M_\odot$ in the lowest mass range. The separate

power-law sections were normalized to join smoothly at the

mass where the value of x changed.

2. We found the total absolute magnitude $M_V$ and inte-

grated color (U-V) by multiplying the number of stars in

each mass interval by the intensity corresponding to the

absolute V and U magnitudes for each star, and summing over

all mass intervals. The U and V absolute magnitudes were

derived from $M_V$-log $(M/M_\odot)$ and $(U-V)$-$M_V$ relations for main sequence stars. For log$(M/M_\odot) < 0.0$, data from Allen (1973) was used. For $0.0 <$ log$(M/M_\odot) < 1.0$, data comes from the models of Kelsall and Stromgren (1969), using the bolometric corrections of Code et al. (1976). Data for the most massive stars $(1.0 <$ log$(M/M_\odot) < 2.0)$ was taken from the models of Chiosi et al. (1978) using the bolometric corrections of Morton (1969). The following simple relations were found to adequately represent the $M_V$-log$(M/M_\odot)$ data:

$$M_V = -10.7 \text{ log}(M/M_\odot) + 4.8 \quad , \quad \text{log}(M/M_\odot) < 0.0 \qquad (19)$$

$$M_V = -6.46 \text{ log}(M/M_\odot) + 4.8 \quad , \quad 0.0 < \text{log}(M/M_\odot) < 1.3 \qquad (20)$$

$$M_V = -3.43 \text{ log}(M/M_\odot) + 0.9 \quad , \quad 1.3 < \text{log}(M/M_\odot) < 2.0 \qquad (21)$$

The $(U-V)$-$M_V$ relation was derived from the main sequence colors listed by Allen (1973). The following adequately represents the $(U-V)$-$M_V$ data:

$$(U-V) = -1.4 \qquad\qquad , \quad M_V < -4 \qquad (22)$$

$$(U-V) = 0.26 \, M_V - 0.38 \quad , \quad -4 < M_V < 6 \qquad (23)$$

$$(U-V) = 0.62 \, M_V - 2.55 \quad , \quad M_V < 6 \qquad (24)$$

Since the models use only main sequence colors, they will be strictly correct only for young clusters. Since we chose the brightest, and hence probably youngest clusters

to observe spectroscopically, this is adequate, at least
for a first look at the properties of the clusters.

The results of three model calculations are listed
in Table 15. This table lists, for each set of x values,
the number of massive stars in various mass ranges for a
cluster with $M_U = -14$, and the cluster's (U-V) color.
Model A uses an approximation to the Miller and Scalo (1979)
solar neightborhood IMF. Model B uses an approximation to
the IMF for massive stars found by Ostriker, Richstone and
Thuan (1974). Both these models predict on the order of
100 stars more massive than about 40 $M_\odot$. Since the value
of W(Hβ) in the LSB HII regions requires a $M_{upp}$ of 40 $M_\odot$ or
less, there must be a real cutoff in the stellar mass dis-
tribution if the model IMFs are valid. Model C has a very
steep massive star IMF, for which W(Hβ) would imply $M_{upp} \cong$
30 $M_\odot$. This model predicts a significant number of stars
(at least 50) above 30 $M_\odot$. Thus, there is probably a real
cutoff in the number of stars above 30 $M_\odot$ or so.

The HII region (U-V) colors can also be used to
study the IMF. The average (U-V) for the LSB HII regions
is -0.32 (σ = 0.30). Models A and B have (U-V) signifi-
cantly bluer than -0.32. The color of model C agrees well
with the average LSB HII region color. Obviously, this
model is not unique, but offers a consistency argument for
a steep massive star IMF. We note that changing $M_{upp}$ from

Table 15. Model Stellar Clusters with $M_U = -14$

| | x | | | Number of Stars in Various Mass Ranges | | | |
|---|---|---|---|---|---|---|---|
| Model | 0.1-2 $M_\odot$ | 2-10 $M_\odot$ | 10-60 $M_\odot$ | 20-35 $M_\odot$ | 35-45 $M_\odot$ | 45-60 $M_\odot$ | (U-V) |
| A | 1. | 1.3 | 2.3 | 900 | 150 | 90 | -1.0 |
| B | 1. | 2.3 | 2.6 | 800 | 130 | 80 | -0.8 |
| C | 1. | 3. | 3.5 | 350 | 30 | 15 | -0.3 |

60 $M_\odot$ to 35 $M_\odot$ changes the integrated (U-V) by only a few hundredths of a magnitude, so the presence of a mass cutoff does not effect this conclusion. It is also of interest to compare the colors of the LSB HII regions with those of the brightest HII region in M 101. The average (U-V) for the M 101 regions, corrected for internal reddening using the $A_V$ values found by Smith (1975), is -0.99 ($\sigma = 0.35$). The normal z test (Section 3.1) shows that the probability that the (U-V) colors of the LSB and M 101 HII regions do not differ is less than 0.1%. It is interesting to note that the (U-V) of the M 101 HII regions agrees with the predicted (U-V) from the model using the Miller and Scalo (1979) IMF.

Although the models presented here are very simplified, we make the following tentative conclusions:

1. If the IMF in the LSB HII regions clusters is similar to that presented by Miller and Scalo (1979) or Ostriker et al. (1978), there is an upper mass limit of about 30-40 $M_\odot$. Even with a steep massive star IMF, there must be few if any stars with masses above 30 $M_\odot$ or so to match the W(H$\beta$) data.

2. The rather red (U-V) colors of the LSB HII regions imply a steep IMF for the massive stars, with x on the order of 3 to 4.

Thus, the low W(Hβ) and red (U-V) colors found for the LSB HII regions require a steep IMF for massive stars, with very few stars above 30-40 $M_\odot$. There appears to be a real lack of massive stars in the LSB HII region star clusters compared to HII regions in the outer parts of M 101. This suggests some global difference in star-forming activity between the LSB and normal galaxies. It would be interesting to observe intrinsically faint HII regions in M 101. If they also have small W(Hβ), we can assume that $M_{upp}$ is a function of the absolute size of the star-forming region, or that there is some gross error in the simple models presented here.

The steep IMF implied for massive star formation in the LSB galaxies may be inconsistent with the broad-band optical colors. Approximate broad-band colors for the LSB galaxies, found from the average total (U-R) photographic color (1.14) and the color interpolation equations, are (U-B) = 0.0, (B-V) = 0.6. From the models of Huchra (1977) and Larson and Tinsley (1978), it would appear impossible to produce a color this blue, even with a constant star formation rate, with x = 3-4. However, the low metallicity of the LSB galaxies will make the galaxies bluer than the simple models predict. It would be very interesting to produce models of evolving galaxies using stellar models of low metal abundance.

## 3.4 Spiral Structure

In this section, we present a discussion of some aspects of the spiral structure of the LSB galaxies. We derive estimates of the strength or amplitude of the spiral pattern in a few LSB galaxies, using methods similar to those of Schweizer (1976). We examine the LSB galaxies in the context of the Roberts, Roberts and Shu (1975) picture of the density wave theory of spiral structure.

In the density wave theory of spiral structure, spiral arms are a manifestation of a rigidly-rotating density wave pattern in the disk mass distribution. The wave pattern rotates with a constant angular velocity $\Omega_p$, while the angular velocity of the material in the galaxy as a function of galactic radius, $\tilde{\omega}$, is $\Omega(\tilde{\omega})$. The velocity component of the disk gas (assumed to be in circular motion around the galactic center) normal to a spiral arm is $w_\perp$:

$$w_\perp = \tilde{\omega} \, (\Omega - \Omega_p) \, \sin i \qquad (25)$$

where i is the pitch angle of the spiral arms. If $w_\perp$ is larger than the sound speed in the gas, $a_s$, gas will approach the crest of the density wave at a supersonic velocity, and a shock front will form. In this picture, compression of gas clouds behind the shock front is responsible for the initiation of star formation, and can therefore

account for the presence of newly-formed stars near the crest of the density wave (Shu 1975).

One important recent discovery, discussed by Schweizer (1976) and Jensen (1977), is the existence of broad spiral density patterns in the underlying old (red) disk stars in spirals. This pattern is most readily understood as a manifestation of a density wave in the mass distribution. From visual inspection of R photographs of the LSB spirals we find some show fairly well-developed global density wave patterns. Examples of such galaxies are: NGC 4411A, UGC 06983, UGC 04841 and NGC 4517A. Others, such as UGC 07557 and NGC 3913, show substantial fragments of such a pattern. Others show little evidence of a global spiral pattern.

Photographs of all LSB galaxies with 4-m plates are shown in Figure 6. These were produced by photographing the digital images displayed on a precision CRT. The contrast has been chosen to try to bring out faint spiral features.

Following Schweizer (1976) we define the quantity A to be the amount of light in the arms, defined as all the light above the underlying axisymmetric disk, and D to be all non-arm light, including light from the underlying disk and central bulge. The quantity A/(D+A) measures the fraction of the total light emitted by the arms. We found the

Figure 6. Photographs of LSB Galaxies--
        Most photographs are 4 arcmin on a side.
        Those showing NGC 5774-5 and NGC 45 are
        8 arcmin on a side.
        p. 116   NGC 4411A, NGC 4411B
        p. 117   NGC 3913, UGC 06922
        p. 118   UGC 06983
        p. 119   UGC 07557, DDO 144
        p. 120   NGC 4517A
        p. 121   DDO 142
        p. 122   DDO 146
        p. 123   NGC 5774-5
        p. 124   UGC 04841, DDO 102
        p. 125   UGC 11868, UGC 04922, NGC 45, UGC A0333
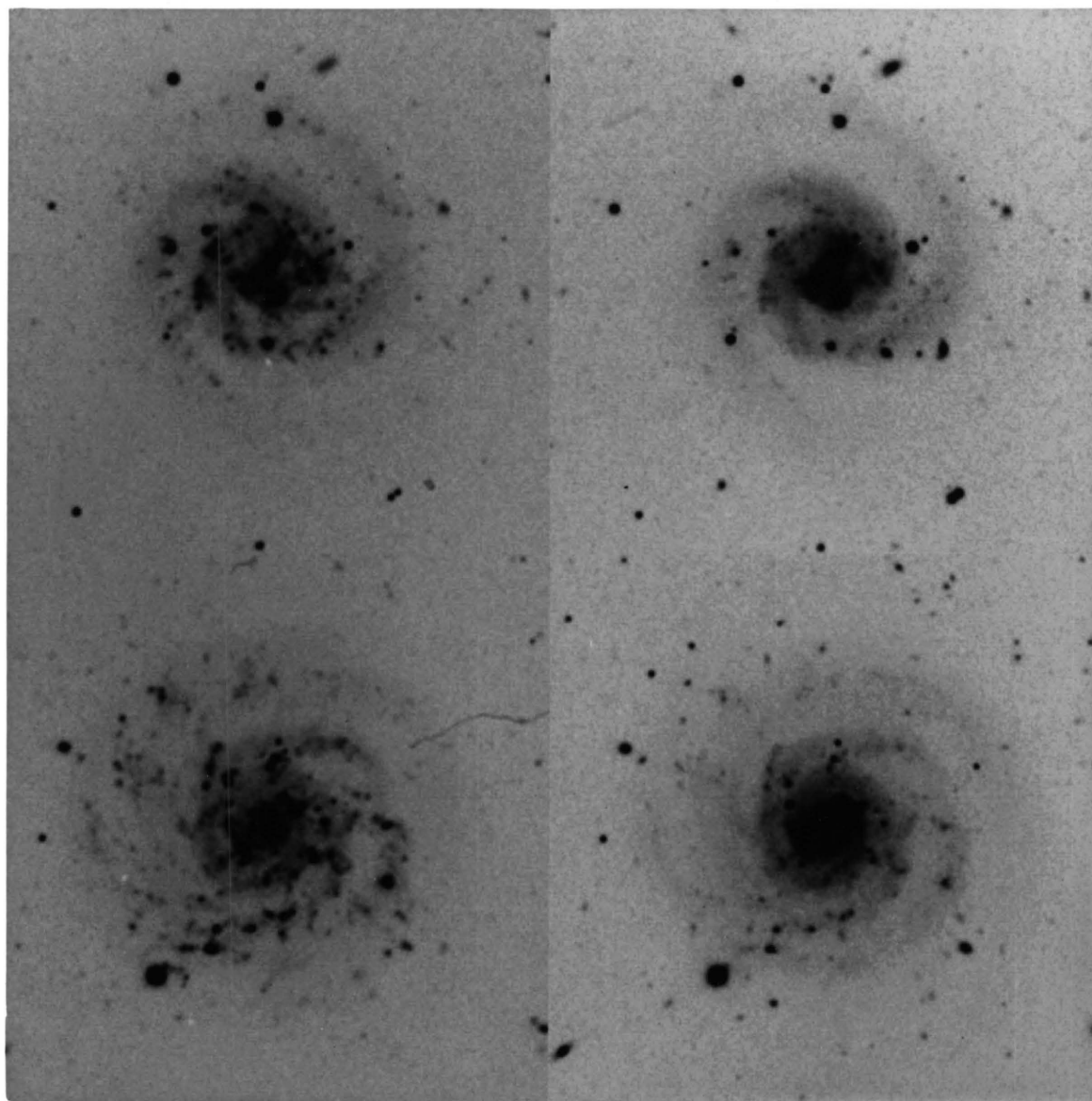
Figure 6. Photographs of LSB Galaxies

upp. left- NGC 4411A (U) , upp. right- NGC 4411A (R)
low. left- NGC 4411B (U) , low. right- NGC 4411B (R)
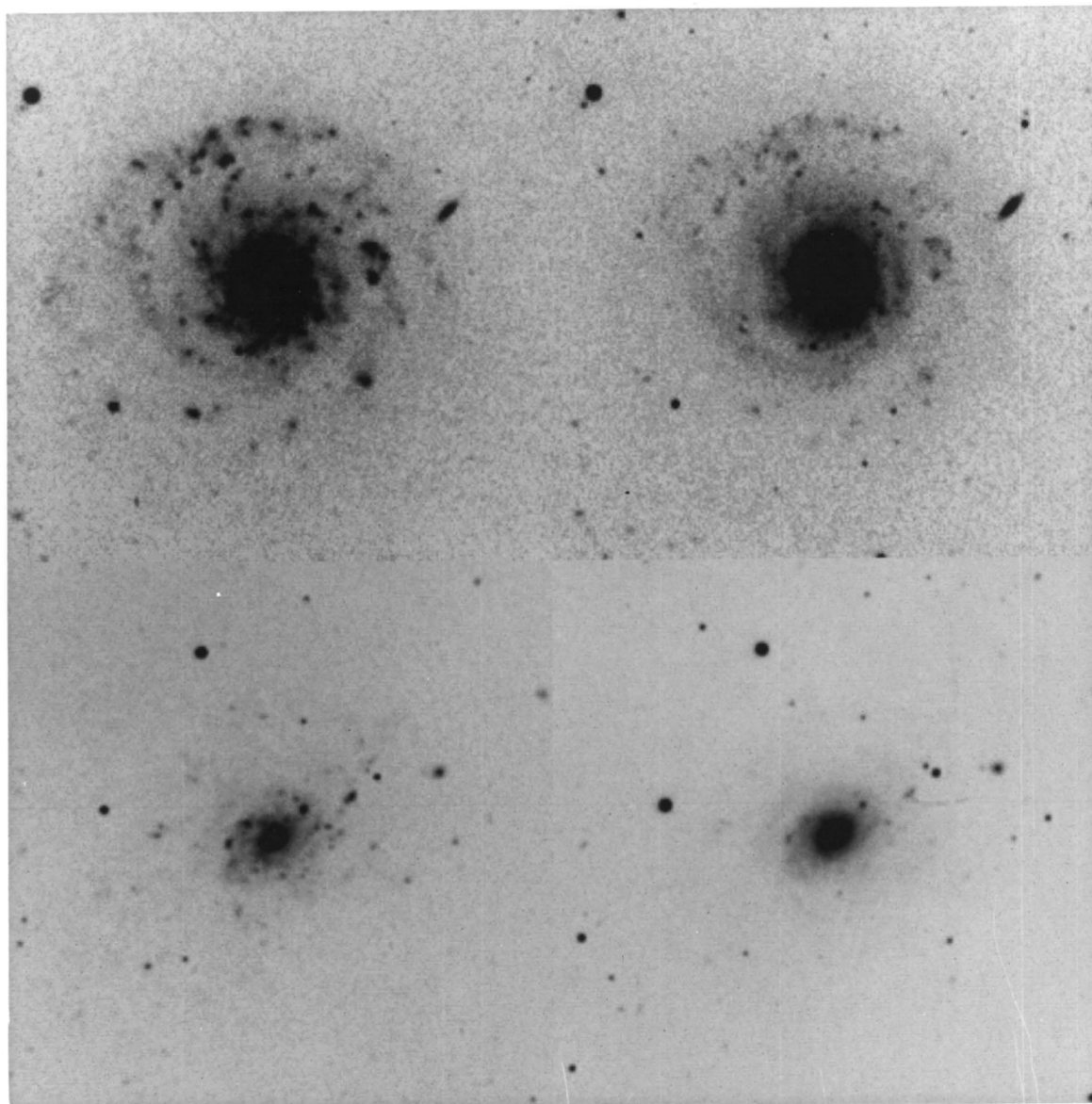
Figure 6. <u>Continued</u>.-- Photographs of LSB Galaxies

upp. left- NGC 3913 (U) , upp. right- NGC 3913 (R)
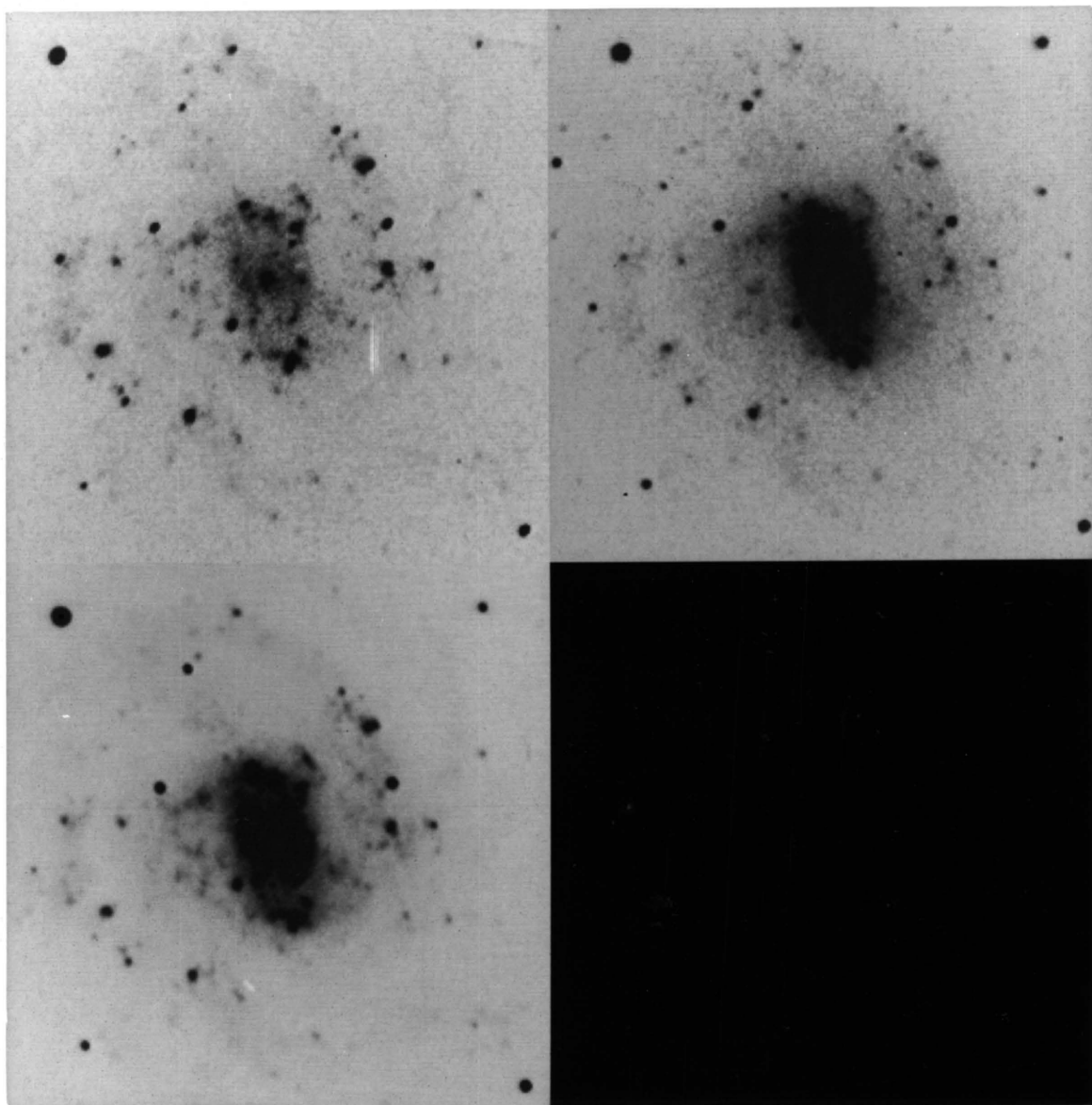low. left- UGC 06922 (U) , low. right- UGC 06922 (R)
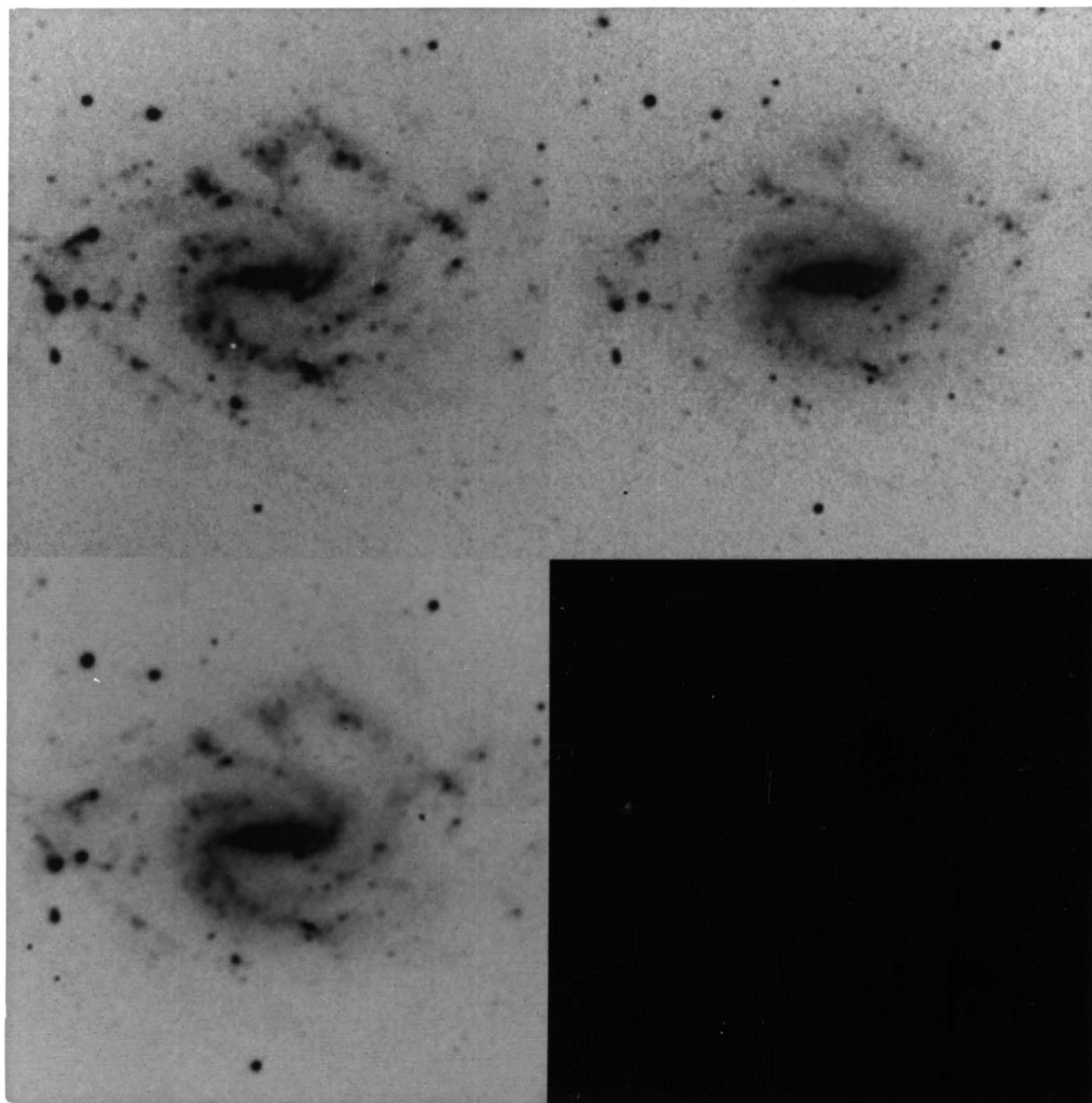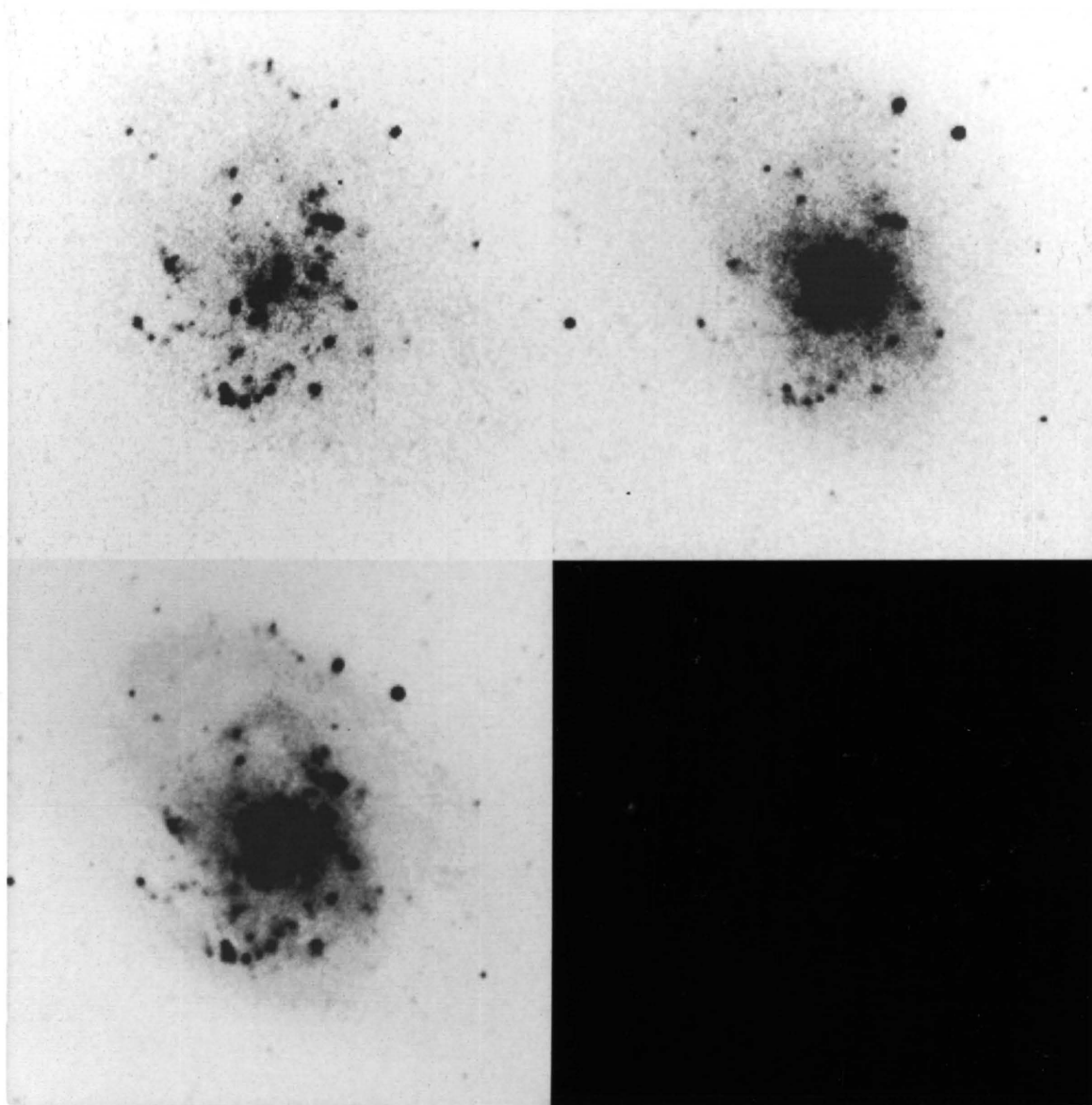
Figure 6. <u>Continued</u>.-- Photographs of LSB Galaxies

upp. left- UGC 06983 (U) , upp. right- UGC 06983 (R)
low. left- UGC 06983 (B)
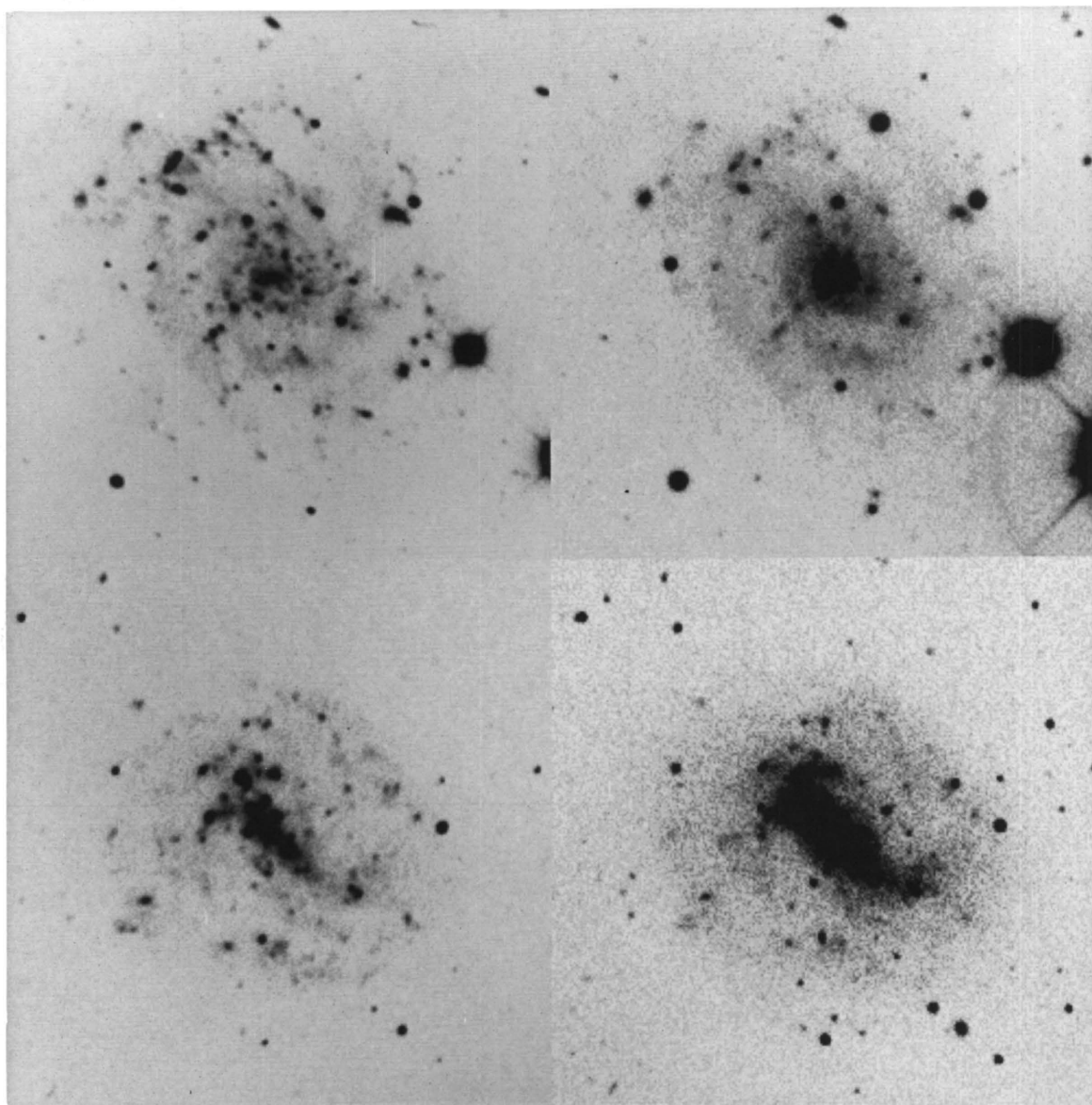
Figure 6. <u>Continued</u>.-- Photographs of LSB Galaxies

upp. left- UGC 07557 (U) , upp. right- UGC 07557 (R)
low. left- DDO 144 (U) , low. right- DDO 144 (R)
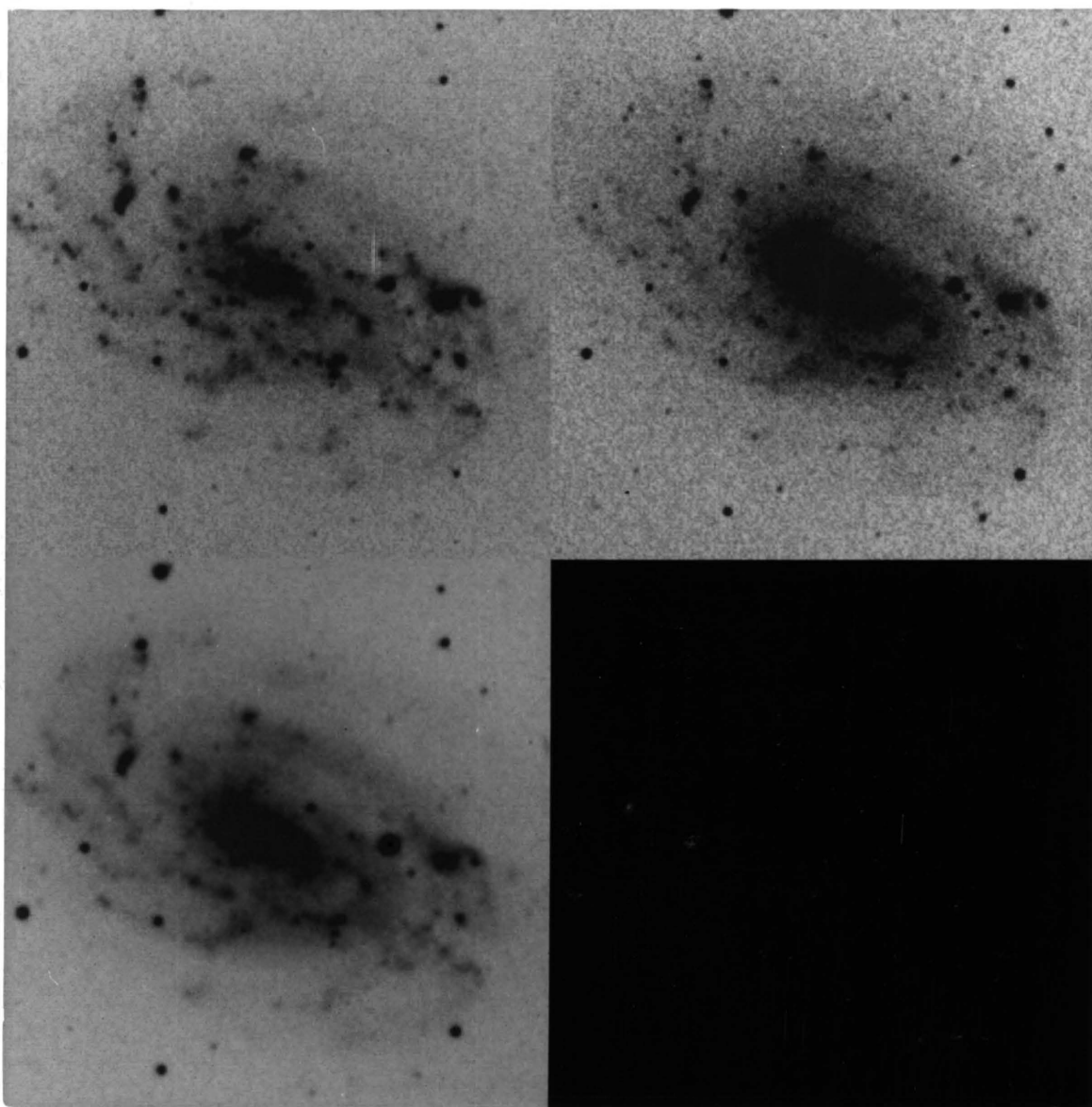
Figure 6. <u>Continued</u>.-- Photographs of LSB Galaxies

upp. left- NGC 4517A (U) , upp. right- NGC 4517A (R)
low. left- NGC 4517A (B)

Figure 6. <u>Continued</u>.-- Photographs of LSB Galaxies

upp. left- DDO 142 (U) , upp. right- DDO 142 (R)
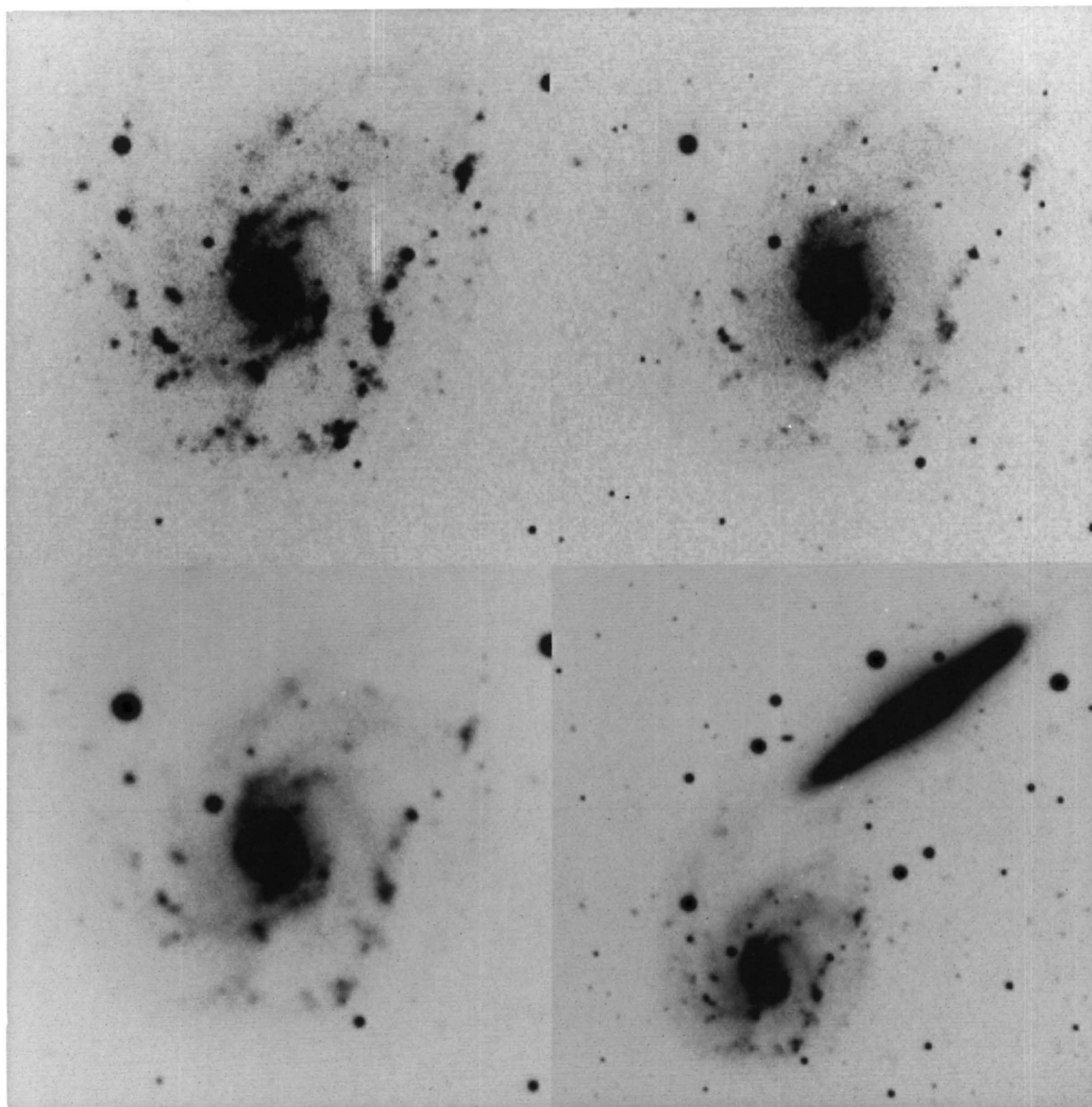low. left- DDO 142 (B)

Figure 6. <u>Continued</u>.-- Photographs of LSB Galaxies

upp. left- DDO 146 (U) , upp. right- DDO 146 (R)
low. left- DDO 146 (B)

Figure 6. <u>Continued</u>.-- Photographs of LSB Galaxies

upp. left- NGC 5774 (U) , upp. right- NGC 5774 (R)
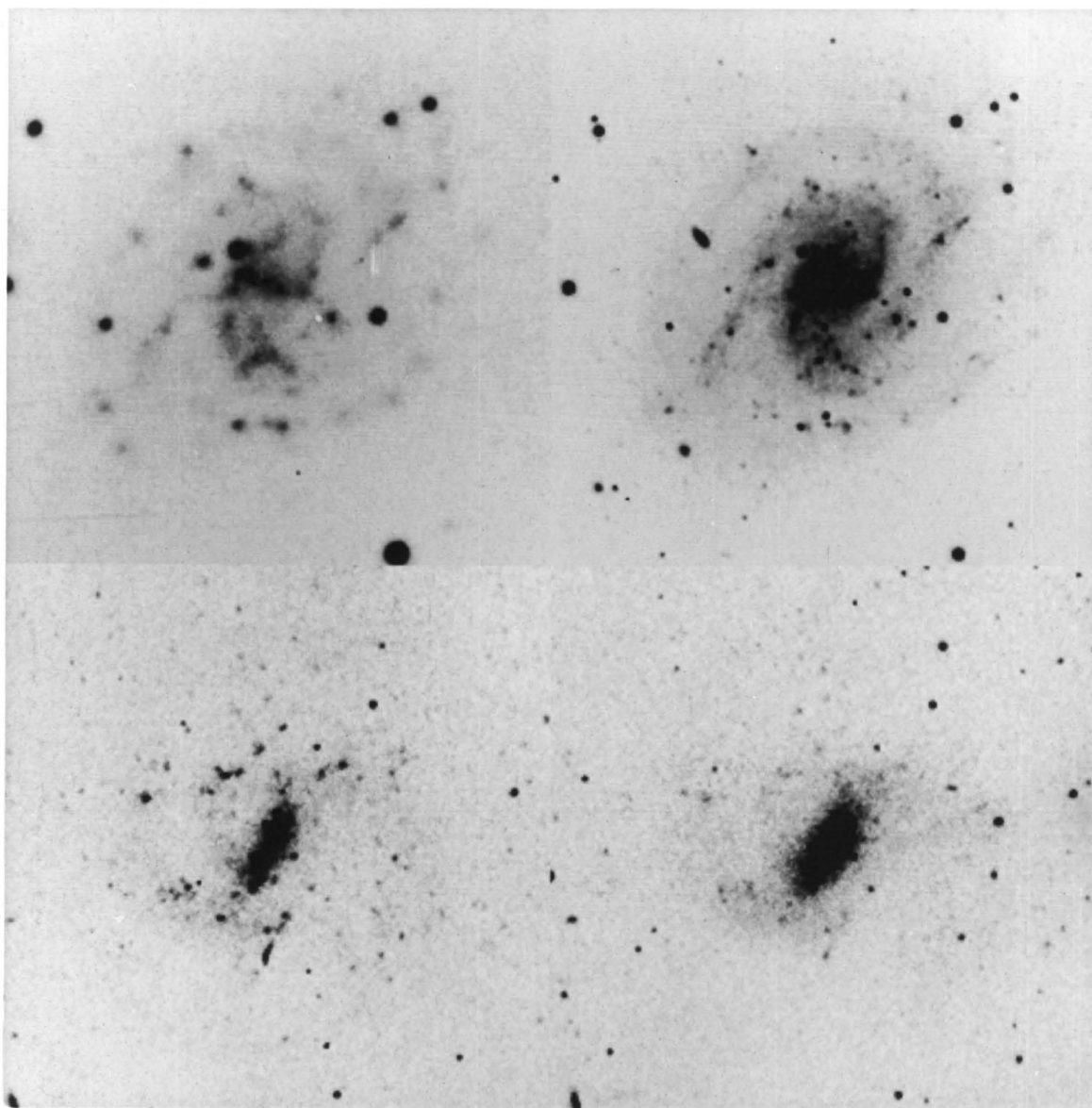low. left- NGC 5774 (B) , low. right- NGC 5774-5 (B)

Figure 6. <u>Continued</u>.-- Photographs of LSB Galaxies

upp. left- UGC 04841 (U) , upp. right- UGC 04841 (R)
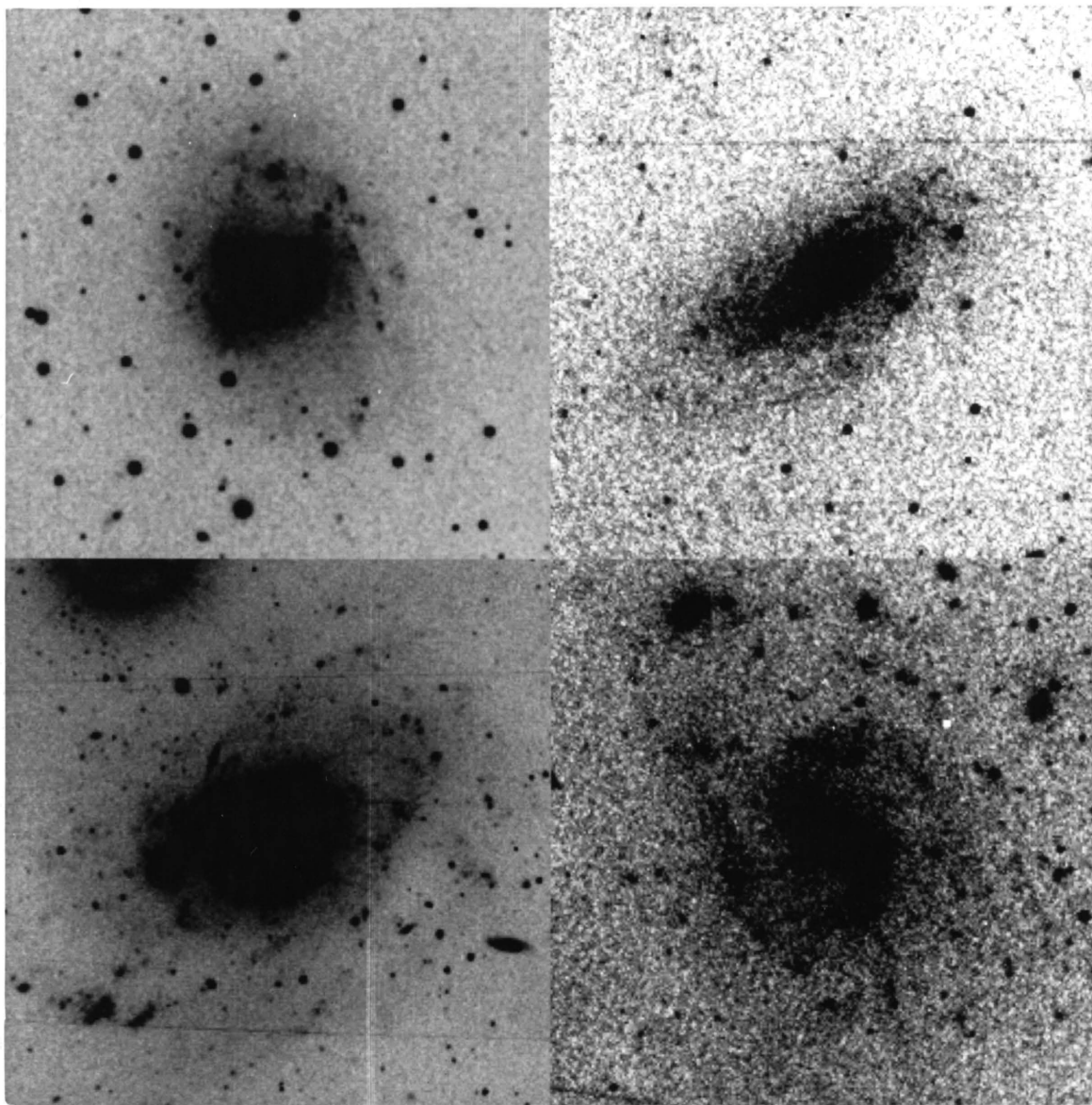low. left- DDO 102 (U) , low. right- DDO 102 (R)

Figure 6. <u>Continued</u>.-- Photographs of LSB Galaxies

upp. left- UGC 11868 (R) , upp. right- UGC 04922 (R)
low. left- NGC 45 (R) , low. right- UGC A0333 (R)

level of the underlying disk by measuring the surface
brightness at a number of points chosen to lie between the
spiral arms. These points fell roughly on a straight line
in the surface brightness versus radius plot, implying an
exponential falloff in intensity, as expected for the disk
component. We fit a straight line to the points in the
surface brightness versus radius plot, to define the under-
lying disk intensity. By comparing the azimuthal luminosity
profiles with the surface brightness of the disk, we could
measure A/(D+A), since the azimuthal profiles measure the
sum of the light in the arms and disk. This assumes that
all the light above the disk level is contributed by the
arms. This assumption is probably valid for galaxies with
well-developed arms, but becomes invalid as the galaxies
become more irregular.

Another parameter measured by Schweizer (1976) is
$\Delta P$, the peak brightness of the arms above the disk, ex-
pressed as a magnitude difference. This is a measure of
the peak-to-trough contrast in the wave pattern. We esti-
mated this quantity for a few LSB spirals by measuring the
surface brightness in a number of small areas along the
crest of the wave and comparing this to the level of the
underlying disk at the same radius.

The quantities A/(D+A) and $\Delta P$, measured for three
LSB spirals with well or moderately well-developed spiral

arms, are listed in Table 16, along with the parameters for
the four giant spirals measured by Schweizer (1976) which
have U measurements. The values of A/(D+A) listed for the
LSB galaxies overlap those of the giant spirals. Thus, the
LSB spirals can have wave amplitudes comparable to those of
the giant spirals studied by Schweizer. However, from
visual appearance, some of the LSB galaxies have signifi-
cantly smaller wave amplitudes than those listed in Table
16.

At a given value of A/(D+A), ΔP appears to be smal-
ler in the LSB galaxies than in the spirals studied by
Schweizer (1976). This would be consistent with the pres-
ence of only weak shock fronts in the gas in the LSB spirals,
as discussed below. For a given amplitude of the broad
spiral wave pattern, as measured by A/(D+A), we expect a
smaller ΔP for galaxies with weak shocks, as the gas com-
pression and hence star formation rate would be lower.

Roberts et al. (1975) have found that the character-
istics of the spiral density wave pattern depend primarily
on two global properties of a galaxy: the degree of central
concentration of the mass, and the total mass divided by
the corotation radius, $\tilde{\omega}_c$, the radius where $\Omega(\tilde{\omega}) = \Omega_p$.
Roberts et al. (1975) have studied a selection of 24 spiral
galaxies with published rotation curves. For each galaxy
in their sample, they estimated $w_{\perp o}$, the shock velocity at

Table 16. Arm Strength Parameters

| | A/(D+A) | | | ΔP (Magnitudes) | | |
|---|---|---|---|---|---|---|
| | U | B | R | U | B | R |
| **LSBs:** | | | | | | |
| NGC 3913 | 0.11 | | 0.09 | 0.39 | | 0.30 |
| UGC 06983 | 0.37 | 0.28 | 0.19 | 0.79 | 0.67 | 0.50 |
| NGC 4411A | 0.53 | | 0.34 | 0.83 | | 0.66 |
| **Schweizer Late-type Spirals:** | | | | | | |
| NGC 3031 | 0.22 | 0.12 | 0.11 | | 1.03 | |
| NGC 5457 | 0.37 | 0.28 | 0.25 | | 1.58 | |
| NGC 4321 | 0.42 | 0.31 | 0.28 | | 1.01 | |
| NGC 4254 | 0.54 | 0.46 | 0.41 | | 1.58 | |

one-half the corotation radius, as a function of $M/\tilde{\omega}_c$,
where M is the total galactic mass, and $\tilde{\omega}_{0.5M}/\tilde{\omega}_c$, where
$\tilde{\omega}_{0.5M}$ is the radius containing half of the total mass. The
first step in estimating $w_{\perp 0}$ using their method is to de-
termine $\tilde{\omega}_c$. They estimate $\tilde{\omega}_c$ from the maximum radial ex-
tent of three indicators: (1) the prominent spiral
structure, (2) the "easily visible" disk, and (3) the dis-
tribution of HII regions. The radii of the "easily visible"
disk listed for galaxies in Roberts et al. (1975) corre-
sponds to about 0.8 times the de Vaucouleurs radius
$r_{deV}$. The radii of the outermost HII regions in the LSB
galaxies corresponds to about 1.2 $r_{deV}$. We have, there-
fore, adopted $r_{deV}$ as a suitable and well-defined estimate
of $\tilde{\omega}_c$ for our galaxies. The other parameter we need for
this analysis is the total mass M. Most observed rotation
curves do not exhibit a falloff after the initial rise, and
thus the total mass is not defined. Roberts et al. (1975)
use an analytic continuation of the observed rotation
curves, based on the disk mass models of Toomre (1963), to
compute a well-defined and finite galactic mass. This fit
allows for a falling rotation curve after the peak observed
velocity. We estimated the total mass of the LSB galaxies
by extending their observed rotation curves from the last
observed point to 1.2 Holmberg radii, using a falling
velocity with slope equal to 0.3 times the maximum velocity

per Holmberg radii.  The slope was estimated from the rotation curve for NGC 157 illustrated in Roberts et al. (1975). The outer integration limit was derived by applying our simple procedure to the rotation curve of NGC 4236 (Shostak 1973), and finding the radius where our mass matched that given by the Toomre (1963) rotation curve fit.  The rotation curve of NGC 4236 is very similar in shape, maximum velocity, and observed radial extent to the observed rotation curves for the LSB galaxies.  Table 17 lists the parameters for the three LSB galaxies with rotation curves (see Section 3.7) and two galaxies with similar parameters from Roberts et al. (1975), M 33 and NGC 4236.  In both the important parameters, the central mass concentration and $M/\tilde{\omega}_c$, the LSB spirals lie between the corresponding parameters for M 33 and NGC 4236.  The value of $w_{\perp 0}$ for M 33 is 8.3 km/sec, for NGC 4236, 6.9 km/sec.  The value of $w_{\perp 0}$ for the LSB galaxies should also lie in this range.

Since the sound speed, $a_s$, probably lies in the range 7-12 km/sec, the value of $w_{\perp 0}$ in the LSB galaxies is low.  We would therefore expect only a weak shock front, if any, to form in the LSB galaxy spiral arms.  Naively, we might try to associate the deficiency of massive stars, found in our HII region analysis, with the weakness of the shock.  However, M 33, with a similar value of $w_{\perp 0}$, does appear to contain many more massive stars than the LSB

Table 17.  Roberts, Roberts and Shu Parameters

| | M $(10^{10}M_{\odot})$ | $\tilde{\omega}_c$ (kpc) | $\tilde{\omega}_{0.5M}$ (kpc) | $M/\tilde{\omega}_c$ | $\tilde{\omega}_{0.5}/\tilde{\omega}_c$ |
|---|---|---|---|---|---|
| NGC 4517A | 1.8 | 9.7 | 10.0 | 0.19 | 1.0 |
| UGC 06983 | 1.8 | 7.7 | 6.5 | 0.23 | 0.8 |
| UGC 07557 | 1.8 | 5.9 | 5.5 | 0.31 | 0.9 |
| M 33 | 1.3 | 2.8 | 3.5 | 0.46 | 1.2 |
| NGC 4236 | 1.7 | 9.6 | 6.9 | 0.18 | 0.7 |

galaxies. This is indicated by the value of the average equivalent width of Hβ in the M 33 HII regions, which is over three times than in the LSB HII regions (Searle 1971). The density wave theory offers no simple explanation for the difference between the initial mass function in the LSB galaxies and a normal galaxy, M 33, which has a similarly low value of $w_{\perp o}$.

### 3.5 Surface Mass Density

In this section, we compare the average surface mass density of LSB and normal late-type galaxies. Galaxies with differing surface mass densities are expected to evolve at different rates, as indicated in the models of Talbot and Arnett (1975). Their models show that galaxies with a low surface mass density should have a higher neutral hydrogen content and bluer colors than galaxies with a high surface mass density. We make no direct comparison between our data and the Talbot and Arnett models, as they assumed an IMF with $x = 1.35$, significantly different from the IMF we believe applicable in the LSB galaxies. The surface mass density is also of interest as a fundamental structural parameter of any disk galaxy. We expect the LSB galaxies to have a low average surface mass density, provided they have a normal mass-to-light ratio.

We calculated the average surface mass density $(\sigma_{0.5M})$ within the radius containing half the total mass as:

$$\sigma_{0.5M} = (1/2 \ M)/(\pi \tilde{\omega}^2_{0.5M}) \tag{26}$$

where $\tilde{\omega}_{0.5M}$ is the radius containing half the total mass
M, as in Section 3.4. Values of $\sigma_{0.5M}$ are listed in Table
18 for the three LSB galaxies with rotation curves (Section
3.6) and all galaxies of type Scd or later from Roberts et
al. (1975). As $\sigma_{0.5M}$ is distance-dependent, we corrected
all distances for the normal galaxies to the Sandage-
Tammann distance scale used for the LSB galaxies, using in-
dividual galaxy distances from Sandage and Tammann (1974a
and 1974c). For the normal late-type galaxies, the average
value of $\sigma_{0.5M}$ is 142 $M_\odot$/pc ($\sigma = 73$), while for the LSB
galaxies the average is 64 $M_\odot$/pc ($\sigma = 33$). The normal z
test (Section 3.1) shows the probability that the mean of
$\sigma_{0.5M}$ for the two samples does not differ is less than 2%.
The galaxy NGC 4236, one of the Roberts et al. galaxies,
has a value of $\sigma_{0.5M}$ lower than the LSB galaxy average.
This galaxy is an excellent example of a galaxy which would
have been placed on the LSB observing list had it not been
for its large angular size (diameter > 12 arcmin).

The surface mass density, along with the velocity
dispersions in the stars and gas, controls the scale heights
of the two mass components. For a given velocity disper-
sion, the lower the surface mass density, the larger the
scale height. Thus the LSB galaxies, with their low average

Table 18.  Surface Mass Density

|  | $\sigma_{0.5M}$ $(M_{\odot}/pc^2)$ |
|---|---|
| **LSBs:** | |
| NGC 4517A | 29 |
| UGC 06983 | 68 |
| UGC 07557 | 95 |
| Average | 64 ($\sigma$ = 33) |
| | |
| **Late-type Spirals from Roberts et al. (1975):** | |
| NGC 598 | 142 |
| NGC 925 | 56 |
| NGC 2403 | 181 |
| NGC 4236 | 57 |
| NGC 4631 | 88 |
| NGC 5457 | 186 |
| NGC 6946 | 267 |
| IC 342 | 161 |
| Average | 142 ($\sigma$ = 73) |

surface mass density, should have scale heights larger than
normal galaxies. It would be very interesting to observa-
tionally compare the scale heights and velocity dispersions
of the LSB and normal galaxies.

### 3.6 Neutral Hydrogen Content

One method of measuring the relative neutral hydro-
gen content of galaxies is to divide the total hydrogen
mass, $M_H$, by some measure of the luminosity, L. Some au-
thors derive luminosities from Holmberg magnitudes, others
use de Vaucouleurs magnitudes. Different authors use dif-
ferent corrections to the observed luminosity to account
for Galactic and internal extinction, in an attempt to de-
rive a true, or at least a face-on, luminosity. The
average $M_H/L$ at a given Hubble type can vary by as much as
0.2 dex (60%) depending on the sample used and the proce-
dure for deriving L (Sullivan and Johnson 1978). We com-
pute luminosities using the de Vaucouleurs $B_T$ magnitude
system. We corrected our total B magnitudes for Galactic
and internal extinction following the precepts of de Vaucou-
leurs et al. (1976). For the internal absorption correc-
tion, we assumed all galaxies were of type Sd. Any
uncertainty caused by this will be negligible, as the gal-
axies are mostly face-on, so the internal absorption correc-
tions are small. Table 19 lists the fully corrected B
magnitude, $B_T^O$, and $M_H/L_B$ for the LSB galaxies. Also listed

Table 19.  Hydrogen Mass to Luminosity Ratio

| | $B_T^o$ | $M_H/L_B$ (solar units) |
|---|---|---|
| NGC 45 | 11.13 | 1.14 |
| UGC 04841 | 12.83 | 0.60 |
| UGC 04922 | 13.50 | 0.65 |
| NGC 3913 | 13.09 | 0.33 |
| UGC 06922 | 13.97 | 0.56 |
| UGC 06983 | 12.71 | 0.74 |
| NGC 4411A | 13.46 | 0.40 |
| NGC 4411B | 12.88 | 0.36 |
| UGC 07557 | 13.28 | 0.87 |
| NGC 4517A | 12.55 | 0.68 |
| DDO 144 | 13.24 | 0.46 |
| DDO 142 | 12.51 | 0.62 |
| DDO 146 | 12.60 | 0.41 |
| NGC 5774 | 12.37 | 0.83 |
| UGC 11868 | 13.68 | 0.45 |
| LSB Average | | 0.61 ($\sigma = 0.22$) |
| Shostak (1978) Scd-Sm Average | | 0.37 |
| de Vaucouleurs (1977) Scd-Sm Average | | 0.32 |

in Table 19 are the average value of $M_H/L_B$ for galaxies of
type Scd, Sd, Sdm and Sm from two sources: de Vaucouleurs
(1977) and Shostak (1978). These authors use the $B_T$ magni-
tude system, so our results are directly comparable to
theirs. The ratio $M_H/L_B$ is distance-independent.

The average $M_H/L_B$ value for the LSB sample is about
1.8 times that of the other late-type galaxies. Using the
Student t test (Langley 1971), we find the probability that
the mean $M_H/L_B$ for the LSB sample does not differ from the
mean for the Shostak (1978) or de Vaucouleurs (1977) late-
type samples is less than 0.2%.

The three galaxies judged from their luminosity pro-
files to have early Hubble types (Section 3.1) have high
$M_H/L_B$. For their type as defined by their profiles, all
three galaxies all hydrogen-rich in the sense used by de
Vaucouleurs (1977): their $M_H/L_B$ is greater than the average
for their type by a factor of at least 3.2.

Another way of measuring the HI content of galaxies
is to find the fraction of the total galactic mass, $M_T$, in
the form of neutral hydrogen. This quantity is more funda-
mental than $M_H/L_B$, but the ambiguity in defining the total
mass of a galaxy makes it more difficult to readily compare
different galaxies using this quantity. We make limited use
of this quantity, by calculating it only for the three LSB
galaxies with masses determined from rotation curves using

our approximation to the Roberts et al. (1975) analysis

(Section 3.4). Table 20 lists $M_H$, $M_T$ and $M_H/M_T$ for these

three galaxies and for five late-type galaxies with masses

from Roberts et al. (1975). The hydrogen masses for these

five galaxies were taken from Rogstad and Shostak (1972).

The average value of $M_H/M_T$ for the LSB galaxies is

roughly twice that of the normal galaxies. However, the

normal z test (Section 3.1) does not indicate a significant

difference between the mean $M_H/M_T$ for the LSB and normal

galaxies.

### 3.7 Mass-to-light Ratio

The individual HII region velocities measured from

the long-slit spectra (Section 2.6) were combined to form a

rotation curve for each galaxy. The observed velocities

($V_{obs}$) were corrected for galaxy inclination and projection

effects due to the misalignment of the spectrograph slit

and the major axis of the galaxy. Both these corrections

are incorporated in the following equation:

$$V(r) = (V_{obs} - V_{sys}) \frac{(\sec^2 i - \tan^2 i \cos^2 \theta)^{\frac{1}{2}}}{\sin i \cos \theta} \quad (27)$$

where i is the galaxy inclination, $V(r)$ is the corrected

velocity relative to the systemic velocity of the galaxy

($V_{sys}$) and $\theta$ is the angle between the spectrograph slit

and the major axis of the galaxy. We adopted the velocities

Table 20.  Hydrogen Mass to Total Mass Ratio

| | $M_{HI}$ $(10^9 M_\odot)$ | $M_T$ $(10^{10} M_\odot)$ | $M_{HI}/M_T$ |
|---|---|---|---|
| **LSBs:** | | | |
| UGC 06983 | 4.8 | 1.8 | 0.27 |
| UGC 07557 | 2.3 | 1.8 | 0.13 |
| NGC 4517A | 7.4 | 1.8 | 0.41 |
| Average | | | 0.27 ($\sigma$ = 0.14) |
| **Normal Late-type Spirals:** | | | |
| M 33 | 1.64 | 1.3 | 0.13 |
| NGC 2403 | 3.5 | 2.3 | 0.15 |
| M 101 | 18.5 | 14.5 | 0.13 |
| NGC 6946 | 21.2 | 11.5 | 0.18 |
| IC 342 | 14.7 | 8.8 | 0.17 |
| Average | | | 0.15 ($\sigma$ = 0.02) |

determined from the 21-cm line as the systemic velocities. Systemic velocities estimated from the distribution of the individual velocity points agreed with the 21-cm velocities to within 10 km/sec.

The mass of the galaxy as a function of radius was obtained using a standard disk model (cf. Burbidge and Burbidge 1975). The Kuzmin integral was integrated by a combination of Simpson's rule and analytic integration. The computer program used was tested using the rotation curve for NGC 4378 from Rubin et al. (1978). The program results agreed precisely with the values of mass as a function of radius published in that paper.

The rotation curves are shown in Figures 7-9. The individual velocity points are plotted with different symbols for points on either side of the galaxy center. The solid line is the fit to the points used by the program which calculates the mass.

The local mass to blue luminosity ratio ($M/L_B$) for several annuli are listed in Table 21. Corrections for Galactic and internal absorption were made using the procedures of Rubin, Ford and Thonnard (1978). The local $M/L_B$ increases substantially from the inner kiloparsec outwards in all three galaxies. This phenomena has been observed in several other galaxies for which detailed rotation curves and surface photometry exist. These include NGC 4378
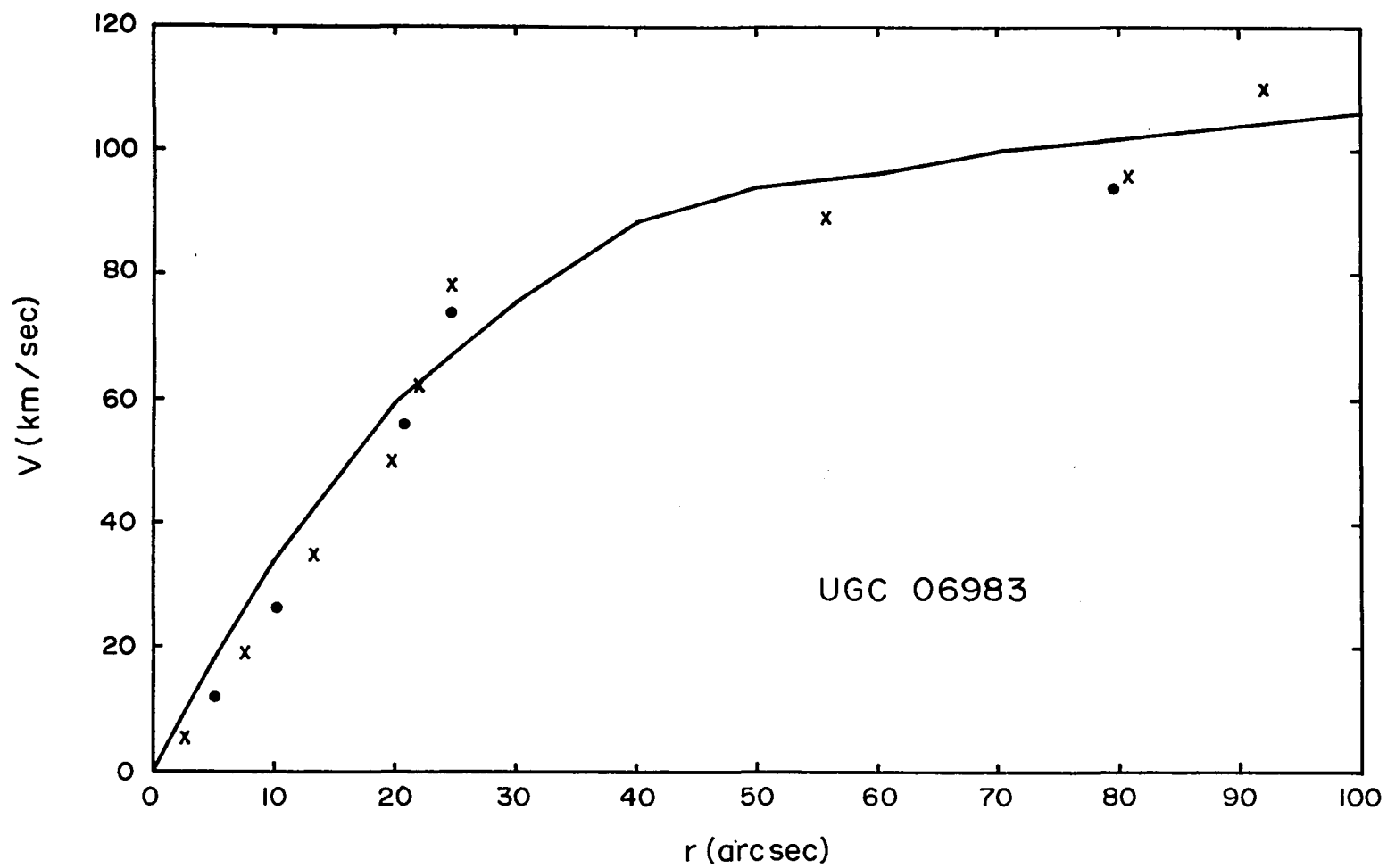
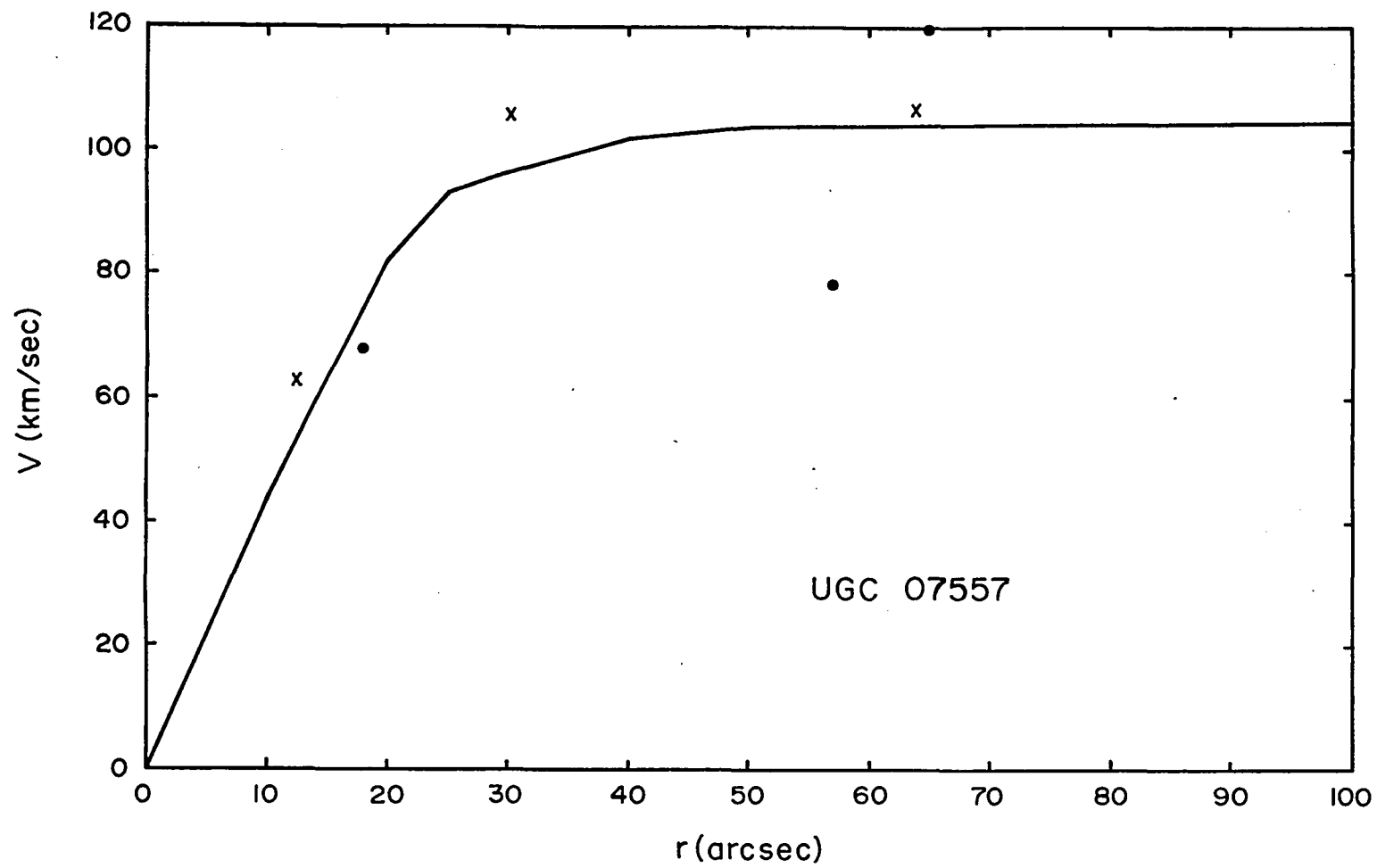Figure 7. Rotation Curve for UGC 06983.
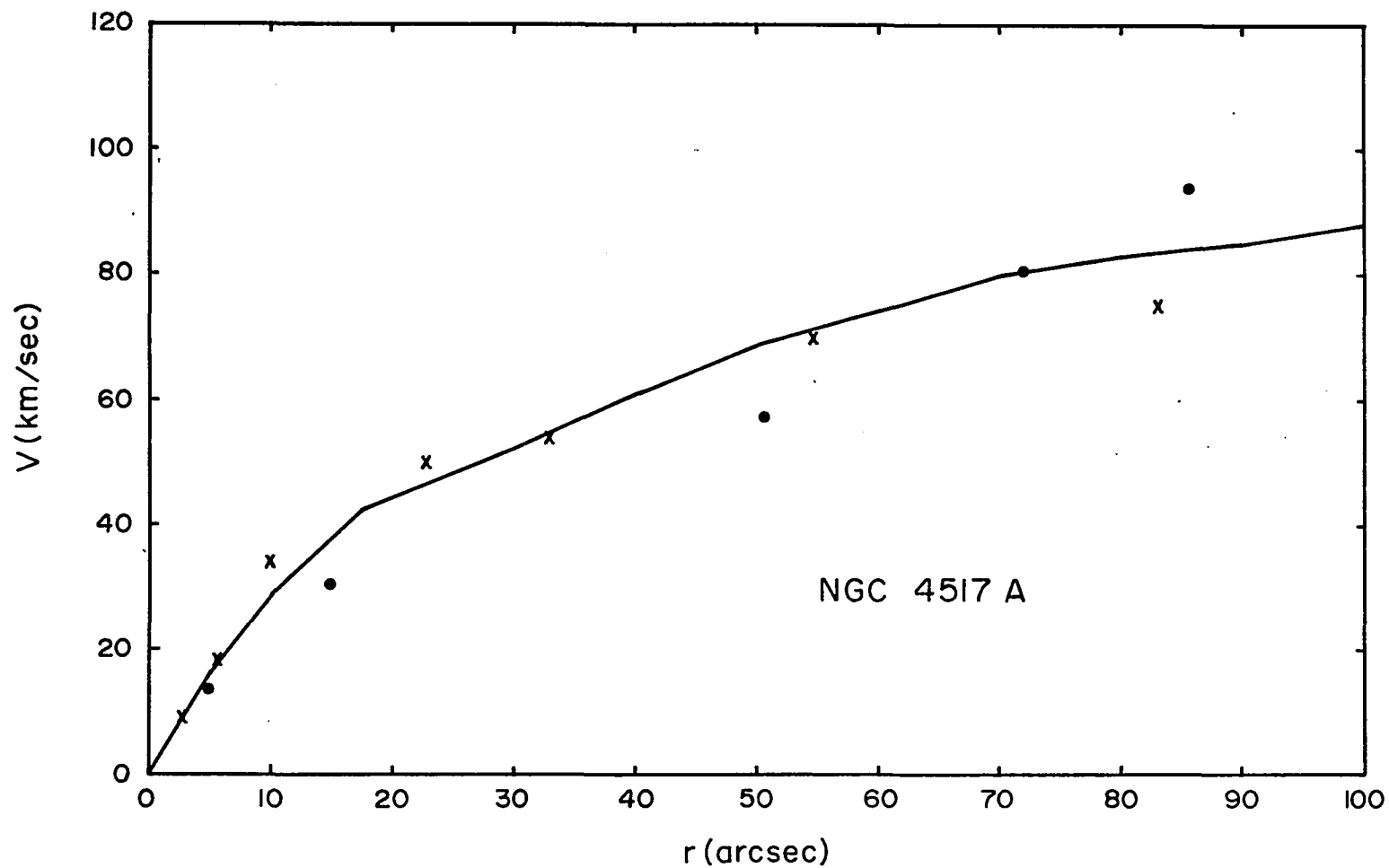
Figure 8.   Rotation Curve for UGC 07557.

Figure 9. Rotation Curve for NGC 4517A.

Table 21. Annular $M/L_B$ Measurements

| Annulus (kpc) | $M/L_B$ (solar units) | | |
|---|---|---|---|
| | UGC 06983 | UGC 07557 | NGC 4517A |
| 0-1.1 | 1.0 | 2.4 | 0.4 |
| 1.1-2.1 | 3.4 | 8.3 | 0.9 |
| 2.1-4.1 | 5.6 | 9.3 | 1.5 |
| 4.1-6.1 | 6.8 | 8.3 | 2.3 |
| 6.1-8.1 | 8.0 | | 2.8 |
| 8.1-10.1 | | | 3.3 |

(Rubin et al. 1978), NGC 7217 (Peterson et al. 1978) and
NGC 4594 (Schweizer 1978). These three galaxies are all
early-type spirals of large mass. The three LSB galaxies
are of late type. Our observations suggest that the in-
crease of M/L from the inner kiloparsec to the outer re-
gions is not associated with the presence of a dominant
bulge component. Either this increase in M/L is a general
property of spiral galaxies or a similar error exists in
the interpretation of rotation curves as a mass indicator
for both early and late spirals.

The integrated values of $M/L_B$ within the de Vaucou-
leurs radii ($r_{dev}$) for UGC 06983, UGC 07557 and NGC 4517A
are 5.9, 8.1, and 2.3, respectively, for an average of 5.4
($\sigma = 2.9$). The average $M/L_B$ within $r_{dev}$ for a sample of
eleven spirals observed by Rubin et al. (1978) is 3.7
($\sigma = 1.9$). The average for the five galaxies of latest
type (Sbc-c or Sc) observed by Rubin et al. is 2.6 ($\sigma = 0.8$).
Only one of their galaxies (NGC 4378) definitely has $M/L_B$
greater than UGC 06983 and UGC 07557. The normal z test
(Section 3.1) shows no significant difference between the
average $M/L_B$ for the LSB galaxies and either the entire
Rubin et al. sample or only the five latest galaxies. Thus,
the very limited nature of our sample makes it impossible
to say whether the average $M/L_B$ for the LSB galaxies is
higher than for normal spirals. We note that the mass of

UGC 07557 may be in error because of uncertain inclination corrections as it is close to face-on (b/a = 0.8).

We can also study the masses of the LSB spirals using their 21-cm line widths. Masses determined from 21-cm line widths depend on assumptions made concerning the shape and extent of the rotation curve. We follow the simple procedure of Faber and Gallagher (1979). They calculate the mass ($M_{HO}$) within the Holmberg radius as simply:

$$M_{HO} = R_{HO} \ V_{HO}^2/G \tag{28}$$

where $V_{HO}$ is the rotational velocity at the Holmberg radius $R_{HO}$. For galaxies with 21-cm line widths, they calculate $V_{HO}$ from $V_{max}$, the velocity width corrected for inclination, as:

$$V_{HO}^2 = V_{max}^2/1.25 \tag{29}$$

We calculated $M_{HO}$ in this way for all LSB galaxies with b/a $\leq$ 0.86 (i $\leq$ 31°). We calculated $L_B$ in the Faber and Gallagher system, using $B_T$ magnitudes corrected for internal absorption as in the RC2 (see Section 3.5) and the Faber and Gallagher Galactic absorption correction. The resulting $M/L_B$ ratios are listed in Table 22. The average value is 5.7 ($\sigma$ = 2.1). This value is almost identical to the average value Faber and Gallagher derive from 21-cm line widths for Scd galaxies (5.8). However, they derive a

Table 22.  $M/L_B$ from 21-cm Widths

|  | $M/L_B$ (solar units) |
|---|---|
| NGC 45 | 9.5 |
| UGC 04841 | 7.3 |
| UGC 04922 | 6.2 |
| UGC 06983 | 6.8 |
| UGC 07557 | 8.0 |
| NGC 4517A | 2.9 |
| DDO 144 | 4.9 |
| DDO 142 | 4.4 |
| DDO 146 | 4.1 |
| NGC 5774 | 2.3 |
| UGC 11868 | 5.3 |
| UGC 06922 | 7.0 |
| Average | 5.7 ($\sigma$ = 2.1) |

smaller value, 3.1, for Sdm galaxies. It seems unlikely that the actual $M/L_B$ ratio changes by a factor of 2 from type Scd to Sdm. The variation in $M/L_B$ with type at these late types probably reflects more on uncertainties in measuring $M/L_B$ using this technique. The average 21-cm $M/L_B$ for Sc, Scd and Sdm galaxies derived by Faber and Gallagher is 4.6. We find no statistically significant difference between this mean $M/L_B$ and the LSB data listed in Table 22, using the Student t test (Langley 1971).

As discussed in Section 2.7, our 21-cm line widths may be slightly underestimated. If we assume our line widths are too small by 10% and make an appropriate correction, the LSB average $M/L_B$ becomes 6.8 ($\sigma = 2.5$). The Student t test shows that the probability that this LSB $M/L_B$ average and the Faber and Gallagher Sc, Scd and Sdm $M/L_B$ average do not differ is about 2%. Another factor, which would tend to work in the opposite direction, is the bias towards face-on galaxies in the LSB sample. The 21-cm line widths of nearly face-on galaxies includes a substantial contribution from noncircular motion. This is shown by the substantial line widths (40-80 km/sec) measured for the face-on galaxies NGC 3913, 4411A and 4411B. Without a knowledge of the velocity dispersion perpendicular to the plane ($\Delta V_z$) we cannot accurately evaluate this contribution to the observed line width. A very crude correction for

this effect can be estimated by assuming the actual circular velocity width, $\Delta V_c$, can be derived from the measured velocity width, $\Delta V_{obs}$, and $\Delta V_z$ using the following simple relation:

$$\Delta V_c{}^2 = (\Delta V_{obs}{}^2 - \Delta V_z{}^2)^{\frac{1}{2}} \tag{30}$$

With $\Delta V_z = 40$ km/sec, the average $M/L_B$ ratio for the LSB sample is lowered by about 10%. After making this correction for face-on bias, we find, using the Student t test, no significant difference between the LSB and Sc, Scd and Sdm average $M/L_B$, whether or not we make the correction for possible line width underestimation.

Thus, we find no conclusive evidence for a difference in M/L between the LSB and normal galaxies. There is a suggestion that the M/L ratio of the LSB spirals may be higher than that of normal spirals of late type, by no more than about 50%. However, the scatter in the values of M/L for both LSB and normal galaxies is large.

CHAPTER 4

CONCLUSIONS AND RECOMMENDATIONS
FOR FUTURE WORK

This work has presented a large quantity of varied observational material on a number of low surface brightness spiral galaxies. The following form the primary conclusions of this work:

1. There exist intrinsically bright spiral galaxies with average surface luminosities about 1/3 that of normal spirals. These galaxies have extrapolated central disk surface brightnesses nearly a factor of 3 fainter than the value found by Freeman (1970) to characterize the majority of spirals. These systems have $M_B$ between -17 and -20. Thus they are brighter than dwarf galaxies.

2. The primary reason these galaxies appear to have low optical surface brightness disks is because they have low average surface mass densities. A higher than normal M/L ratio may also contribute to their low surface brightness. However, with the available data, we cannot definitely tell if the average LSB M/L ratio is significantly higher than normal.

3.  The emission-line spectra of the LSB galaxy HII regions suggest a lack of massive stars in their ionizing clusters, compared to HII regions in galaxies such as M 33 and M 101.  These spectra provide only an upper limit for the average metal abundance in the gas.  The unusual radiation field prevents a firm estimate of the metal abundance.

4.  The broad band colors (both the integrated infrared colors and the optical colors of the old disk population) indicate a stellar population of low metal abundance.  The estimated metal abundance of a typical LSB spiral is on the order of 1/5 solar.

5.  The spiral density wave theory as presented in Roberts et al. (1975) can perhaps explain the weak shocks and low star formation efficiency (as evidenced by the high $M_H/L$ ratio) in the LSB galaxies.  This theory does not offer any simple explanation of the unusual mass function of the massive stars.

Perhaps the most interesting properties of the LSB galaxies are the apparent deficiency of massive stars and the low metal abundance in the stars.  The low metal abundance is probably the consequence of the low proportion of massive stars, rather than a consequence of a high gas/star ratio.  Although the HI mass fraction is relatively large, the mass of HI still comprises less than half the total mass.  In a simple galactic evolution model, (Tinsley

1976), the metallicity of the gas depends only on the logarithm of the inverse of the gas mass fraction. If we assume a HI mass fraction of 25% for the LSB galaxies, and a value half as large for normal late-type galaxies, the difference in metallicity between LSB and normal late spirals predicted by the simple model is only about 30%. The LSB galaxies appear to have an overall metal abundance a factor of two or more lower than normal spirals of late Hubble type. To account for this low metallicity, we are forced to postulate a lower than normal yield of heavy elements. This would be a natural result of an initial mass function with a deficiency of massive stars.

We can make a very crude estimate of the effect of varying the IMF on the average metal abundance of a galaxy by calculating the amount of mass ejected by massive stars, as a fraction of the total mass forming stars, for various IMFs. This should give a crude idea of the relative metal abundance for galaxies with differenct IMFs, as this ejected gas enriches the interstellar medium with metals. In this context, massive stars are those which recycle enriched matter into the interstellar medium, say stars with masses 2 $M_\odot$ and larger. We calculated this ejected mass fraction assuming all massive stars leave a 1 $M_\odot$ remnant. This calculation was performed for two of the IMFs used in Section 3.3, the Miller and Scalo (1979) IMF (model A), and

the steep massive star IMF (model C). The ejected mass fraction will depend somewhat on the details of the low-mass IMF, as changing this changes the proportion of mass locked up in non-evolving stars. Also, the metallicity of the ejected gas will vary with initial stellar mass. We are encouraged that the predicted metallicity ratio, estimated using IMFs we believe appropriate for the normal and LSB galaxies, is similar to the metallicity ratio inferred from our observations.

Our data suggest that the main difference in the evolution of the LSB and normal galaxies is in the massive star IMF, with the LSB galaxies having fewer massive stars. Kormendy (1977b) has discussed another type of galaxy, the filamentary arm spiral, which may be similar to the LSB galaxies in this respect. The filamentary arm spirals, such as NGC 2841, have many short spiral filaments, but lack global spiral structure. Kormendy cites two members of this class as having HII regions much fainter than expected. He speculates that these galaxies may be deficient in massive stars because of a lack of density wave driven star formation. These galaxies have disks of normal surface brightness. Perhaps a strong shock, absent in both LSB and filamentary arm spirals, is needed to make massive stars efficiently. Unfortunately, as pointed out in Section 3.4, the lack of massive stars probably cannot be explained quite

so easily. M 33, a galaxy predicted to have weak shocks, does have an IMF with a larger proportion of massive stars than the LSB galaxies.

As for future observational work, perhaps the most immediate need is to investigate whether factors other than the lack of massive stars may be causing the low $W(H\beta)$ in the LSB HII regions. Observations of a number of HII regions of low absolute luminosity in a normal galaxy such as M 101 should help in disentangling any effects of age or absolute luminosity of the HII region from effects of the IMF. Spectra and colors of HII regions in filamentary arm spirals should also be obtained to determine how they compare with the LSB HII regions.

Also needed are observations of emission lines in the LSB HII regions sensitive to the stellar ionizing temperature and the electron temperature of the gas, such as the He II $\lambda$ 5876 line or the [OIII] $\lambda$ 4363 line. These observations will allow measurement of the chemical abundances in the ionized gas in the LSB HII regions. We expect these lines to be very weak. Perhaps the best place to measure these lines will be in the HII regions of NGC 4236, as it is relatively nearby. First, of course, we must verify that the HII regions in NGC 4236 have spectra similar to those of the galaxies in the present sample.

It would be very useful to have a totally independent check on our conclusion that there are relatively few massive stars in the LSB galaxies. Observations of the equivalent width of Hα integrated over an entire galaxy might provide such a check. Cohen (1976) has presented such W(Hα) data for a number of normal galaxies, finding a decrease of W(Hα) with increasing (B-V). She attributes this decrease to the decreasing amount of light emitted by the hottest O stars for galaxies with redder colors. Our interpretation of the LSB colors implies their low metallicity makes them bluer than expected for the number of massive stars they contain. Thus, we expect a lower W(Hα) at a given (B-V) for the LSB galaxies.

The study of edge-on LSB galaxies should help elucidate any effects of the scale height of the stars and gas on the evolution of these galaxies. The obvious problem is identifying edge-on LSB galaxies. These systems might be identified from their size/infrared magnitude ratio. If any nearby edge-on LSB galaxies can be found, we can measure the scale height of the neutral gas with the Very Large Array observing in the 21-cm line.

There are several 21-cm observations of face-on galaxies that would be of great interest. One is the measurement of the spiral arm peak-to-trough density contrast in the gas. If the gas scale height is large, perhaps the gas

is not as effected by the density wave as in a normal galaxy. This could be determined by comparing the peak-to-trough arm contrast in the gas with the arm contrast in the stars (Section 3.4). In face-on galaxies, measurement of the velocity dispersion in the gas with high velocity resolution would be useful. This, along with an estimate of the disk surface mass density, would make possible an estimate of the gas scale height.

# LIST OF REFERENCES

Aaronson, M. 1977, Ph.D. Dissertation, Harvard University.

_____, J. G. Cohen, J. Mould and M. Malkan. 1978, Ap. J. 223, 824.

Aaronson, M., J. Huchra and J. Mould. 1979, Ap. J., 229, 1.

Allen, C. W. 1973, Astrophysical Quantities, (London: Athlone Press).

Balick, B. and C. Sneden. 1976, Ap. J., 208, 336.

Bevington, P. R. 1969, Data Reduction and Error Analysis for the Physical Sciences, (New York: McGraw-Hill Book Company), p. 105.

Burbidge, E. M. and G. R. Burbidge. 1975, Galaxies and the Universe, eds. A. Sandage, M. Sandage and J. Kristian (Chicago: University of Chicago Press), Chap. 3.

Burnstein, D. 1978, Ph.D. Dissertation, University of California at Santa Cruz.

_____ and C. Heiles. 1978, Ap. J., 225, 40.

Chiosi, C., E. Nasi and S. R. Sreenivasan. 1978, A. & A., 63, 103.

Code, A. D., J. Davis, R. C. Bless and R. Hanbury-Brown. 1976, Ap. J., 203, 417.

Cohen, J. G. 1976, Ap. J., 203, 587.

Crow, E. L., F. A. Davis and M. W. Maxfield. 1960, Statistics Manual, p. 53.

de Vaucouleurs, G. 1953, M.N.R.A.S., 113, 134.

_____. 1977, in The Evolution of Galaxies and Stellar Populations, eds. B. M. Tinsley and R. B. Larson (New Haven, Connecticut: Yale University Observatory), p. 43.

158

de Vaucouleurs, G and A. de Vaucouleurs. 1972, <u>M.N.R.A.S.</u>, <u>77</u>, 1.

_____ and H. Corwin. 1976, <u>Second Reference Catalog of Bright Galaxies</u> (Austin: University of Texas Press).

Dickel, J. R. and H. J. Rood. 1978, <u>Ap. J.</u>, <u>223</u>, 391.

Faber, S. M. 1977, in <u>The Evolution of Galaxies and Stellar Populations</u>, eds. B. M. Tinsley and R. B. Larson (New Haven Connecticut: Yale University Observatory), p. 157.

_____ and J. S. Gallagher. 1979, <u>Ann. Rev. Astron. Astrophys.</u>, <u>17</u>, 135.

Fisher, J. R. and R. B. Tully. 1975, <u>Astr. and Ap.</u>, <u>44</u>, 151.

Freeman, K. C. 1970, <u>Ap. J.</u>, <u>160</u>, 811.

_____. 1976, in <u>Galaxies</u>, eds. K. Freeman, R. C. Larson and B. Tinsley (Geneva: Geneva Observatory), p. 31.

Frogel, J. A., S. E. Persson, M. Aaronson and K. Mattews. 1978, <u>Ap. J.</u>, <u>220</u>, 75.

Goad, L. E. 1975, Ph.D. Dissertation, Harvard University.

Huchra, J. P. 1977, <u>Ap. J.</u>, <u>217</u>, 928.

Jensen, E. B. 1977, Ph.D. Dissertation, The University of Arizona.

_____, K. M. Strom and S. E. Strom. 1976, <u>Ap. J.</u>, <u>209</u>, 748.

Kelsall, T. and B. Stromgren. 1969, in <u>Stellar Astronomy</u>, vol. 1, eds. H. Chiu, R. L. Warasila and J. L. Remo (New York: Gordon and Breach), p. 237.

Kitt Peak National Observatory. 1977, Ritchey-Chretien Spectrograph Operation Manual.

Kormendy, J. 1977a, <u>Ap. J.</u>, <u>217</u>, 406.

_____. 1977b, in <u>The Evolution of Galaxies and Stellar Populations</u>, eds. B. M. Tinsley and R. B. Larson (New Haven: Yale University Press), p. 131.

Landolt, A. U. 1973, A. J., 78, 959.

Langley, R. 1971, Practical Statistics Simply Explained
        (New York: Dover Publications, Inc.), p. 160.

Larson, R. B. and B. M. Tinsley. 1978, Ap. J., 219, 46.

Miller, G. E. and J. M. Scalo. 1979, Ap. J. S. S., 41, 513.

Moffett, T. J. and T. G. Barnes. 1979, A. J., 84, 627.

Morton, D. C. 1969, Ap. J., 158, 629.

Ostriker, J. P., D. O. Richstone and T. X. Thuan. 1974,
        Ap. J., 188, L87.

Peterson, C. J., V. C. Rubin, W. K. Ford and M. S. Roberts.
        1978, Ap. J., 226, 770.

Peterson, B. M., S. E. Strom and K. M. Strom. 1979, A. J.,
        84, 735.

Purcell, E. M. 1969, Ap. J., 158, 433.

Roberts, W. W., M. S. Roberts and F. Shu. 1975, Ap. J.,
        196, 381.

Rogstad, D. H. and G. S. Shostak. 1972, Ap. J., 176, 315.

Rubin, V. C., W. K. Ford, K. M. Strom, S. E. Strom and W.
        Romanishin. 1978, Ap. J., 224, 782.

Rubin, V. C., W. K. Ford and N. Thonnard. 1978, Ap. J.
        (Letters), 225, L107.

Sandage, A. 1973, Ap. J., 183, 711.

_____ and G. A. Tammann. 1974a, Ap. J., 190, 525.

_____. 1974b, Ap. J., 194, 223.

_____. 1974c, Ap. J., 194, 559.

Sarazin, C. L. 1976, Ap. J., 208, 323.

_____. 1977, Ap. J., 211, 772.

Schweizer, F. 1976, Ap. J. Suppl., 31, 313.

_____. 1978, Ap. J., 220, 98.

Searle, L.  1971, Ap. J.,168, 327.

Shields, G. A. and L. Searle.  1978, Ap. J., 222, 821.

Shields, G. A. and B. M. Tinsley.  1976, Ap. J., 203, 66.

Shostak, G. S.  1973, A.A., 24, 411.

_____.  1978, A.A., 68, 321.

Shu, F. H.  1975, in La Dynamique des Galaxies Spirales,
        ed. L. Weliachew (Paris:  Centre National de la
        Recherche Scientifique), p. 309.

Smith, H. E.  1975, Ap. J., 199, 591.

Strom, S. E.  1978, personal communication, Astronomer,
        Kitt Peak National Observatory.

Strom, K. M. and S. E. Strom.  1978, A. J., 83, 73.

_____, E. B. Jensen, J. Moller, L. A. Thompson and T. X.
        Thuan.  1977, Ap. J., 212, 335.

Sullivan, W. T. and P. E. Johnson.  1978, Ap. J., 225, 751.

Talbot, R. J. and W. D. Arnett.  1975, Ap. J., 197, 551.

Talbot, R. J., E. B. Jensen and R. J. Dufour.  1979, Ap. J.,
        229, 91.

Thuan, T. X. and P. Seitzer.  1979, Ap. J., 231, 680.

Tinsley, B. M.  1976, in Galaxies, eds. K. Freeman, R. C.
        Larson and B. Tinsley (Geneva:  Geneva Observatory),
        p. 205.

Toomre, A.  1963, Ap. J., 138, 385.

Tully, R. B. and J. R. Fisher.  1977, A. A., 54, 661.

van den Bergh, S.  1966, A. J., 71, 922.

Walker, M. F.  1964, A. J., 69, 744.

Wells, D.  1975, KPNO and CTIO Quarterly Bull., July-Sept.,
        p. 12.

Whitford, A. E.  1958, A. J., 63, 201.

Yoshizawa, M and K. Wakamatsu.  1975, <u>A. A.</u>, <u>44</u>, 363.